Ground ice stratigraphy of the Inuvik-Tuktoyaktuk corridor

by

Alejandro Alvarez

A thesis submitted in partial fulfilment of the requirements for the degree of

Master of Science

Department of Earth and Atmospheric Sciences

University of Alberta

Abstract

In order to understand permafrost and paleoenvironmental conditions in the Mackenzie Delta Region, permafrost cores were collected in the winter of 2017, near the newly developed Inuvik-Tuktoyaktuk Highway (ITH), NWT, by the NWT Geological Survey, NWT Department of Infrastructure, the University of Alberta's Permafrost Archives Science Laboratory (PACS Lab), and partners as part of the Sentinel Drilling program. This study analyzed five cores (BH-1, BH-2, BH-3, BH-4, and BH-8) located within hilltops, riparian, and peatland terrains, recording various depositional environments. Cores were analyzed for stratigraphy, density, cryostructures, water isotopes ($\delta^{18}O$ and $\delta^{2}H$) and radiocarbon dating to determine the origin of the sedimentary records and associated ground ice.

This study highlights that the Mackenzie Delta region and its ground ice history have been extensively preconditioned by deglaciation, landscape evolution and climatic change, resulting in a landscape with reduced ground ice relative to the late Pleistocene surface. Collectively, these results indicate that deposits within low-relief areas (such as peatlands, lacustrine and riparian zones) are characterized by hosting ice-poor sediments with isotopic values, similar to modern-day, local isotopic composition. BH-1 and BH-3 are comprised of ice-poor diamicts with an isotopic composition between $\delta^{18}O$ -23‰ to -19‰, with a co-isotope slope lower than the local meteoric water line. These isotopic values indicate deep thaw following deglaciation, and subsequent talik formation, and likely enhanced by the Early Holocene thaw followed by stabilization and permafrost aggradation. Likewise, BH-4 and BH-8 are underlain by modest ice contents, in the form of Holocene-aged segregated ice within lacustrine and glaciolacustrine deposits. Radiocarbon dates and sedimentary structures indicate a changing landscape following

deglaciation. Local lakes from ~11,500 to 9000 years ago, subsequently drained or lowered, developing epigenetic permafrost, and transitioning to syngenetic peat in the early Holocene. Lastly, deposits within high-relief areas, such as hummocky and ice-cored terrain, show little evidence of being affected by Holocene thaw. The ice within BH-2, located on a hilltop remnant of glaciofluvial outwash deposits, had depleted Pleistocene values ranging between $\delta^{18}O$ -30‰ to -27‰, at depths greater than 6-meters below the surface. This borehole included buried glacier ice and primary till below 11m depth, likely buried by glaciofluvial outwash in an ice-marginal landsystem.

Overall, these results highlight the ground ice heterogeneity within the Mackenzie Delta region. This heterogeneity is primarily a function of landscape geologic history, including, first and foremost, the preservation or eradication of relict ice during deglaciation processes such as talik development within lakes and fluvial networks, and mass-wasting processes, and subsequent climatic warming during the early Holocene. The result of these landscape-wide processes over the Holocene suggests that the landscape today is less ice-rich than the late Pleistocene landscape. Since the distribution and abundance of ground ice are strongly related to the geologic history of permafrost regions, future work will focus on placing these observations into a Quaternary geologic context and allow future trajectories of thermokarst to be identified.

.

Preface

This thesis is organized into five chapters, with chapter 4 representing a manuscript to be summited for publication – the thesis and the manuscript result from collaborative efforts from multiple researchers and organizations. The studies were designed by myself (Alejandro Alvarez) and my thesis supervisor Dr. Duane Froese. I was responsible for conducting laboratory analyses, compiling results, creating all the figures, and writing thesis chapters and manuscripts, which were subsequently edited and improved by my supervisory committee and co-authors. My supervisor, Duane Froese, assisted in developing the thesis structure, supported themes and objectives and helped design the methodology. Dr. Steve Kokelj and the Northwest Territories Geological Survey and Department of Infrastructures collected the cores used for this study in 2017 as part of the Sentinel Program. Chapter 4 is a co-authored manuscript with Drs. Duane Froese and Steve Kokelj have assisted in creating the manuscript framework and provided numerous constructive feedback. I (Alejandro Alvarez) wrote the manuscript and created all the figures.

Chapter 4 is in preparation to be submitted to a journal as: Alvarez, A., Kokelj, S.V., and Froese, D.G. Holocene thermokarst landscape conditioning across the Pleistocene-Holocene transition: an example from the southern Inuvik-Tuktoyaktuk Highway, NW Canada.

Acknowledgments

First and foremost, I would like to thank my thesis supervisor and mentor, Dr. Duane Froese. Over the last five years, Dr. Froese has undoubtedly made me a better scientist. I want to thank Dr. Froese for his endless and continuous support in writing, research, and fieldwork opportunities. I would also like to recognize that working under Duane has dramatically improved my lab, communication, and critical thinking skills. Lastly, I am forever grateful for the chance to do fieldwork in Inuvik and Tuktoyaktuk in 2017. This invaluable opportunity of getting mucky on thaw slumps, especially as a second-year undergraduate student, is a big reason I have pursued a Master of Science and will continue to pursue a Ph.D.

Thank you, the Natural Sciences and Engineering Research Council (NSERC), Northern Scientific Training Program (NSTP) and Ualberta North for providing the funding necessary to complete this thesis. Thank you to NSERC Permafrost Net for numerous research talks, meetings, and networking experiences. Thank you to the Geological Survey of Northwest Territories and Aurora Research institute for in-kind support, including helicopter time, data inquiries, and guidance.

I would like to respectfully acknowledge that this research took place in the traditional lands and homeland of the Inuvialuit and Gwich'in. I want to thank the Inuvialuit Land Administration (ILA), Inuvialuit Regional Corporation (IRC), Inuvik Hunters and Trappers Committee (IHTC), Gwich'in Tribal Council, and the Gwich'in Renewable Resource Board for their comments and support of research.

A huge thank you to many individuals who have made this research possible. I owe special thanks to Dr. Steve Kokelj for his guidance and extensive knowledge of the Mackenzie Delta Region. The last two spring fieldwork seasons have had many priceless experiences and lessons. I want to thank my colleagues Casey Buchanan and Joe Young for initially teaching me laboratory and fieldwork techniques. I want to thank Alexandre Chiasson for always helping me with ArcGIS, including mapping and database organizing. I want to thank Alister Monteath for his help on the Geotek Scanner, especially during the covid shutdowns. And lastly, a massive thanks to Joel Pumple. Joel is an attentive and caring lab manager. Joel is always ready to help, even if he’s busy, and I will always be grateful to have him as our lab manager.

Lastly, I want to thank my family and friends. Thank you to my parents for supporting (or pushing) my degrees. A special thank you to my dad for being interested in my research and choosing to give feedback on my thesis. Thanks to my two younger brothers. And lastly, thank you to my partner, Kayla Blackadar, for her kindness, support, and patience during my time as a student, especially when I leave for fieldwork, sometimes months at a time.

Table of Contents

List of Tables

List of Figures

Chapter 1: Introduction

Permafrost, or ground that remains below 0°C for two or more years, is the binding agent cementing northern landscapes. The definition of permafrost represents a thermal condition, regardless of the presence or absence of ground ice; consequently, permafrost is a product of climate (Mackay, 1972; Murton and Ballantyne, 2017). The sensitivity and impacts of climate change on permafrost is primarily related to the nature and amount of ground ice in the host materials that may potentially lose cohesion with thaw, and may develop terrain effects from subsidence, termed thermokarst. The magnitude of thermokarst development is largely a function of the abundance of excess ice, *i.e.,* ice that exceeds the pore space of the host sediments. Since thermokarst poses a significant threat via thermokarst, northern landscapes underlain by ice-rich permafrost have the potential to dramatically transform the surficial terrain in response to climate change (Jorgenson et al., 2006; Lantz and Kokelj, 2008).

Tuktoyaktuk Coastlands and Anderson Plain Continuous Permafrost:

The Inuvik – Tuktoyaktuk Highway (ITH) is a 138 km long highway extending from Inuvik to Tuktoyaktuk, NWT, which officially opened in 2017, ultimately connecting all three Canadian coasts. The ITH is arguably the most challenging road built in Canada in the last 50 years, given it traverses a region of ice-rich permafrost located in the continuous permafrost zone (permafrost underlying 90-100% of the landscape), with permafrost depths varying from 100m to 500m near Inuvik and Tuktoyaktuk, respectively (Figure 1.1b; Kokelj et al., 2017). The ITH crosses ecological zones from open-canopy boreal forest (near Inuvik) to dwarf-shrub tundra (near Tuktoyaktuk) that is associated with a change in annual mean ground temperatures from -3°C at Inuvik to -7°C at Tuktoyaktuk (Rampton, 1988; Kokelj et al., 2017).

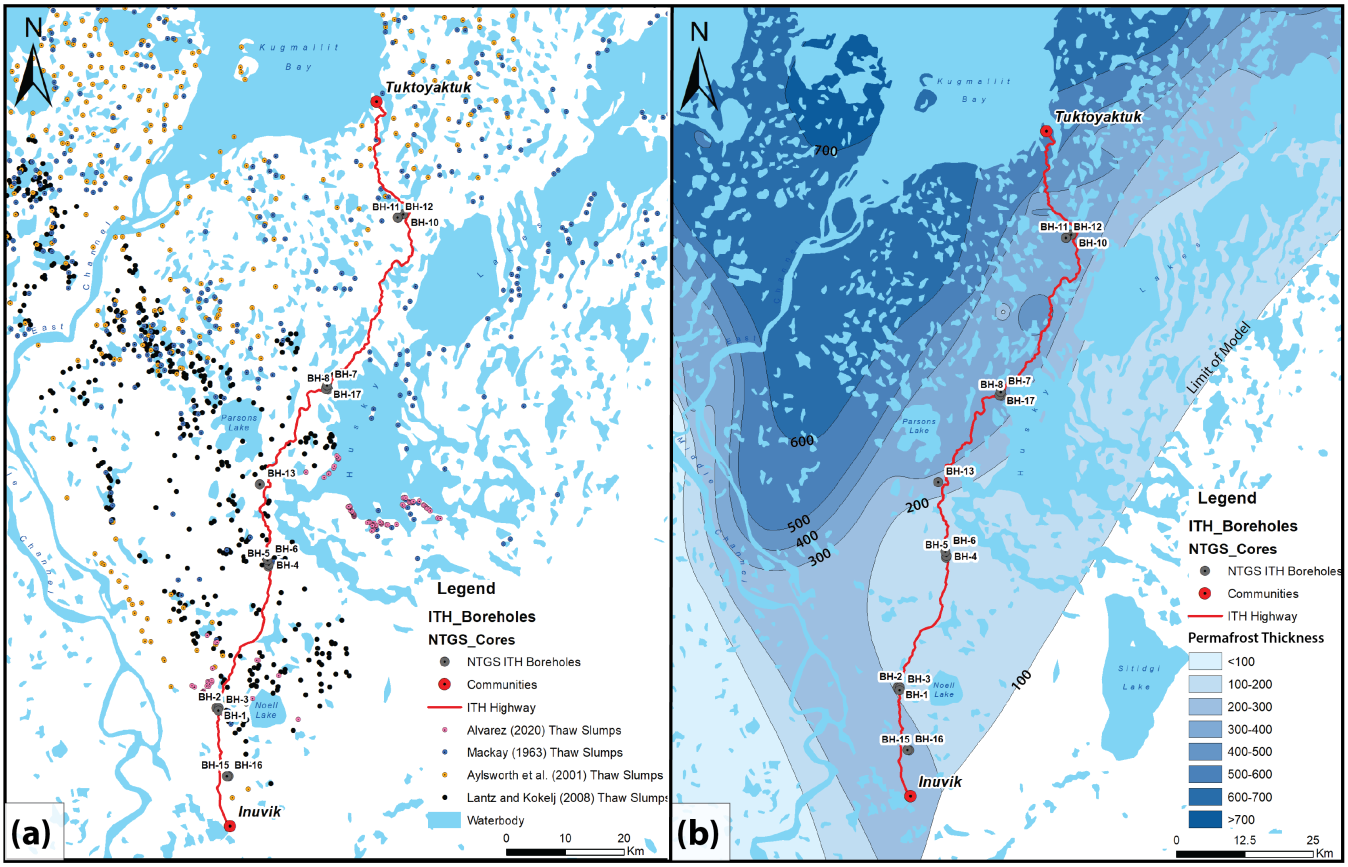

.

Figure 1.1: Study Region – the Mackenzie Delta Region and the ITH .
(a) Figure shows the ITH (red line) traversing the Sentinel boreholes collected in 2017, as well as an inventory retrogressive thaw slumps (past and active) of in the study area. (b) Modeled depth of permafrost for the study region (Smith and Duong, 2012).

The ITH traverses ice-rich continuous permafrost encompassing two physiographic regions, the Tuktoyaktuk Coastlands and Anderson Plain, characterized by thousands of tundra lakes coupled with rolling hills and plains (Burn and Kokelj, 2009; Kokelj et al., 2017b). The Anderson plain is defined as gently undulating or rolling terrain, with moderate relief (~250 masl) controlled by the underlying bedrock (Rampton, 1988; Rudy et al., 2019). Overall, the surficial geology of the Anderson plain is composed of fine-grained till within rolling terrain and thick peatlands (1-4m thick) within low-relief and poorly drained areas (Aylsworth et al., 2001; Rudy et al., 2019). The Tuktoyaktuk Coastlands are defined as low-lying terrains with a maximum elevation reaching 60 masl (Rampton, 1988). The surficial geology of the Tuktoyaktuk coastlands is characterized by gently rolling terrain with tills and organic terrain within lacustrine and glaciolacustrine plains (Duk-Rodkin and Lemmen, 2000; Rudy et al., 2019).

The ITH is especially sensitive to future thaw because of the abundance of excess ice, i.e., ground ice that exceeds the pore space of the host sediments. This excess ice is a catalyst for ground materials which may potentially lose cohesion with thaw, and may develop terrain effects from subsidence, termed thermokarst (Murton et al., 2005). A prominent illustration of thermokarst along the ITH are retrogressive thaw slumps, which represent large mass-movements (landslides) in hillslopes composed of ice-rich permafrost (Figure 1.1a). Alarmingly, these features have taken on new significance as they appear to have substantially increased in frequency and magnitude in northwestern Canada in the last two decades (Lantz and Kokelj, 2008; Segal et al., 2016; Lewkowicz and Way, 2019). Thermokarst has the potential to strongly alter the hydrology, soil processes, and vegetation of many northern environments. Additionally, thermokarst represents a significant threat to subsidence and instability of Arctic infrastructure (Lantz et al., 2009; Kokelj and Jorgenson, 2013; Kokelj et al., 2014; Steedman et al., 2017).

Table 2.1: Main climatic indices from recorded air temperatures at Environment Canada station, located in Inuvik from 2000 to 2020.

Climatic year		2000-2001	2001-2002	2002-2003	2003-2004	2004-2005	2005-2006	2006-2007	2007-2008	2008-2009	2009-2010	Mean (2000-2010)
Thaw season	Start	May. 30	May. 29	May.07	May. 19	May. 19	May. 13	May. 09	May.22	May. 13	May. 17	-
	End	Sep. 23	Oct. 07	Oct. 02	Oct. 08	Sep. 28	Sep. 26	Oct. 07	Sep. 25	Sep. 25	Sep. 24	-
	Duration (days)	116	131	148	142	132	136	151	162	135	130	**138**
	Avg. Temp. T°C	10.3	9.9	8.4	8.8	10.3	8.5	10.0	10.9	8.9	9.4	**9.5**
	Thawing index (TI)	1193	1293	1242	1242	1367	1151	1502	1353	1205	1228	**1278**
Freezing season	Start	Sep. 24	Oct. 08	Oct. 03	Oct. 09	Sep. 28	Sep. 27	Oct. 08	Sep. 26	Sep. 26	Sep. 25	-
	End	May.28	May.06	May. 18	May. 18	May. 12	May. 08	May. 21	May. 12	May. 16	May. 13	-
	Duration (days)	249	210	227	221	226	223	225	228	232	230	**227**
	Avg. Temp. T°C	-16.7	-19.0	-15.8	-20.1	-18.5	-17.3	-17.6	-17.3	-17.4	-15.6	**-17.5**
	Freezing index (FI)	-4143	-4021	-3628	-4460	-4190	-3891	-3986	-4001	-4081	-3587	**-3999**
Mean Annual Air Temperature (°C)		-8.1	-7.9	-6.3	-8.8	-7.9	-7.6	-6.6	-7.4	-7.8	-6.5	-7.5
Climatic year		**2010-2011**	**2011-2012**	**2012-2013**	**2013-2014**	**2014-2015**	**2015-2016**	**2016-2017**	**2017-2018**	**2019-2020**	**2019-2020**	**Mean (2010-2020)**
Thaw season	Start	May. 18	May. 15	May. 11	May. 16	May. 02	May. 07	May. 06	May. 13	May. 09	May. 10	-
	End	Sep. 23	Oct. 05	Oct. 08	Oct. 23	Oct. 03	Oct. 04	Oct. 07	Oct. 10	Sep. 23	Oct. 06	-
	Duration (days)	128	140	150	160	154	150	154	150	137	149	**147**
	Avg. Temp. T°C	11.1	10.3	11.9	8.7	8.8	9.0	9.2	10.3	7.4	9.3	**9.6**
	Thawing index (TI)	1445	1462	1774	1365	1347	1342	1407	1518	1067	1362	**1409**
Freezing season	Start	Sep. 24	Oct. 06	Oct. 09	Oct. 24	Oct. 04	Oct. 05	Oct. 08	Oct. 11	Sep. 24	Oct. 06	-
	End	May. 14	May. 10	May. 15	May. 01	May. 06	May. 05	May. 12	May. 08	May. 09	May. 18	-
	Duration (days)	232	216	218	189	214	212	216	209	228	224	**216**
	Avg. Temp. T°C	-16.2	-18.9	-20.2	-17.6	-15.8	-15.7	-16.2	-14.8	-12.8	-17.1	**-16.5**
	Freezing index (FI)	-3803	-4137	-4422	-3368	-3392	-3335	-3530	-3085	-2910	-3859	**-3584**
Mean Annual Air Temperature (°C)		-8.1	-7.4	-7.2	-5.8	-5.6	-5.5	-5.7	-4.4	-5.1	-6.7	-6.2

Late Quaternary Glaciations and Environmental Setting of the Northwestern Canadian Arctic:

Pre-Laurentide Deposition:

The complex sedimentary deposition underlying northwestern Arctic Canada contains marine sands and clay, alluvial and aeolian sands, tills and diamictons, many incorporating ground ice (Rampton and Mackay, 1971; Rampton, 1988; Wolfe et al., 2020). The lowermost units, the Kendall sediments and Hooper clay, were likely deposited during the last Sangamonian (MIS 5e) interglaciation, representing deposits from marine transgression (Wolfe et al., 2020). The overlying Kidluit Formation denotes pre-Laurentide alluvial sands deposited in a landscape dominated by large braided rivers (Murton et al., 2017; Wolfe et al., 2020). These large ancient rivers, flowing into the Arctic Ocean, have been dated between 76 and 27 ka via optically stimulated luminescence (Murton et al., 2017). The overlying Kittigazuit Formation is interpreted as eolian sands reworked from the Kidluit (Murton et al., 2017; Wolfe et al., 2020). These aeolian sands, dated between ca. 30 and 13ka, likely formed as the Laurentide Ice Sheet advanced northward, effectively blocking and abandoning portions of the large paleo-rivers, leading to extensive depositions of fine-grained sediments.

Laurentide Ice Sheet: Toker Point Stade and Sitidgi Stade

The landscape of the Mackenzie Delta and the Tuktoyaktuk Coastlands is a direct result of the Laurentide Ice Sheet (LIS) (Duk-Rodkin and Lemmen, 2000). The LIS reached it maximum ~18,000 ^{14}C years BP and persisted as late as ~13,100 ^{14}C years BP (Rampton, 1988; Hill, 1996; Duk-Rodkin and Lemmen, 2000; Kokelj et al., 2017a). However, the exact timing and extent of the Laurentide glaciation remains poorly constrained. The LIS reached the Mackenzie Delta region twice during the last glacial cycle, the Toker Point Stade and the subsequent younger Sitidgi Stade. The Toker Point Member, of the Tuktoyaktuk Formation, is a grey, pebbly clay till deposited by the northward advance of the LIS into the Tuktoyaktuk area, reaching its maximum extent ca. 30 ka (Mackay and Dallimore, 1992; Murton et al., 2015). During the glacial maximum, ice thickness throughout western Arctic Canada reached at least 600 to 1000m (Duk-Rodkin and Hughes, 1992; Lacelle et al., 2018). Following the retreat of the LIS, a second readvance (or stillstand), defined as the Sitidgi Stade, extended the ice sheet in the southern part of the Tuktoyaktuk Coastlands (Rampton, 1988). The limit of the Sitidgi Stade, previously defined by Hughes (1987) as the Tutsieta Lake glacial advance, is defined by a hummocky landform, deposited by the LIS representing the ice limit while it persisted near Inuvik (Rampton, 1988). The Sitidgi Stade dates to approximately ca. 15 300 cal. yr BP (Rampton, 1988; Murton et al., 2007)

Thesis Objectives

This thesis focuses on five deep boreholes along the Inuvik-Tuktoyaktuk Highway, with an emphasis on reconstructing the sedimentological record and ground ice evolution between the Last Glacial Maximum and present day. Results from this study will increase our understanding of climate change and future thermokarst in continuous permafrost within northern Canada and develop a set of tools that can be used in other regions to evaluate future thaw trajectories for northern landscapes.

The objectives of this thesis are, therefore, to:

(1) Determine the depositional history of the five boreholes along the Inuvik-Tuktoyaltuk Highway;

(2) Determine the ground ice genesis hosted within these continuous permafrost settings; and

(3) Evaluate the evolution and heterogeneity of ground ice within a glaciated permafrost settings in relation to early Holocene and recent warming.

Collectively, the aim of this study is to quantify the age, ground ice setting and abundance in relation to terrain units to estimate the impacts of early Holocene thaw. In this study, we use stratigraphy, sediment descriptions, cryostratigraphy and water isotopes, to determine which sediments are prone to hosting excess ice within different terrains.

Organization of the thesis

Chapter 2 of the thesis presents a technical communication on laboratory methods used in this study. Additionally, it provides introductory information on the methods utilized, including Geotek Density scanning, stratigraphy, cryostratigraphy, till and diamict classification, water isotope analyses, radiocarbon dating, and ground ice classification.

Chapter 3 is a literature review of ground ice and ground ice forms typically hosted within the Mackenzie Delta region. This review includes commonly used ground ice definitions and examples of different ground ice forms typically found within the Mackenzie Delta Region, Klondike, and central Mackenzie Valley.

Chapter 4 presents a manuscript tittled "Holocene thermokarst landscape conditioning across the Pleistocene-Holocene transition: an example from the southern Inuvik-Tuktoyaktuk Highway, NW Canada" detailing the stratigraphy and ground-ice evolution of 5 boreholes along the Inuvik-Tuktoyaktuk Highway.

Chapter 5 presents the thesis conclusions and recommendations for future work.

References:

Associate Committee on Geotechnical Research National (ACGR), 1988, Glossary of Permafrost and Related Ground-Ice Terms: National Research Council of Canada, v. Technical, p. 156, doi:10.4224/20378888.

Aylsworth, J.M., Burgess, M.M., Desrochers, D.T., Duk-Rodkin, A., Robertson, T., and Traunor, J.A., 2001, Surficial geology, subsurface materials, and thaw sentivity of sediments: Bulletin of the Geological Survey of Canada, p. 41–48.

Burn, C.R., and Kokelj, S. V., 2009, The environment and permafrost of the Mackenzie Delta area: Permafrost and Periglacial Processes, v. 20, p. 83–105, doi:10.1002/ppp.655.

Cardyn, R., Clark, I.D., Lacelle, D., Lauriol, B., Zdanowicz, C., and Calmels, F., 2007, Molar gas ratios of air entrapped in ice: A new tool to determine the origin of relict massive ground ice bodies in permafrost: Quaternary Research, v. 68, p. 239–248, doi:10.1016/j.yqres.2007.05.003.

Clark, I.D., and Lauriol, B., 1997, Aufeis of the Firth River basin, Northern Yukon, Canada: Insights into permafrost hydrogeology and karst: Arctic and Alpine Research, v. 29, p. 240–252, doi:10.2307/1552053.

Crites, H., Kokelj, S. V, and Lacelle, D., 2020, Icings and groundwater conditions in permafrost catchments of northwestern Canada: Scientific Reports, v. 10, doi:10.1038/s41598-020-60322-w.

Duk-Rodkin, A., and Hughes, O.L., 1992, Pleistocene montane glaciations in the Mackenzie Mountains, Northwest Territories: Geographie Physique et Quaternaire, v. 46, p. 69–83, doi:10.7202/032889ar.

Duk-Rodkin, A., and Lemmen, D.S., 2000, Glacial history of the Mackenzie region: Bulletin of the Geological Survey of Canada, p. 11–20, doi:10.4095/211903.

French, H., 2007, The Periglacial Environment, 3rd edn: Wiley, Chichester, 458 p.

French, H.M., and Pollard, W.H., 1986, Ground-ice investigations, Klondike District, Yukon Territory:, www.nrcresearchpress.com (accessed December 2019).

Froese, D.G., Zazula, G.D., and Reyes, A. V, 2006, Seasonality of the late Pleistocene Dawson tephra and exceptional preservation of a buried riparian surface in central Yukon Territory, Canada: Quaternary Science Reviews, v. 25, p. 1542–1551, doi:10.1016/j.quascirev.2006.01.028.

Hill, P.R., 1996, Late Quaternary sequence stratigraphy of the Mackenzie Delta: Canadian Journal of Earth Sciences, v. 33, p. 1064–1074, doi:10.1139/e96-081.

Hughes, O.L., 1987, Late Wisconsinan Laurentide glacial limits of northwestern Canada: the Tutsieta Lake and Kelly Lake phases: Geological Survery of Canada, p. 25, doi:10.4095/122385.

Jorgenson, M.T., Shur, Y.L., and Pullman, E.R., 2006, Abrupt increase in permafrost degradation in Arctic Alaska: Geophysical Research Letters, v. 33, p. 2–5, doi:10.1029/2005GL024960.

Knight, P.G., 1997, The basal ice layer of glaciers and ice sheets: Quaternary Science Reviews, v. 16, p. 975–993, doi:10.1016/S0277-3791(97)00033-4.

Kokelj, S. V., and Jorgenson, M.T., 2013, Advances in thermokarst research: Permafrost and Periglacial Processes, v. 24, p. 108–119, doi:10.1002/ppp.1779.

Kokelj, S. V, Lantz, T.C., Tunnicliffe, J., Segal, R., and Lacelle, D., 2017a, Climate-driven thaw of permafrost preserved glacial landscapes, northwestern Canada: GEOLOGY, v. 45,

doi:10.1130/G38626.1.
Kokelj, S. V., Lantz, T.C., Wolfe, S.A., Kanigan, J.C., Morse, P.D., Coutts, R., Molina-Giraldo, N., and Burn, C.R., 2014, Distribution and activity of ice wedges across the forest-tundra transition, western arctic Canada: Journal of Geophysical Research: Earth Surface, v. 119, p. 2032–2047, doi:10.1002/2014JF003085.
Kokelj, S. V., Palmer, M.J., Lantz, T.C., and Burn, C.R., 2017b, Ground Temperatures and Permafrost Warming from Forest to Tundra, Tuktoyaktuk Coastlands and Anderson Plain, NWT, Canada: Permafrost and Periglacial Processes, v. 28, p. 543–551, doi:10.1002/PPP.1934.
Lacelle, D., 2002, Ground ice investigation in the far northwest of Canada: , p. 101.
Lacelle, D., Fisher, D., Clark, I.D., and Berinstain, A., 2008, Distinguishing between vapor- and liquid-formed ground ice in the northern martian regolith and potential for biosignatures preserved in ice bodies: Icarus, v. 197, p. 458–469, doi:10.1016/j.icarus.2008.05.017.
Lacelle, D., Fisher, D.A., Coulombe, S., Fortier, D., and Frappier, R., 2018, Buried remnants of the Laurentide Ice Sheet and connections to its surface elevation: Scientific Reports, v. 8, doi:10.1038/s41598-018-31166-2.
Lacelle, D., Lauriol, B., Clark, I.D., Cardyn, R., and Zdanowicz, C., 2007, Nature and origin of a Pleistocene-age massive ground-ice body exposed in the Chapman Lake moraine complex, central Yukon Territory, Canada: Quaternary Research, v. 68, p. 249–260, doi:10.1016/j.yqres.2007.05.002.
Lacelle, D., St-Jean, M., Lauriol, B., Clark, I.D., Lewkowicz, A., Froese, D.G., Kuehn, S.C., and Zazula, G., 2009, Burial and preservation of a 30,000 year old perennial snowbank in Red Creek valley, Ogilvie Mountains, central Yukon, Canada: Quaternary Science Reviews, v. 28, p. 3401–3413, doi:10.1016/j.quascirev.2009.09.013.
Lantz, T.C., and Kokelj, S. V., 2008, Increasing rates of retrogressive thaw slump activity in the Mackenzie Delta region, N.W.T., Canada: Geophysical Research Letters, v. 35, p. 1–5, doi:10.1029/2007GL032433.
Lantz, T.C., Kokelj, S. V., Gergel, S.E., and Henry, G.H.R., 2009, Relative impacts of disturbance and temperature: Persistent changes in microenvironment and vegetation in retrogressive thaw slumps: Global Change Biology, v. 15, p. 1664–1675, doi:10.1111/j.1365-2486.2009.01917.x.
Lewkowicz, A.G., and Way, R.G., 2019, Extremes of summer climate trigger thousands of thermokarst landslides in a High Arctic environment: Nature Communications, v. 10, p. 1–11, doi:10.1038/s41467-019-09314-7.
Mackay, J.R., 1993, Air temperature, snow cover, creep of frozen ground, and the time of ice-wedge cracking, western Arctic coast: Canadian Journal of Earth Sciences, v. 30, p. 1720–1729, doi:10.1139/e93-151.
Mackay, J.R., 1983, Downward water movement into frozen ground, western arctic coast, Canada.: Canadian Journal of Earth Sciences, v. 20, p. 120–134, doi:10.1139/e83-012.
Mackay, J.R., 1989, Massive ice: some field criteria for the identification of ice types: Current Research, Part G, Geological Survey of Canada, Paper, p. 5–11.
Mackay, J.R., 1998, Pingo growth and collapse, Tuktoyaktuk Peninsula area, western arctic coast, Canada: A long-term field study: Geographie Physique et Quaternaire, v. 52, p. 271–323, doi:10.7202/004847ar.
Mackay, J.R., 1990, Some observations on the growth and deformation of epigenetic, syngenetic and anti-syngenetic ice wedges: Permafrost and Periglacial Processes, v. 1, p. 15–29,

doi:10.1002/ppp.3430010104.
Mackay, J.R., 1971, The Origin of Massive Icy Beds in Permafrost, Western Arctic Coast, Canada: Canadian Journal of Earth Sciences, v. 8, p. 397–422, doi:10.1139/e71-043.
Mackay, J.R., 1972, The World Of Underground Ice: Annals of the Association of American Geographers, v. 62, p. 1–22, doi:10.1111/j.1467-8306.1972.tb00839.x.
Mackay, J.R., and Dallimore, S.R., 1992, Massive ice of the Tuktoyaktuk area, western Arctic coast, Canada: Canadian Journal of Earth Sciences, v. 29, p. 1235–1249, doi:10.1139/e92-099.
Moorman, B.J., and Michel, F.A., 2000, The burial of ice in the proglacial environment of Bylot Island, Arctic Canada: Permafrost and Periglacial Processes, v. 11, p. 161–175, doi:10.1002/1099-1530(200007/09)11:3<161::AID-PPP347>3.0.CO;2-F.
Morse, P.D., and Burn, C.R., 2013, Field observations of syngenetic ice wedge polygons, outer Mackenzie Delta, western Arctic coast, Canada: Journal of Geophysical Research: Earth Surface, v. 118, p. 1320–1332, doi:10.1002/jgrf.20086.
Murton, J.B., 2005, Ground-ice stratigraphy and formation at North Head, Tuktoyaktuk Coastlands, western Arctic Canada: A product of glacier-permafrost interactions: Permafrost and Periglacial Processes, v. 16, p. 31–50, doi:10.1002/ppp.513.
Murton, J.B., and Ballantyne, C.K., 2017, Periglacial and permafrost ground models for Great Britain, *in* Geological Society Engineering Geology Special Publication, v. 28, p. 501–579, doi:10.1144/EGSP28.5.
Murton, J.B., Bateman, M.D., Telka, A.M., Waller, R., Whiteman, C., and Kuzmina, S., 2017, Early to mid Wisconsin Fluvial Deposits and Palaeoenvironment of the Kidluit Formation, Tuktoyaktuk Coastlands, Western Arctic Canada: Permafrost and Periglacial Processes, v. 28, p. 523–533, doi:10.1002/ppp.1946.
Murton, J.B., Bateman, M.D., Waller, R.I., Sciences, G., and Whiteman, C.A., 2015, Late Wisconsin glaciation of Hadwen and Summer islands , Tuktoyaktuk Coastlands ,: 68e Conférence Canadienne de Géotechnique et 7e Conférence Canadienne sur le Pergélisol, 20 au 23 septembre 2015, Québec, Québec.,.
Murton, J.B., Frechen, M., and Maddy, D., 2007, Luminescence dating of mid- to Late Wisconsinan aeolian sand as a constraint on the last advance of the Laurentide Ice Sheet across the Tuktoyaktuk Coastlands, western Arctic Canada: Canadian Journal of Earth Sciences, v. 44, p. 857–869, doi:10.1139/E07-015.
Murton, J.B., Whiteman, C.A., Waller, R.I., Pollard, W.H., Clark, I.D., and Dallimore, S.R., 2005, Basal ice facies and supraglacial melt-out till of the Laurentide Ice Sheet, Tuktoyaktuk Coastlands, western Arctic Canada: Quaternary Science Reviews, v. 24, p. 681–708, doi:10.1016/j.quascirev.2004.06.008.
O'Neill, H.B., Wolfe, S.A., and Duchesne, C., 2019, New ground ice maps for Canada using a paleogeographic modelling approach: Cryosphere, v. 13, p. 753–773, doi:10.5194/tc-13-753-2019.
Rampton, V.N.; Mackay, J.R., 1971, Massive ice and icy sediments throughout the Tuktoyaktuk Peninsula, Richards Island, and nearby areas, district of Mackenzie: Geol Surv Can, Pap 71-21,.
Rampton, V.N., 1991, Observations on buried glacier ice and massive segregated ice, Western Arctic Coast, Canada: Discussion: Permafrost and Periglacial Processes, v. 2, p. 163–165, doi:10.1002/ppp.3430020209.
Rampton, V.N., 1988, Quaternary Geology of the Tuktoyaktuk Coastlands, Northwest

Territories: Geological Survey of Canada, p. 1–107, doi:10.1126/science.ns-6.149S.521-a.
Rudy, A.C.A., Morse, P.D., Kokelj, S. V, Sladen, W.E., and Smith, S.L., 2019, A New Protocol to Map Permafrost Geomorphic Features and Advance Thaw-Susceptibility Modelling, *in* p. 661–669, doi:10.1061/9780784482599.076.
Segal, R.A., Lantz, T.C., and Kokelj, S. V., 2016, Acceleration of thaw slump activity in glaciated landscapes of the Western Canadian Arctic: Environmental Research Letters, v. 11, doi:10.1088/1748-9326/11/3/034025.
Shur, Y., French, H.M., Bray, M.T., and Anderson, D.A., 2004, Syngenetic permafrost growth: Cryostratigraphic observations from the CRREL tunnel near Fairbanks, Alaska: Permafrost and Periglacial Processes, v. 15, p. 339–347, doi:10.1002/ppp.486.
Steedman, A.E., Lantz, T.C., and Kokelj, S. V., 2017, Spatio-Temporal Variation in High-Centre Polygons and Ice-Wedge Melt Ponds, Tuktoyaktuk Coastlands, Northwest Territories: Permafrost and Periglacial Processes, v. 28, p. 66–78, doi:10.1002/ppp.1880.
Wolfe, S., Murton, J., Bateman, M., and Barlow, J., 2020, Oriented-lake development in the context of late Quaternary landscape evolution, McKinley Bay Coastal Plain, western Arctic Canada: Quaternary Science Reviews, v. 242, p. 106414, doi:10.1016/j.quascirev.2020.106414.

Chapter 2: Methods

This chapter presents the methods used to analyze the geotechnical and geochemical properties of sedimentary units to explore the relations between permafrost and excess-ice hosted glaciated landscapes along the Inuvik – Tuktoyaktuk Highway. This chapter is organized into sections that detail the workflow of this study, from core retrieval to subsampling. These descriptions outline the collection, Geotek bulk-density scanning, cryostratigraphy, till classification, water isotopes, radiocarbon dating and ground-ice classification.

2.1 NTGS-17 Sentinel Core Collection:

Drilling along the ITH was carried out in March 2017 by the Northwest Territories Geological Survey, NWT Department of Infrastructure, PACS lab and other partners and universities. The NTGS fieldwork consisted of obtaining cores, known as the 'Sentinel' cores, along the ITH right-of-way situated within hilltops, riparian, and peatland terrains. Overall, the 13 coring sites were selected base upon Rampton (1988) surficial geology map and regional description of the area. Cores were recovered, up to a depth of 20m, using a mobile 2012 Prospector P1 RC/DD drilling rig from Midnight Sun Drilling Inc (Ensom et al., 2020). The drilling rig used a CRREL drilling barrel (4-inch diameter) with diamond-coated cutting teeth. All core samples were sectioned in the field, logged, and boxed (Figure 2.1). Initial core descriptions, such as visible ice content and soil descriptions were done at the Western Arctic Research Center located in Inuvik (Ensom et al., 2020). Cores were split lengthwise, and one half was used for gravimetric water content, done in the Western Arctic Research Center by the Northwest Territories Geological Survey, and for geotechnical analysis done by Tetra Tech, outlined in

Ensom et al., (2020). The second half of the boreholes were transported frozen to the University of Alberta's Permafrost Archives Science (PACS) Lab.

This study analyzed five cores (BH-1, BH-2, BH-3, BH-4, and BH-8) within hilltops, riparian, and peatland terrains, recording various depositional environments. These cores underwent a geotek density scan, and analyzed the cryostructures and stratigraphy before being subsampled at the University of Alberta to analyze water isotopes, and radiocarbon dating to determine the origin of the sedimentary and ground ice records. A summary of workflow is shown in Figure 2.2.

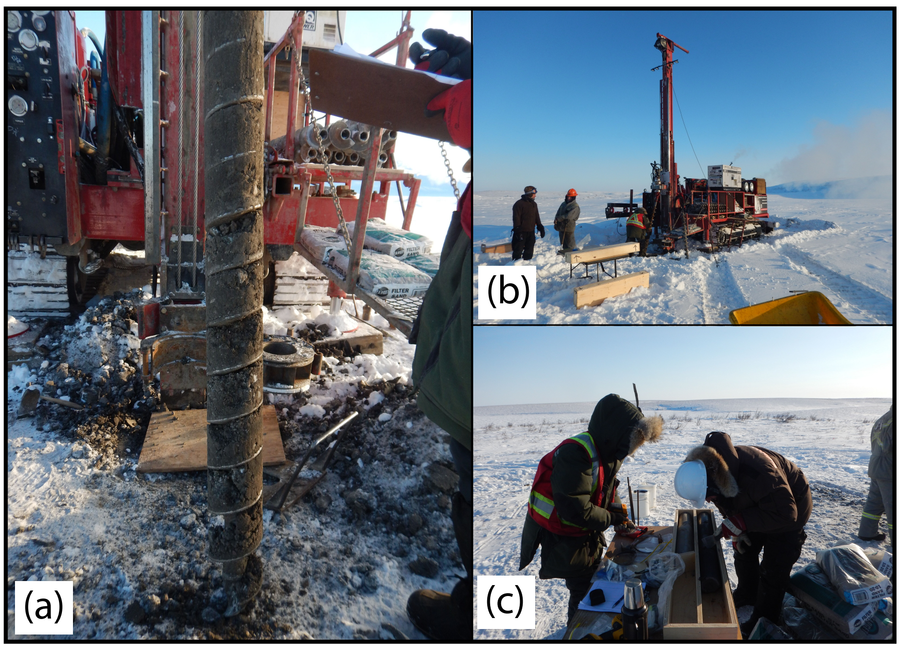

Figure 2.1: Northwest Geological Survey (NTGS) Sentinel core retrieval.
Photos taken by Tim Ensom in March 2017: (a) extraction of permafrost cores. (b) solid stem auger. (c) logging and storing cores

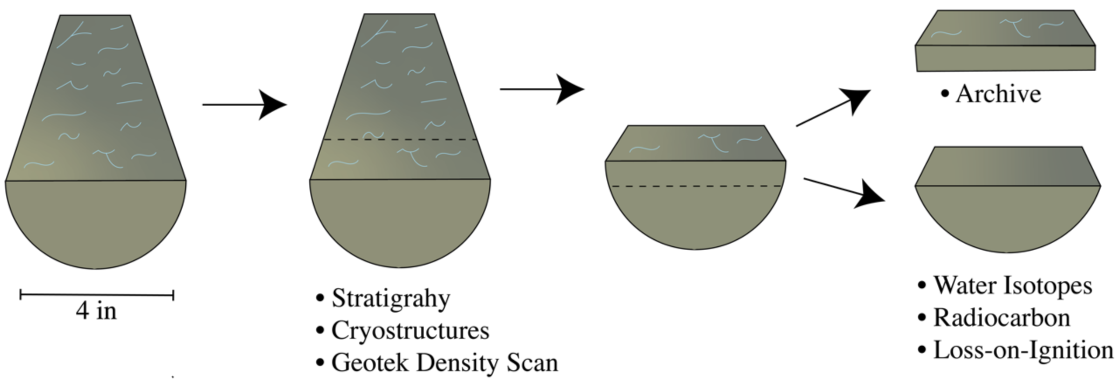

Figure 2.2: Summary of workflow outlined in this methods chapter.
Half the core (cut lengthwise) was shipped to the University of Alberta from Inuvik, NWT. Before subsampling, stratigraphy and cryostructures were analyzed coupled with Geotek density measurements. These cores were further subsampled to determine the water isotopes, and radiocarbon for the core. Figure adapted from Bandara's MSc. Thesis (2017).

2.2 Geotek Multi System Core Logger (MSCL)

The Geotek Multi System Core Logger (MSCL) is an automated system that uses a Caesium-137 (^{137}Cs) source and detector to provide gamma density measurements. Gamma-ray attenuation was measured at 1 cm intervals, for 5 seconds using a 5 mm aperture on half-cores. In addition, the Geotek MSCL software (Geotek, 2008) was used to convert raw gamma density values to bulk sediment densities (g/cm^3). The Geotek is a rapid, non-destructive method to compare and determine different types of sediments present in the study location. Table 3.0 shows a table of representative bulk densities that have been used in previous studies.

The calibration of the MSCL for permafrost cored was developed by the PACS lab and outlined in Pumple et al., (in prep, 2022). We developed an aluminum calibration piece housed within a PVC pipe and surrounded with frozen water. This new calibration system aided in, (1) an increase in 0.5 cm resolution relative to 1 cm from the Geotek calibration piece. This change in calibration resolution resulted in visually picking clearer points to process raw data in the Geotek software. (2) Increased the range of density measurements within frozen sediments (0.9 g/cm^3 (ice) to >2.4 g/cm (clast-rich sediments). Overall, the calibration results in accurate density measurements for frozen sediments.

Sediment Type	**Density (g/cm^3)**
Diamict	> 2.03
Coarse Sand	2.03
Fine Sand	1.98
Very Fine Sand	1.91
Silt	1.83 – 1.38
Clay	1.38 – 1.26

Table 2.1: Summary of representative bulk densities values for marine sediments. Table is summarized from Hamilton, 1970.

2.3 Cryostratigraphy

Cryostratigraphy is the study of frozen layers in the Earth's crust (French and Shur, 2010). While cryostructures describe the shape and distribution of ice hosted within frozen sediments (Murton and French, 1994). Permafrost studies regularly use cryostructures to identify the genesis of ground ice and to interpret the history of the frozen material (French and Shur, 2010). The development of cryostructures reflects: (1) moisture availability; (2) the nature of freezing (epigenetic, syngenetic or polygenetic); and (3) the properties of the soil (packing of grains and grain size) (Gilbert et al., 2016).

This study has adopted a modified classification scheme used by Murton and French (1994), as shown in Figure 2.3. Six main cryostructures were observed throughout the cores, including suspended, lenticular, layered, irregular reticulate, and organic-matrix and Solid (S). Suspended (Su), or ataxitic, is defined as individual mineral grains (clay to sand), rock clasts or aggregates suspended in ice, often associated with massive ice and ice-rich sediments (Murton and French, 1994). Lenticular (Le) is defined as a lens-shaped body of ice in sediment, often developed by ice-segregation within fine-grained sediments (Murton and French, 1994; Murton, 2013). Layered (La), or bedded, is defined as continuous layers of alternating ice and sediment, often developed by segregated or intrusive ice (French, 2007; French and Shur, 2010). Layered and Lenticular can have any thickness, length or orientation and may be parallel, wavy or non-parallel relative to other layered and lenticular cryostructures (Murton and French, 1994; Shur and Jorgenson, 1998). Irregular reticulate (Ri) is a three-dimensional non-oriented web-like structure composed of ice-rich veins encompassing a sediment block, often associated with silt-clay or diamict units (French and Shur, 2010). Organic-matrix (O) is an ice-rich structure controlled by organic fibers in soil/peat (Kanevskiy et al., 2013; Murton, 2013).

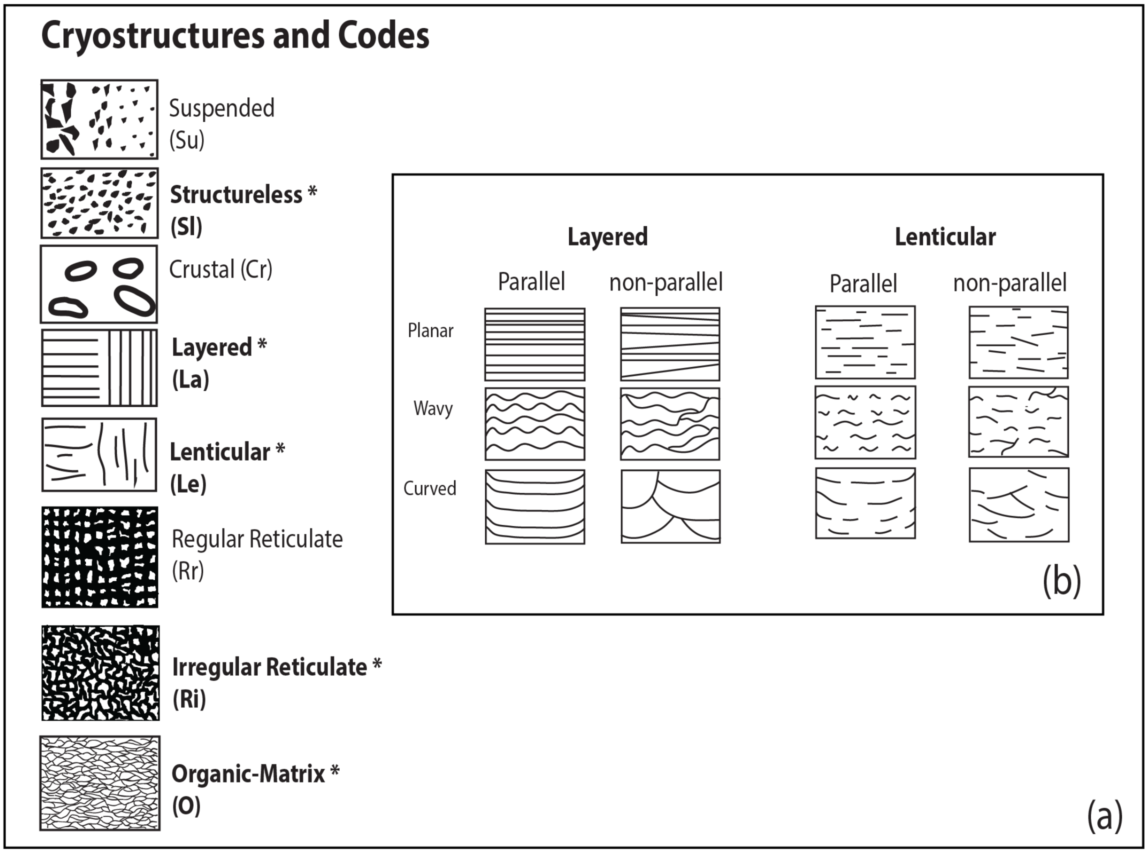

Figure 2.3: Modified classification of cryostructures

(a) Cryostructures and codes; Ice is shown in black and sediment in white. **(b)** Further classification for Lenticular and Layered cryostructures (modified from Murton and French, 1994).
Note: the dominant cryostructures in this study are bolded

Previous workers have shown that cryostructures may be strongly related to the freezing history of the permafrost, and the material hosting the ice. Certain types of cryostructures are formed due to the freezing history of permafrost, i.e., syngenetic or epigenetic permafrost , Table 2.2, (Mackay, 1974; Murton and French, 1994; Shur et al., 2004; Bray et al., 2006; French and Shur, 2010; French, 2011; Calmels et al., 2012; Murton, 2013). Syngenetic permafrost forms during cold-climate sedimentation, causing the base of the active layer to aggrade upwards; common cryostructures include organic-rich matrix, layered and lenticular (Figure 2.4a,c,d) (Shur and Jorgenson, 1998; French and Shur, 2010). Epigenetic permafrost forms after the deposition of host sediment resulting in downwards aggradation of permafrost; common cryostructure include reticulate and structureless (Figure 2.4b, e) (French and Shur, 2010).

Table 2.2: The formation of syngenetic and epigenetic permafrost; and associated cryostructures. Adapted from Shur and Jorgenson (1988).

Syngenetic Permafrost	**Epigenetic Permafrost**
Deposition during permafrost aggradation	Deposition in the absence of permafrost
Age of ice increases with depth	Age of ice increase with depth
Uncompacted Soil	Compacted Soil
Permafrost thickness is dependent on sediment accumulation rate	Permafrost thickness is dependent on ground temperature gradient
Permafrost aggrades upwards	Permafrost aggrades downwards
Common Cryostructures: Organic-rich matrix, Layered and Lenticular	**Common Cryostructures:** Reticulate and Structureless

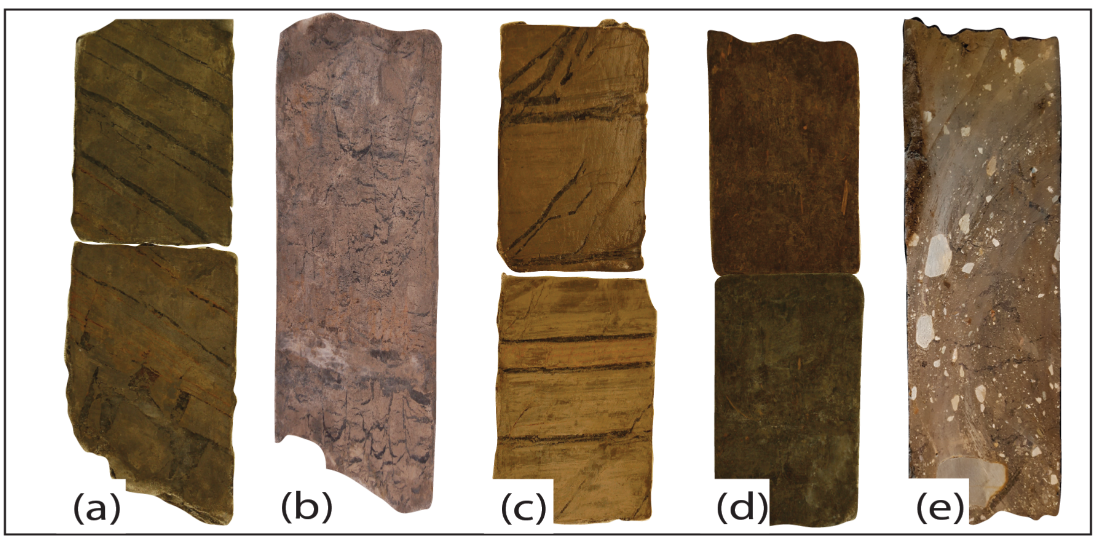

Figure 2.4: Core Segments with representative cryostructures
(a) BH-8 clay and silt unit with angled, planar layered cryostructures at a depth of 6.2m; (b) BH-4 clay and silt unit with irregular reticulate cryostructures at depth of 6.4m; (c) BH-8 clay and till unit with parallel and planar layered cryostructures and sub-vertical lenticular cryostructures at a depth of 9.3m; (d) peat unit with organic-matrix cryostructures; and (e) BH-1 ice-poor diamic unit with a structureless cryostructure at a depth of 10m.

Secondly, the properties of the hosting material also dictate the development of cryostructures. Fine-grained clay and silty sediments (i.e., frost-susceptible soils) tend to develop lenticular, layered, reticulate and structureless cryostructures (Murton and French, 1994; Murton, 2013). Contrary, coarse-grained sediments (sand, gravel, bedrock), and organic-rich soils tend to develop pore-ice and organic-matrix cryostructures (Murton and French, 1994; Kanevskiy et al., 2013; Murton, 2013). A summary of host material and associated cryostructures is shown in Table 2.3.

Table 2.3: Summary of cryostructures and most common host materials. Adapted from Murton (2013)

Cryostructure	**Common host material**
Structureless/Pore (Sl)	Coarse Sediments (Sand, Gravel, Bedrock)
Organic-matrix (O)	Organic-rich soils (ex. peatlands)
Lenticular (Le)	Fine-grained frost-susceptible soils (clay and silts)
Layered (La)	Fine-grained frost-susceptible soils (clay and silts)
Reticulate (R)	Silt-Clay mixtures, Diamicts (ex. Tills)
Suspended/Solid (Su)	Massive Ice, icy-sediments

2.4 Till and Diamict Classification:

Determining the origin of a diamict allows additional information to inform the types of ground ice. Further, it allows for improved prediction of ground ice across different geologic settings. This study focused on the differences between a (1) primary till, defined as material deposited by a uniquely glacial process; (2) secondary till, a primary till that has been subsequently mobilized by non-glacial processes; and (3) diamict, a non-glaciogenic, general term to describe poorly to non-sorted sediment containing a mix of clasts and fine-grained material (Evans et al., 2006; Benn and Evans, 2010). Primary till can be further subdivided into three endmembers, lodgement, deformation and melt-out till. Table 2.4 shows a summary of characteristics commonly used to discriminate between them. Lodgement till is defined as sediment deposited by plastering of glacial debris from a sliding glacier due to pressure melting and frictional drag (Evans et al., 2006). Deformation till is defined as sediment deposited and subsequently disintegrated or homogenized by subglacial shearing stresses (Benn and Evans, 2010). Lastly, melt-out till is defined as sediment deposited/released by the melting of stagnant or slowly moving debris-rich glacier ice and deposited without subsequent transportation or deformation (Evans et al., 2006).

Table 2.4: Summary of characteristic used to discriminate between the three primary till end-members.

Characteristics	**Lodgment Till**	**Deformation Till**	**Melt-Out Till**
Clast Shape	• Striated/Faceted Clast • Stoss/Less asymmetry	• Variable	• Variable
Texture	• Bimodal (Silt and Clasts)	• Variable • Can be very fine-grained	• Bimodal (Silt and Clasts)
Fabric	• Strong 'a-axis' fabric orientation is parallel to flow	• 'a-axis' fabric orientation is determined by shear stress.	• Variable
Structures	• Massive • 'Blocky' Appearance	• Variable • Folds/Boudinage • Other rotational indicators	• Variable

Subsampling:

All five boreholes were cut lengthwise using a rock saw with a diamond blade in the PACS lab core cutting at -5°C. These 2cm lengthwise core segments were then sub-sampled using a table saw with a diamond blade at 5cm intervals perpendicular to the lengthwise cut (parallel to stratigraphy). After that, these 2cm x 5cm x 5cm subsamples were bagged into Nasco Whirl-Pak bags and labelled with an index number, and their corresponding depths. The Nasco Whirl-Pak bags were used as they are sterile and provide an excellent seal when the subsamples are thawed out. Lastly, before any analysis, a dremmel was used to shave off ~2mm from the surface area of the subsamples to mitigate contamination.

2.5 Water Isotope Analysis

Stable water isotopes (oxygen and hydrogen) can be used as proxies for paleo-climate (Lacelle, 2011; Opel et al., 2011). Isotope fractionation, the change in the relative abundance of the isotopes, is controlled by the evaporation effect (kinetic fractionation) and Rayleigh fractionation (Dansgaard, 1964; Lacelle, 2011). The latter reflects the depletion of heavy isotopes (^{2}H and ^{18}O) due to a decrease in temperature and/or an increase in altitude and latitude as precipitation moves from coast to inland (Dansgaard, 1964). The stable water isotope analysis of ground ice within permafrost provides an isotopic composition of precipitation, which can be strongly correlated to temperature, providing a paleoclimate proxy. This paleoclimate proxy allows for distinguishing Pleistocene- and Holocene-aged bodies of ice.

Isotopes ratios are reported in δ-notation in parts per thousand (‰), as shown in equation 1

$$\delta = \left(\frac{R_{sample}}{R_{standard}} - 1\right) \times 1000\,‰ \qquad \textit{Eq.1}$$

Where R_{sample} is the molar ratio (^{1}H/^{2}H or ^{16}O/^{18}O) of a specific sample and $R_{standard}$ is the molar ratio of Vienna Standard Mean Ocean Water (VSMOW)

Following sampling, the frozen subsamples were stored in a fridge overnight at a temperature of 4°C to prepare for water isotope (δD/δ^{18}O) analysis. Thawing the subsamples in sealed bags in the refrigerator prevents isotope fractionation. Pore waters from the subsamples were extracted with a 3ml Sterile Slip Tip syringe and injected into 2ml vials through a 0.20μm syringe filter. Pore water extraction was done via two methods depending on the volume of pore water, and type of sediment hosting the water: (1) extracted directly from the Whirl-Pak bag, such as peats and coarse-grained sediments; or (2) after centrifuging for several minutes to separate the water from fine-grained sediments. All vials were stored in the refrigerator, without headspace, for subsequent water isotope analysis.

Water isotope analysis was performed on Picarro L2130-*i* Analyzer to obtain δ^{18}O and δD, with Trajon SGEµL syringe. Oxygen and hydrogen values are in reference to Vienna Standard Mean Ocean Water (VSMOW). Two water reference standards, USGS 45 (δ^{18}O = -2.2‰ , δD = -10.3‰) and USGS 46 (δ^{18}O = -29.8‰ , δD = -235.8‰) were used, and an internal reference water (QCDI), was used to track analytical precision and accuracy. We estimate the analytical accuracy of the Picarro analyzer is ±0.5‰ and ±0.1‰ for δD and δ^{18}O, respectively, based on repeat analysis of the QCDI internal water standard.

Table 2.5: Water references used in this study.

Standards	**δD VSMOW (‰)**	**δ^{18}O VSMOW (‰)**	**Reference**
USGS 45	-10.3	-2.2	U.S Geological Survey, 2014a
USGS 46	-235.8	-29.8	U.S Geological Survey, 2014b
QCDI	-148.9	-19.08	Pumpel, 2016

Water isotopes are commonly used as a paleoclimatic indicator via co-isotopes plots and deuterium excess. A co-isotope plot (δD as a function of δ^{18}O) is used to provide insights into the genesis of permafrost during deposition (Lacelle, 2011). Co-isotopes calculate the regression slope ($S_{D\text{-}18O}$) between δD and δ^{18}O relative to the local meteoric water line (LMWL) and global meteoric water line (GMWL), shown in equations 2 and 3, respectively (Lacelle, 2011). Thawing and freezing of pore ice within the stratigraphic deposits causes deviations from the LMWL slope.

These changes can be diagnostic to determine their depositional environment (Lacelle et al., 2004). The LMWL was calculated using data from the Global Network of Isotopes in Precipitation (GNIP).

$$\boldsymbol{LMWL}: \qquad \delta D = 7.16 * \delta^{18}O - 5.6 \qquad \textit{Eq.2.}$$

$$\boldsymbol{GMWL}: \qquad \delta D = 8 * \delta^{18}O + 10 \qquad \textit{Eq.3.} \text{ (Craig, 1961)}$$

In general, co-isotope slopes can suggest different origins of the ice (water). Co-isotope slopes greater than the LMWL (~7) are typically associated with freezing of water from atmospheric sources; co-isotope slopes less than 7 suggests evaporative enrichment (Lacelle, 2002; Lacelle et al., 2004, Fritz et al., 2022).

The intercept value for the GMWL (+10‰) is defined as deuterium excess (d-excess) on a global scale influenced by kinetic evaporation. D-excess is a climate proxy used to indicate non-equilibrium effects such as evaporation, and relative humidity evaporation (at a constant moisture level) for depositional environments with simple topography far enough from ocean-atmosphere influences (Dansgaard, 1964; Lacelle, 2011; Porter et al., 2016). D-excess (*d*) can be calculated for any sample using equation 4.

$$d = \delta D - 8\delta^{18}O \qquad \textit{Eq.4.} \text{ (Dangaard, 1964)}$$

2.6 Radiocarbon Dating

To understand the chronology of the deposited units within the boreholes, this study used five radiocarbon dates (^{14}C yrs BP) located within peatlands along the ITH. These organic samples were obtained from BH-1, BH-4, and BH-8. Two radiocarbon dates were obtained for BH-1. The uppermost radiocarbon sample (BH1-60) at a depth of 2.1m was selected in the peat unit above the massive-ice unit; the lowermost sample (BH1-141) at a depth of 7.0 m was selected near the contact between the massive ice and ice-poor diamict units. A single radiocarbon sample was obtained for BH-4; the sample (BH4-92) was obtained in the fine-grained unit at a depth of 4.6 m. Two radiocarbon samples were obtained for BH-8. The uppermost sample (BH8-75) was selected at a depth of 4.1m, near the peat and fine-grained contact; the second sample (BH8-11.3) was selected near the base of the core at a depth of 11.3 m.

The five organic samples required an acid-base-acid (ABA) pre-treatment wash for 14C dating to remove any contamination. ABA consisted of a 3-step process: (1) samples were heated to 70°C and washed in 1M HCl for 30 minutes; (2) washed in 1M NaOH for 60 minutes; and (3) washed in1M HCl for 30 minutes. Samples were subsequently rinsed with ultrapure water until neutral and freeze-dried. Prepared samples were shipped to the A.E Lalonde AMS Laboratory, University of Ottawa. Calibration – in the University of Ottawa – was performed using OxCal v4.2.4 (Bronk Ramsey, 2009) and IntCal13/Bomb 13 calibration. Samples were analyzed with two, well dated internal standards, FIRI-F and AVR07-PAL, for age, analytical precision and accuracy (Table 2.6).

Table 2.6: Radiocarbon standards used in this study

Standards	**Age (^{14}C yr BP)**	**Material**	**Reference**
FIRI-F	4,510	Wood shavings	Boaretto et al., 2002
AVR07-PAL	Non-finite, last interglacial	Wood shavings	Reyes et al., 2010, Martinez et al., 2020

2.7 Ground Ice Discriminating Tools:

Ground ice within permafrost provides a paleoenvironmental proxy indicative of past processes at the time of its formation (Lacelle, 2011). Discriminating between different types of ground ice is fundamental to increase our understanding of climate change and future thermokarst in northern Canada and develop a set of tools that can be used in other regions to evaluate future thaw trajectories for northern landscapes. A summary of ground ice discriminating tools is shown in Table 2.7.

This study used four different tools used to discriminate different types of large ground ice bodies. (1) Stratigraphy can be used to provide a context for ground ice in relation to adjacent units. For example, buried glacier ice is likely to be covered by till during incomplete deglaciation; therefore, the overlying upper contact of buried glacier ice is most likely a diamicton (Mackay, 1989). Additionally, the nature of contacts with enclosing sediments provides context into the the type of ground ice. For example, intrusive ice typically has sharp contacts with enclosing sediments (Mackay, 1989). (2) Structures, such as deformations, foliations, and banded appearance within large ice bodies can be discriminating tools. For example, glacial deformations can be associated with buried glacier ice, while vertical foliations are diagnostic of wedge ice. (3) Stable water isotopes (δ^{18}O and δD), preserved in permafrost, cab be a proxy which aids to distinguish Pleistocene- and Holocene-aged bodies of ice. Lastly, (4) δ^{18}O - δD regression slope analysis, is a tool use to interpret a ground ice genesis between atmospheric sources (a slope like the LMWL) or groundwater (a slope lower than the LMWL).

Types of Ground Ice	Ground Ice Discriminating Tools			
	Stratigraphy	**Structures**	**Oxygen ($\delta^{18}O$) Isotopes**	**δD-$\delta^{18}O$ regression slope**
Pore Ice	Found within frozen ground.	None. Infill of pore space with water.	Holocene ice: -15 to -25‰ Or Pleistocene ice: ~ -33 to -30‰	Slope may or may not be similar to LWML
Buried Glacier Ice	Typically found within primary till.	Foliations and glacial deformations development during ice movement	Pleistocene ice: ~ -33 to -30‰	Slope may or may not be similar to LWML
Buried Surface Ice	Upper and lower contacts do not provide context	May be subjected to glacial deformation, but Holocene ice should not have prominent deformations. Typically forms a tabular appearance.	Holocene ice: -15 to -25‰ Or Pleistocene ice: ~ -33 to -30‰	Regression slope will plot similar to LMWL (slope ~7)
Wedge Ice	Upper and lower contacts do not provide context	Vertical Foliations	Holocene ice: -15 to -25‰ Or Pleistocene ice: ~ -33 to -30‰	Regression slope will plot similar to LMWL (slope ~7)
Segregated Ice	Upper and lower contacts do not provide context	May be subjected to glacial deformation, but Holocene ice should not have prominent deformations	Holocene ice: -15 to -25‰ Or Pleistocene ice: ~ -33 to -30‰	Slope may or may not be similar to LWML

Injection Ice	Upper and lower contacts do not provide context. Typically, will have sharp contact with enclosing material.	May be subjected to glacial deformation, but Holocene ice should not have prominent deformations. May have a tabular or massive appearance.	Holocene ice: -15 to -25‰ Or Pleistocene ice: ~ -33 to -30‰	Slope may or may not be similar to LWML
Segregate - Intrusive Ice	Upper contact may or may not be glacial till, underlying unit should be coarse-grained (sand)	Upper contact may or may not be glacial till, underlying unit should be coarse-grained (sand). Typically has a banded appearance.	Depleted Values: ~ -33 to -30‰	Regression slope will plot on a much lower regression slope

Table 2.7: Summary of the tools used in this study to determine the origin on massive ice bodies underlying permafrost within the Mackenzie Delta region, the Tuktoyaktuk Coastlands, and other similar Arctic Settings.

References:

Bandara, S., 2017, Records of atmospheric mercury deposition and post-depositional mobility in peat permafrost archives from central and northern Yukon, Canada: 119 p., https://doi.org/10.7939/R3KD1R04P.

Benn, D.I., and Evans, D.J.A., 2010, Glaciers and Glaciation, 2nd edition: Hodder Arnold Publication, 816 p., doi:https://doi.org/10.4324/9780203785010.

Boaretto, E. et al., 2002, Summary findings of the fourth international radiocarbon intercomparison (FIRI)(1998–2001): Journal of Quaternary Science, v. 17, p. 633–637, doi:10.1002/JQS.702.

Bray, M.T., French, H.M., and Shur, Y., 2006, Further cryostratigraphic observations in the CRREL permafrost tunnel, Fox, Alaska: Permafrost and Periglacial Processes, v. 17, p. 233–243, doi:10.1002/ppp.558.

Bronk Ramsey, C., 2009, Bayesian Analysis of Radiocarbon Dates: Radiocarbon, v. 51, p. 337–360, doi:10.1017/s0033822200033865.

Calmels, F., Froese, D.G., and Clavano, W.R., 2012, Cryostratigraphic record of permafrost degradation and recovery following historic (1898-1992) surface disturbances in the klondike region, central yukon territory 1,2: Canadian Journal of Earth Sciences, v. 49, p. 938–952, doi:10.1139/E2012-023.

Craig, H., 1961, Standard for reporting concentrations of deuterium and oxygen-18 in natural waters: Science, v. 133, p. 1833–1834, doi:10.1126/science.133.3467.1833.

Dansgaard, W., 1964, Stable isotopes in precipitation: Tellus, v. 16, p. 436–468, doi:10.3402/tellusa.v16i4.8993.

E.L, H., 1970, SOUND VELOCITY AND RELATED PROPERTIES OF MARINE SEDIMENTS, NORTH PACIFIC: J Geophys Res, v. 75, p. 4423–4446, doi:10.1029/jb075i023p04423.

Ensom, T., Morse, P.D., Kokelj, S. V, Macdonald, E., Young, J., Tank, S., Grozic, E., and Castagner, A., 2020, Permafrost geotechnical borehole data synthesis: 2013–2017 Inuvik-Tuktoyaktuk region, Northwest Territories; Northwest Territories Geological Survey, NWT Open Report 2019-012; Geological Survey of Canada, Open File 8652.:

Evans, D.J.A., Phillips, E.R., Hiemstra, J.F., and Auton, C.A., 2006, Subglacial till: Formation, sedimentary characteristics and classification: Earth-Science Reviews, v. 78, p. 115–176, doi:10.1016/j.earscirev.2006.04.001.

French, H., 2011, Frozen sediments and previously-frozen sediments: Geological Society Special Publication, v. 354, p. 153–166, doi:10.1144/SP354.9.

French, H., 2007, The Periglacial Environment, 3rd edn: Wiley, Chichester, 458 p.

French, H., and Shur, Y., 2010, The principles of cryostratigraphy: Earth-Science Reviews, v. 101, p. 190–206, doi:10.1016/j.earscirev.2010.04.002.

Geotek, 2008, Multi-Sensor Core Logger Manual:, www.geotek.co.uk (accessed May 2021).

Gilbert, G.L., Kanevskiy, M., and Murton, J.B., 2016, Recent Advances (2008–2015) in the Study of Ground Ice and Cryostratigraphy, *in* Permafrost and Periglacial Processes, v. 27, p. 377–389, doi:10.1002/ppp.1912.

Kanevskiy, M., Shur, Y., Jorgenson, M.T., Ping, C.L., Michaelson, G.J., Fortier, D., Stephani, E., Dillon, M., and Tumskoy, V., 2013, Ground ice in the upper permafrost of the Beaufort Sea coast of Alaska: Cold Regions Science and Technology, v. 85, p. 56–70, doi:10.1016/j.coldregions.2012.08.002.

Lacelle, D., 2002, Ground ice investigation in the far northwest of Canada: , p. 101.
Lacelle, D., 2011, On the δ18O, δD and D-excess relations in meteoric precipitation and during equilibrium freezing: Theoretical approach and field examples: Permafrost and Periglacial Processes, v. 22, p. 13–25, doi:10.1002/ppp.712.
Lacelle, D., Bjornson, J., Lauriol, B., Clark, I.D., and Troutet, Y., 2004, Segregated-intrusive ice of subglacial meltwater origin in retrogressive thaw flow headwalls, Richardson Mountains, NWT, Canada: Quaternary Science Reviews, v. 23, p. 681–696, doi:10.1016/j.quascirev.2003.09.005.
Mackay, J.R., 1989, Massive ice: some field criteria for the identification of ice types: Current Research, Part G, Geological Survey of Canada, Paper, p. 5–11.
Murton, J.B., 2013, Ground Ice and Cryostratigraphy, *in* Treatise on Geomorphology, v. 8, p. 173–201, doi:10.1016/B978-0-12-374739-6.00206-2.
Murton, J.B., and French, H.M., 1994, Cryostructures in permafrost, Tuktoyaktuk coastlands, western Arctic Canada: Canadian Journal of Earth Sciences, v. 31, p. 737–747, doi:10.1139/e94-067.
Murton, J.B., Whiteman, C.A., Waller, R.I., Pollard, W.H., Clark, I.D., and Dallimore, S.R., 2005, Basal ice facies and supraglacial melt-out till of the Laurentide Ice Sheet, Tuktoyaktuk Coastlands, western Arctic Canada: Quaternary Science Reviews, v. 24, p. 681–708, doi:10.1016/j.quascirev.2004.06.008.
Opel, T., Dereviagin, A.Y., Meyer, H., Schirrmeister, L., and Wetterich, S., 2011, Palaeoclimatic information from stable water isotopes of Holocene ice wedges on the Dmitrii Laptev Strait, northeast Siberia, Russia: Permafrost and Periglacial Processes, v. 22, p. 84–100, doi:10.1002/ppp.667.
Pumple, J., Monteath, A., Harvey, J., Alvarez, A., Moustaei, M., Froese., D. Non-destructive permafrost core characterization using multi-sensor core logging. In preperation. 2022
Rampton, V.N.; Mackay, J.R., 1971, Massive ice and icy sediments throughout the Tuktoyaktuk Peninsula, Richards Island, and nearby areas, district of Mackenzie: Geol Surv Can, Pap 71-21,.
Rampton, V.N., 1988, Quaternary Geology of the Tuktoyaktuk Coastlands, Northwest Territories: Geological Survey of Canada, p. 1–107, doi:10.1126/science.ns-6.149S.521-a.
Reyes, A. V., Froese, D.G., and Jensen, B.J.L., 2010, Permafrost response to last interglacial warming: Field evidence from non-glaciated Yukon and Alaska: Quaternary Science Reviews, v. 29, p. 3256–3274, doi:10.1016/j.quascirev.2010.07.013.
Ross Mackay, J., 1974, RETICULATE ICE VEINS IN PERMAFROST, NORTHERN CANADA.: Canadian Geotechnical Journal, v. 11, p. 230–237, doi:10.1139/t74-019.
Shur, Y., French, H.M., Bray, M.T., and Anderson, D.A., 2004, Syngenetic permafrost growth: Cryostratigraphic observations from the CRREL tunnel near Fairbanks, Alaska: Permafrost and Periglacial Processes, v. 15, p. 339–347, doi:10.1002/ppp.486.
Shur, Y., and Jorgenson, M., 1998, Cryostructure development on the floodplain of the Colville River Delta, northern Alaska: Permafrost, Seventh International Conference, p. 993–999, http://www.arlis.org/docs/vol1/ICOP/40770716/CD-ROM/Proceedings/PDF001189/150193.pdf.

Chapter 3: A review of ground ice types with examples from Mackenzie Delta Region, Klondike, and central Mackenzie Valley.

3.1 Introduction

Ground ice is a generic term used to designate all forms of ice found within permafrost regardless of form or genesis. Ground ice plays an important role in landscape modification, resulting in either landform formation (e.g., pingos, palsas, and peat plateaus) or landform degradation (thermokarst). The amount and form of ground ice are dictated by the nature of permafrost (epigenetic or syngenetic), type of host sediments, glacial and paleoenvironmental history, source of moisture, and freezing mechanism (thermal, hydrological, or burial conditions) (Mackay, 1972; French, 2007; Wolfe, 2017). Ground ice, and its thaw potential, have encouraged the characterization, classification, and discrimination of different ground ice forms to understand foreseeable impacts on permafrost landscapes. In this chapter, I provide a review of ground ice forms typically found within the Mackenzie Delta regions

3.2 Ground Ice Definitions:

Pore ice – ice occurring in the pores of soils and rocks and does not yield excess water upon thaw (ACGR, 1988).

Excess ice – refers to the volume of ice exceeding the total pore space of the host sediments (ACGR, 1988). Excess-ice is sometimes used synonymously with volumetric ice content. The distinction between pore ice and excess ice is related to the water content of the soil. French (2007) suggests the best way to distinguish between excess and pore ice is to thaw the soil and note the presence or absence of supernatant water. If supernatant water is present (i.e., water visible after thawing a sample), it indicates the frozen sample had excess ice. Likewise, an absence of supernatant water after thawing suggests primarily pore ice is present.

Ice-rich permafrost – refers to permafrost containing excess ice. It's a qualitative term describing permafrost's thaw sensitivity (ACGR, 1988). Although this term is mainly used loosely to describe permafrost with excess ice, others, have defined ice-rich permafrost as permafrost with >20% excess ice content (Grosse et al., 2011).

Icy-sediments – sediments which contain excess ice in the form of multiple lenses. Rampton and Mackay,(1971), define this as gravimetric ice content up to 250%.

Massive ice (massive icy bodies) – are large ice bodies, several meters thick, with a gravimetric ice content exceeding 250% (Mackay, 1971). Likewise, other workers have used tabular massive ground ice to describe these large ice bodies.

Massive Ice and Icy Sediments (MI-IS) – is a combination of the two former terms, massive ice and icy sediments. This term is commonly used when the distinction between massive ice and icy-sediments is not possible due to (1) complex stratigraphic sequences with variable ice content, or (2) when the ice content is unknown (Murton et al., 2005).

Although most ground ice definitions are adequate, the term 'Massive Ice' originally defined by Mackay (1971) is problematic. In Mackay's (1971; 1972, and 1989) usage, massive ice describes all large ice bodies, including bedded, foliated, tabular and deformed ice bodies. However, the term 'massive' in a geologic context refers to a rock or sedimentary units with a homogenous texture and lacking structures (Neuendorf et al., 2011). Meanwhile, 'tabular' is defined as a plane where two dimensions are longer than the third or a flat (table-like) rectangular form (Neuendorf et al., 2011). By these geological definitions, the use of massive and tabular to represent all forms of ground ice bodies is problematic since defining textures, and structural properties which aid genetic interpretation may be lost. A foliated ice-wedge, or a deformed buried glacier body, should not be described as massive ice since they may retain structures which aid in the interpretation of the ice body origin. In contrast, a large, segregated ice lens without structure, or aufeis with sheet-like structures, should be referred to as large bodies of ice with a massive appearance, and tabular structure, respectively.

In this chapter, I will use the term ground ice bodies, instead of massive ice, to describe numerous ground ice forms encountered amidst fieldwork opportunities across the Mackenzie Delta Region, the Klondike and central Mackenzie valley (Figure 3.1)

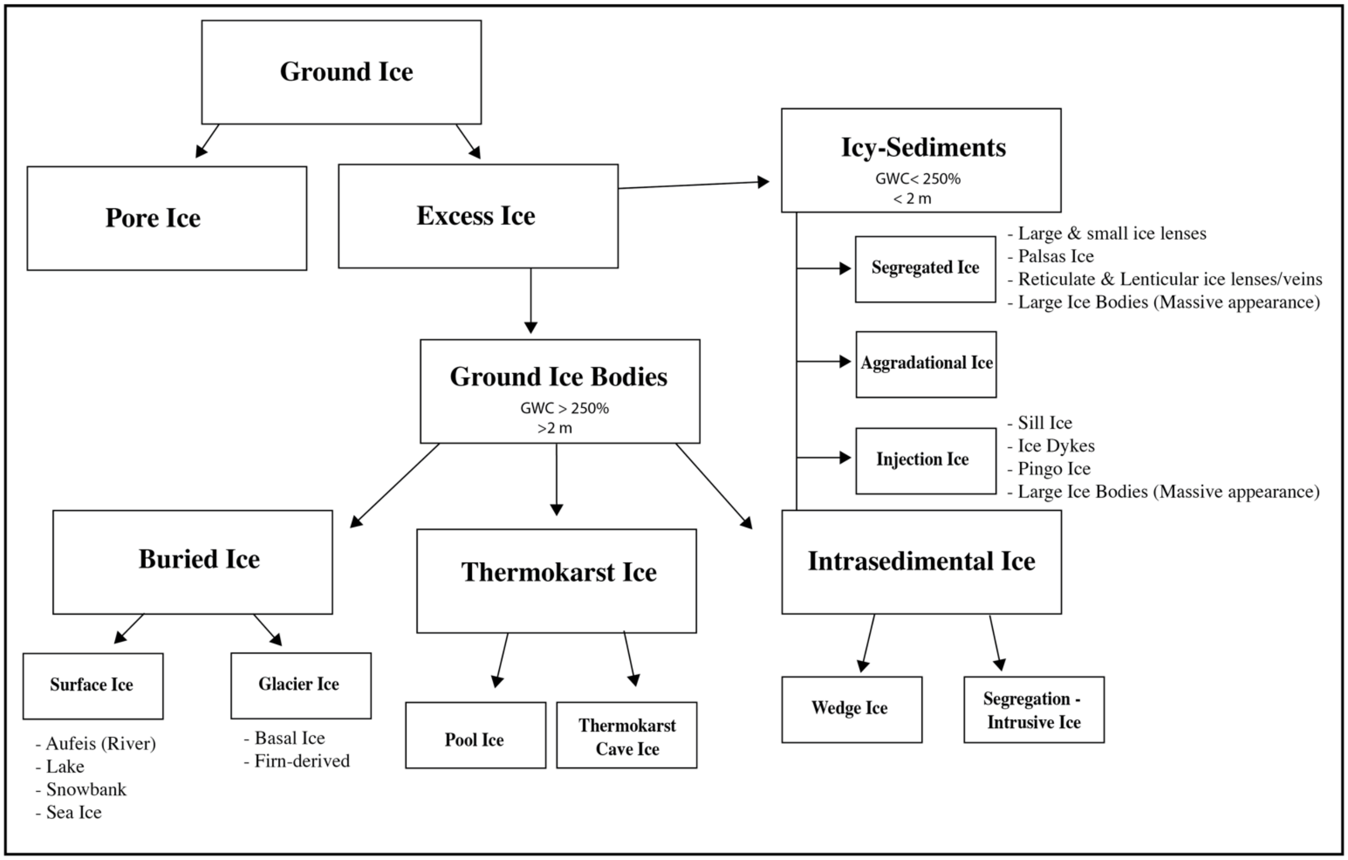

Figure 3.1: General classification of ground ice commonly found in ice-rich permafrost settings. Ground ice bodies is used instead of massive ice to describe large ground ice bodies. Adapted from French (2007)

3.3 Ground Ice Characterization and Classifications

Ground ice found within sediments can be described, characterized, and classified in many ways. Ground ice can be characterized by either ground ice content or the nature of permafrost. These ground ice characterizations coupled with diagnostic tools, including stratigraphy (Mackay, 1989; Murton et al., 2005), geochemistry (Lacelle et al., 2004; Cardyn et al., 2007; Lacelle and Vasil'chuk, 2013), cryostratigraphy (Murton and French, 1994; Shur and Jorgenson, 1998), and petrography (Pollard, 1990; Coulombe et al., 2019) has been fundamental in the characterization of ground ice bodies and the subsequent progress in its classification. Ground ice is classified into two main systems, genetic and non-genetic. The former are classifications that use diagnostic tools to identify an ice form and derive a potential genesis, while the latter provide descriptive and visual classifications that are not used for interpretation.

3.3.1 Ice Content Characterization:

Ground ice content is the amount of ice hosted within frozen sediment or rock. It is typically reported as gravimetric (dry-weight basis), volumetric (volume basis), or excess ice content.

Gravimetric water content (GWC) is the ratio between the mass of the frozen sample to the dry mass of the sample [1] (Van Everdingen, 1998). Volumetric ice content (VIC) is the ratio between the volume of the frozen sample to the volume of the whole sample [2] (Van Everdingen, 1998). Excess ice content (EIC) is the volume of ground ice which exceeds the pore scape (i.e., excess ice) to the volume of the whole sample [4,5,6].(Van Everdingen, 1998; Kokelj and Burn, 2003)

$$GWC\ (\%) = \frac{mass\ most\ soil\ (g)}{mass\ of\ dry\ soil\ (g)} \times\ 100 \qquad [1]\ (\text{Van Everdingen}, 1998)$$

$$VIC\ (\%) = \frac{Volume\ most\ soil\ (cm^3)}{Volume\ of\ dry\ soil\ (cm^3)} \times\ 100 \qquad [2]\ (\text{Van Everdingen}, 1998)$$

$$VIC\ (\%) = \frac{GWC\ \times\ (G_s/0.9)}{1 + (GWC\ \times\ (G_s/0.9))} \times\ 100 \qquad mmm \qquad [3]\ (\text{Shur et al.}, 2021)$$

Where G_s is the specific gravity of soils, which varies between 0.7 (organics) and 2.9 (mineral soils)

$$EIC\ (\%) = \frac{Volume\ of\ Standing\ Water\ \ (cm^3)}{Total\ Volume\ of\ sample\ (cm^3)} \times\ 100 \qquad [4]\ (\text{Murton}, 2013)$$

$$EIC\ (\%) = \frac{V_w\ \times\ 1.09}{S_v\ \times\ (W_v\ \times\ 1.09)} \times 100 \qquad [5]\ (\text{Kokelj and Burn}, 2003)$$

Where W_v is the supernatant (standing) water volume, S_v is the saturated soil volume.

$$EIC\ (\%) = \frac{V_w\ \times\ 1.09}{V_{Ti}/VWC} \times 100 \qquad [6]\ (\text{Shur et al.}, 2021)$$

Where W_v is the supernatant water volume (W_v * 1.09 = excess ice volume), and V_{Ti} is the total ice volume.

3.3.2 Ground Ice Non-genetic Classifications

Pihlainen and Johnston (1963) developed a non-genetic classification based on visible ground ice conditions (Figure 3.2). This classification is purely descriptive, with no indication of genesis or identifying ground ice forms. Three main categories established are 'ice not visible' (i.e., pore ice), 'visible ice – less than 1 inch thick', and 'visible ice – greater than 1 inch thick'.

A. ICE NOT VISIBLE

Group symbol	Subgroup	
	Description	**Symbol**
N	Poorly bonded or friable	Nf
	No excess ice	Nbn
	Well-bonded	Nb
	Excess ice	Nbe

B. VISIBLE ICE – LESS THAN 1 INCH THICK

Group symbol	Subgroup	
	Description	**Symbol**
	Individual ice crystals or inclusions	Vx
	Ice coatings on particles	Vc
	Randomly or irregularly-oriented ice formations	Vr
	Stratified or distinctly-oriented ice formations	Vs

C. VISIBLE ICE – GREATER THAN 1 INCH THICK

Group symbol	Subgroup	
	Description	**Symbol**
ICE	Ice with soil inclusions	ICE + soil type
	Ice without soil inclusions	ICE

Figure 3.2: Non-genetic (visible) ground ice classification proposed by Pihlainen and Johnston (1963), reproduced in French (2007).

Murton and French (1994) developed a non-genetic ground ice classification based on cryostructures, i.e., the distinct sedimentary ice structures found within permafrost. This will be further discussed in section 3.4. Pihlainen and Johnston (1963) and Murton and French (1994) ground ice classifications provide excellent descriptions of ice-poor sediments. They, however, do not provide context to identify or interpret the genesis of ground ice bodies. In Pihlainen and Johnston's (1963), the 'visible ice that greater than 1 inch thick' and Murton and French's (1994) 'suspended cryostructure' categories embody all large ground ice bodies found in permafrost.

3.3.3. Ground Ice Genetic Classifications

One of the earliest attempts to genetically classify ground ice was from the Russian literature (Shumskii, 1964). This classification was one of the first attempts to classify ground ice bodies based on ice formation, unlike previous Russian classifications which focused on nature of permafrost (epigenetic vs syngenetic), visible ice content, or by age (relict vs contemporaneous ice). Shumskii (1964) developed a classification of three distinctly different ice types, with 11 diverse ice sub-types. (1) Constitute ice, developed from the freezing of most soil; (2) cave-vein ice, formed by the infilling of cavities in frozen soil; and (3) buried ice, formed by the surface burial (Figure 3.3).

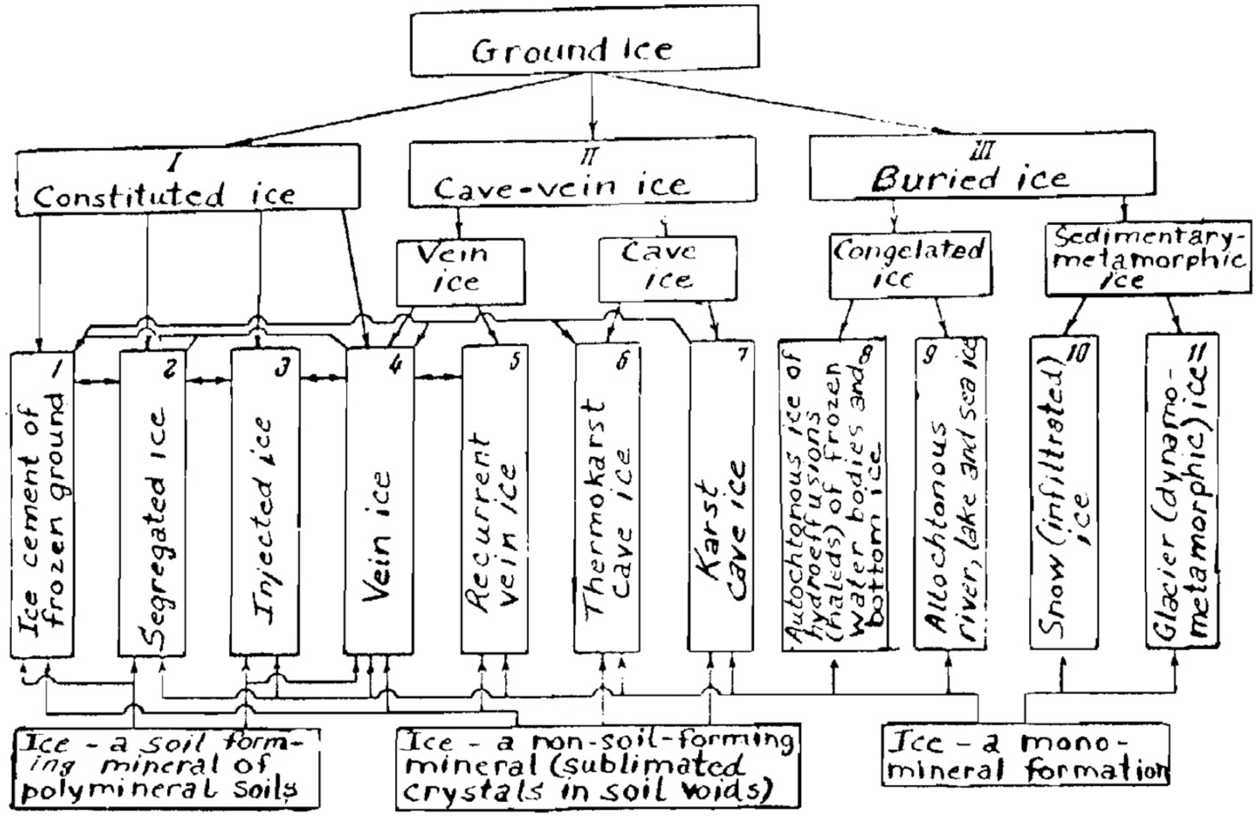

Figure 3.3: Genetic classification of ground ice based upon water freezing process of burial of ice proposed by Shumskii (1964).

One of the earliest North American genetic ground ice classifications was developed by Mackay (1972). Mackay (1972) defined four different ice types, with seven different sub-types based upon the water source and the principal mechanism for water transfer to the freezing plane. The advantage of this classification is that it illustrates the complexities of the water source and transfer mechanism. This classification does not include buried surface ice (e.g., buried glacier ice). However, Murton (2013) adapted this classification to include buried surface ice, but his adaptation coupled aggradational and segregated ice into the same ice form (Fig 3.4). Pollard (1990) proposed a genetic ground ice classification of five ground ice bodies forms based on the water transfer process, while providing petrographic context (i.e., appearance, texture, and fabric characteristics) (Figure 3.5). French (2007) developed a simpler ground ice body classification based on intrasedimental and buried ice, similar to Figure 3.1. Vasilchuk (2012) developed a classification highlighting the complexities of having mutltiple ground ice forms within a startigraphic section. Vasilchuk (2012) suggested two main categories, homogeneous tabular massive ice, which are ice bodies whose genesis and properties are uniform, and heterogenous tabular massive ice, which are bodies whose genesis and properties vary or multiple homogeneous forms in one section. Wolfe (2017) proposed a classification of three main ice types based on the timing of ice genesis relative to the nature of permafrost. Type 1 is formational ice, which forms as permafrost aggrades, including pore and segregated ice. Type 2 is post-formational ice, which forms once permafrost is present, including wedge ice, aggradational ice, and pool ice. Type 3 is relict ice, ice old ice that has been subsequently covered by sediments, including buried ice, along with older ice forms, such as wedge ice and injection ice (Figure 3.6)

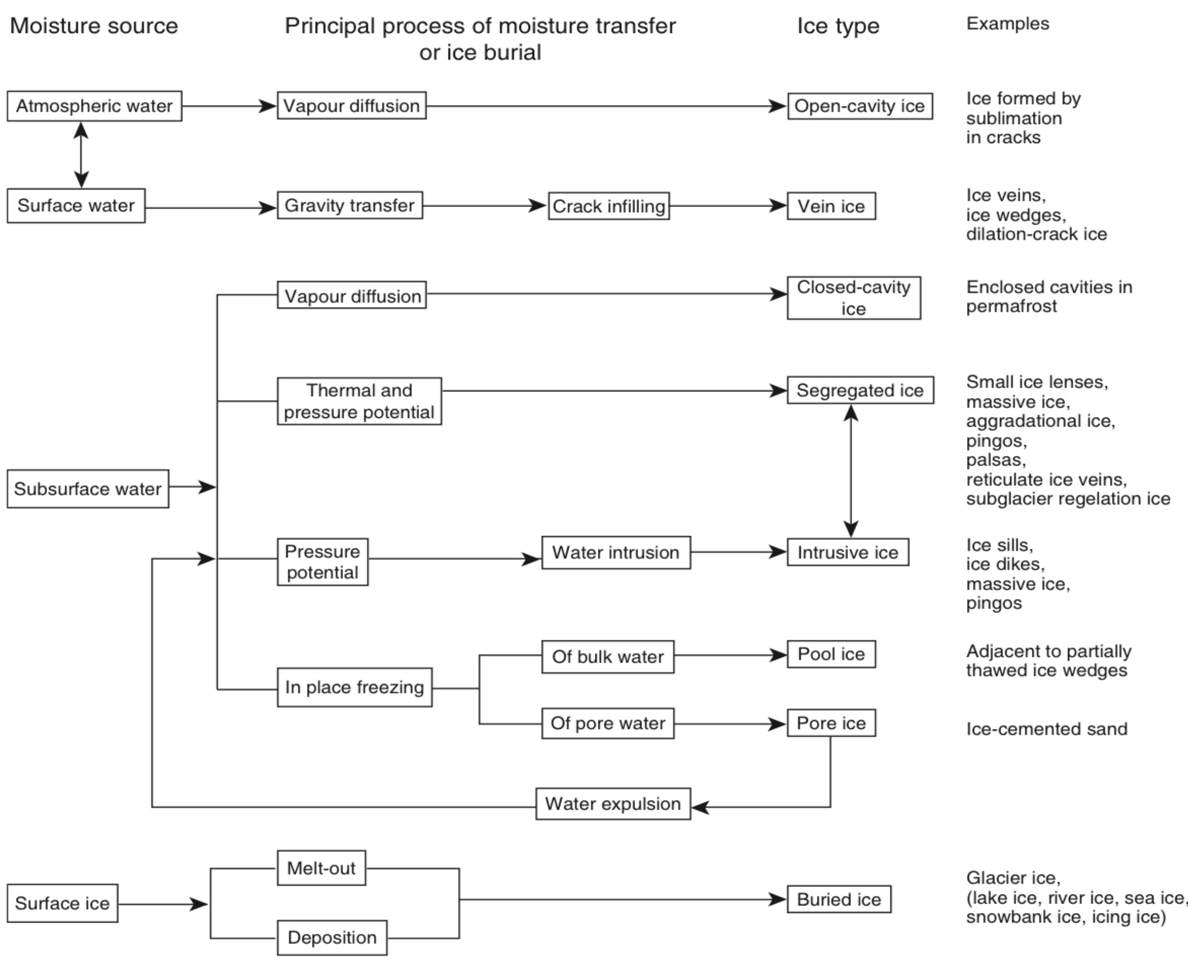

Figure 3.4: Genetic classification of ground ice characterized by water source and the principal transfer process adapted from Mackay (1972) to include buried ice from Murton (2013)

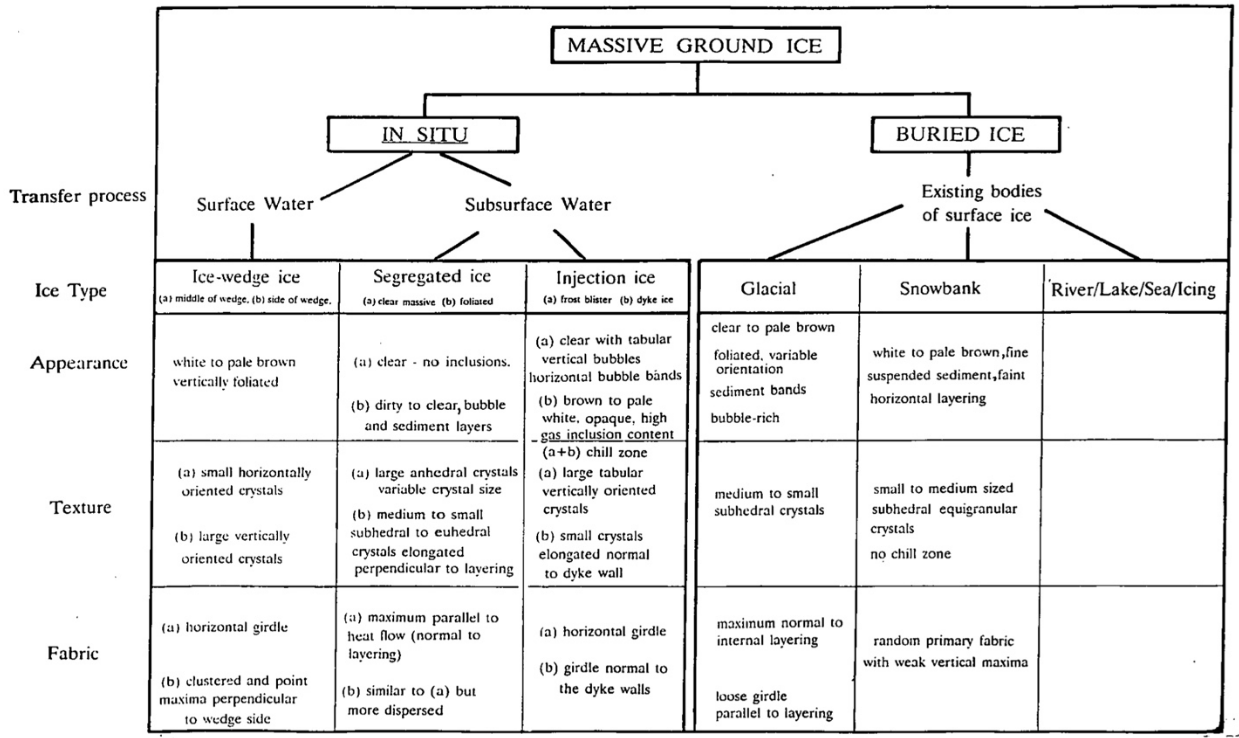

Figure 3.5: Genetic classification of ground ice characterized by petrographic properties proposed by Pollard (1990)

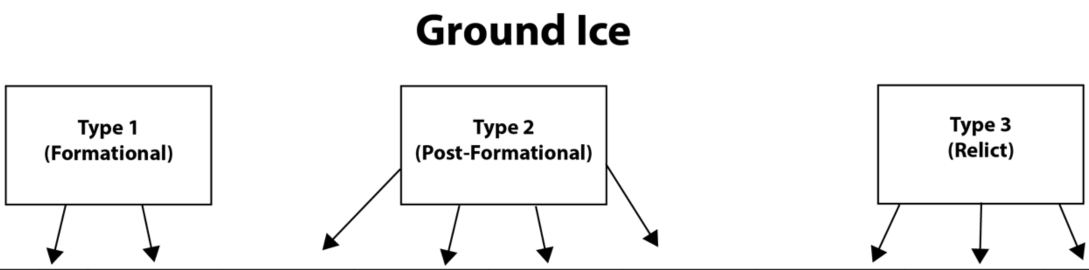

	Ice Type	Pore Ice	Segregated Ice	Aggradational Ice	Wedge Ice	Pool Ice	Injection Ice	Buried Surface Ice	Buried Glacier Ice	Relict Wedge Ice/ injection ice/ segregated ice
Excess Ice potential within terrain units and sediments	**Low**	-	- Outwash deposits - Eolian sands - Bedrock	- Bedrock - thin sediment veneers	- Bedrock - thin sediment veneers	- Bedrock - thin sediment veneers	- Bedrock - thin sediment veneers	- Marine deposits - Glaciolacustrine - Lacustrine	- Marine deposits - Glaciolacustrine - Lacustrine	- Marine deposits - Glaciolacustrine - Lacustrine
	Moderate	-	- Till deposits - Nearshore marine - Lacustrine - Organic - Colluvium - Weather Regolith						- Till blankets - Glaciofluvial outwash - Colluvium	
	High	-	- Lacustrine - Glaciolacustrine - Marine	Near-surface permafrost deposits: - Tills - Lacustrine - Glaciolacustrine - Glaciofluvial - Fluvial - Marine - Colluvial	Wide range of deposits: - Tills - Lacustrine - Glaciolacustrine - Glaciofluvial - Fluvial - Colluvial - Organic deposits	Adjacent to wedge ice.	Wide range of deposits: - Tills - Lacustrine - Glaciolacustrine - Glaciofluvial - Fluvial - Marine - Colluvial - Organic	- Colluvial deposits - Loess sediments - Tephra deposits	- Hummocky till - Moraine deposits	- wide spread of deposits: - Loess sediments - Colluvial deposits

Figure 3.6: Genetic classification of ground ice characterized by their timing of formation relative to that of permafrost and associated excess-ice potential. Figure created from Wolfe (2017) descriptions.

Collectively, these classifications present a challenge. Non-genetic classifications provide little to no indication of ice formation. This may hinder the extent and amount of ground ice, providing little knowledge in predicting ground ice and modelling contexts. In contrast, classifications based on genesis can be problematic, given similar ground ice forms may have multiple origins. As shown in Figure 3.1, some ground ice forms may develop as a ground ice body (>2 m) or as thin lenses within icy sediments. Moreover, classifications based on gravimetric water content may be challenging, especially when dealing with frozen peat. Frozen peat, on account of a density like ice, can have exceptionally high gravimetric water contents ranging between 200 – 2000%, which would classify it under some classifications as a ground ice body. Although these ground ice classifications are not perfect, the overall characterization, classification and discrimination of ground ice coupled with geologic history is useful for predictions of excess-ice hosting sediments.

3.4 Cryostratigraphy, Cryostructures, Cryotextures and Cryofacies:

Cryostratigraphy is the study of frozen layers in the Earth's crust (French and Shur, 2010). Cryostratigraphy is a branch of geocryology. The latter refers to the study of frozen materials (temperature lower than 0°C). Geocryology includes the study of glaciers, and seasonal frost, although it is usually applied to permafrost (ACGR, 1988). Cryostratigraphy in geocryology is comparable to sedimentology and stratigraphy in geology. However, cryostratigraphy differs from stratigraphy by acknowledging that layers of frozen ground contain ground ice structures that are distinct from sedimentary structures (French and Shur, 2010).

Cryotextures refer to the texture of frozen ground, i.e., the microscopic features, such as grain size. Cryotextures are defined as the grain and/or ice crystal size, shape, and fabric and the nature of the contacts between grains and crystals in frozen ground. (Murton and French, 1994; French, 2007). **Cryostructures** refer to the structure of frozen ground, i.e., the visible features and multiple textures of frozen soil. Cryostructures are the shape, size, assembly, quantity and distribution of ice and sediments within frozen ground (Murton and French, 1994). Cryostructures and cryotextures are unique to frozen sediments because frozen water in pores can exceed the pore space, unlike unfrozen deposits. Both cryostructures and cryotextures are influenced by the environment of the freezing process (i.e., syngenetic vs epigenetic) and the nature of the precondition freezing processes (initial water content and extent of moisture migration) (French and Shur, 2010).

Cryofacies are a grouping (or sum) of cryostructures and ice content (Murton and French, 1994). Like facies in a sedimentological scope, cryofacies are purely descriptive and do not infer freezing history. A **Cryofacies Assemblage** is a group of cryofacies used to identify a distinctive cryostratigraphic unit (Murton and French, 1994). Overall, this hierarchical classification provides a framework for interpreting the genesis of ground ice within sediments (Figure 3.7). Figure 3.8, from Murton and French (1994), portrays five cryofacies divided into volumetric ice content, sediment type, and cryostructures.

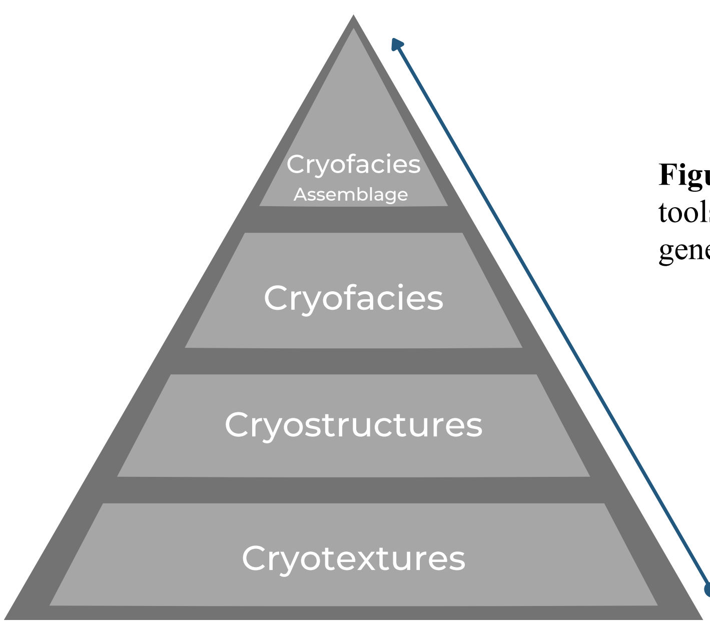

Figure 3.7: Hierarchy of cryostratigraphic tools to identify fabrics and textures to infer a genesis of ground ice and sediments.

Cryofacies type	Volumetric ice content (%)	Cryofacies	Code	Cryostructures
Pure ice	100	Pure ice	I	Le, Le
Sediment-poor ice	>75	Sand-poor ice	SPI	Le, La, Su
		Aggregate-poor ice	API	
Sediment-rich ice	>5 to ≤75	Sand-rich ice	SRI	Le, La, Su
		Aggregate-rich ice	ARI	
Ice-rich sediment	>25 to ≤50	Ice-rich sand	IRS	Sl, Le, La
		Ice-rich mud	IRM	Le, La, Rr, Ri, Cr
		Ice-rich diamicton	IRD	
Ice-poor sediment	≤25	Ice-poor mud	IPM	Sl; various non-ice sedimentary structures
		Ice-poor sand	IPS	
		Ice-poor gravel	IPG	
		Ice-poor diamicton	IPD	
		Ice-poor peat	IPP	

Figure 3.8 Cryofacies classification for ice-rich sediments in the Mackenzie Delta Region from Murton and French (1994).

3.5 Ground Ice Bodies Forms and Defining Characteristics:

Canada's continuous and discontinuous permafrost regions underlie an area with a complex record and history of ground ice. Ground ice within these regions can be classified into two major categories, pore ice and excess ice. The excess ice hosted within the Mackenzie Delta region typically encompasses icy-sediments and ground ice bodies (including buried surface ice, intrasedimental ice, and thermokarst ice) (Figure 3.1**)**. Buried surface ice includes the burial and preservation of glacier ice, snowbank ice, and frozen water bodies (i.e., sea ice, aufeis and lake ice) (Lacelle et al., 2008). Intrasedimental ice is an umbrella term to describe ground ice that has aggraded in place by the freezing of water within *in-situ* sediments, including wedge ice, segregated ice, segregated-intrusive ice, and injection ice (Mackay and Dallimore, 1992). The mechanisms for the growth of intrasedimental ice consist of (1) gravity transfer and thermal contractions for wedge ice; (2) hydrological controlled water injection for hydraulic (open) pingos, segregation – intrusive ice; and (3) water expulsion in frost-susceptible sediments, for segregated ice, and hydrostatic (closed) pingos (Mackay and Dallimore, 1992; Mackay, 1998; Lacelle et al., 2008). Lastly, I propose the term thermokarst ice to encompass large ground ice bodies that form due to thermal-erosion and subsequent re-freezing (i.e., pool ice and thermokarst cave ice).

The preservation of ground ice depends on climatic conditions, the stability of the terrain, and rapid ice burial by placing the ground ice below the active layer. Commonly, rapid burial occurs as colluvial, mass-movements, tephra falls, and aeolian processes or by glacier interactions such as sediments deposited on top of the ice by retreating meltwater sedimentation (such as deltaic sedimentation) or sediment melt-out till (Moorman and Michel, 2000). Moorman and Michel, (2000) describe how retreating glaciers are one of the most effective mechanisms to preserve buried ground ice through the melt-out of entrained sediment. Overall, buried glacier ice has a high preservation potential relative to other buried ice forms. Snowbanks are less likely to be preserved, which may be buried and subsequently preserved by aeolian or colluvial processes (Mackay, 1989; Moorman and Michel, 2000). Lastly, aufeis (river), lake and sea ice are rarely preserved; however, a rapid cover of tephra deposits has been shown to preserve these ice bodies (Froese et al., 2006). Following deposition of large bodies of ice – either buried surface or intrasedimental ice – its preservation depends on the thickness of sediments and the thickness of the active layer. The preservation of ground ice bodies is only possible if the thickness of the overlying sediment/soil cover exceeds the active layer thickness (Cardyn et al., 2007; Lacelle et al., 2009).

Buried Ice Types:

Buried glacier ice forms as a result of incomplete deglaciation, and its subsequently preserved by a cover of glaciogenic material against further thaw (Rampton, 1988; Lacelle, 2002). Two types of buried glacier ice are recognized, including firn-derived glacier ice, and basal ice. Firn-derived glacier ice forms by firn densification and commonly contains a high bubble content and low concentration of glacial debris (Lacelle et al., 2007). Basal glacier ice forms (and modified) by melting and refreezing at the base of warm glaciers (Knight, 1997). Furthermore, basal ice is frequently comprised of low bubble content, a high concentration of glacier debris, and is regularly associated with glacial deformation of the ice and adjacent sediments, as shown in Figure 3.9 (Murton, 2005). Overall, buried glacier ice is commonly associated with: (*i*) foliations and glacial deformations; (*ii*) an upper stratigraphic unit composed of an icy-diamicton; (*iii*) CO_2 concentrations similar to atmospheric values; (*iv)* molar ratios of O_2, N_2, and Ar gasses similar to atmospheric values; (*v*) depleted Pleistocene $\delta^{18}O$ values, ~-33 to -30‰; (*vi)* $\delta D - \delta^{18}O$ regression slope (~7) is similar to the LMWL. Buried glacier ice is typically associated with hummocky topography and moraine belts formed by ice sheets, but it also may be preserved in glaciofluvial outwash, colluvium and till blanket deposits (Wolfe, 2017).

Figure 3.9: Buried Glacier Ice. Example of buried glacier ice from the headwall of a thaw slump near Aklavik (68.113869, -135.676405). This buried glacier ice highlights a banded and moderately deformed ice.

Buried snowbank ice is formed by the accumulation of snow, and subsequently metamorphosed into a tabular ice body – commonly including wind-driven laminations (Figure 3.10) (French and Pollard, 1986). Relict perennial snowbanks rely on rapid burial for preservation; common burial mechanisms include rapid cover of tephra, aeolian or colluvial deposits (Lacelle et al., 2009). Defining characteristics of buried snowbanks consists of: (*i*) little to no debris present; (*ii*) high concentration of bubbles, typically composed of small, euhedral and equigranular crystals; (*iii*) CO_2 concentrations similar to atmospheric values; (*iv)* molar ratios of O_2, N_2, and Ar gasses similar to atmospheric values; (*v*) a wide range of isotopic values strongly dependent on age, may preserve Pleistocene or Holocene-aged isotopes; (*vi)* δD – δ^{18}O regression slope (~7) is similar to the LMWL.

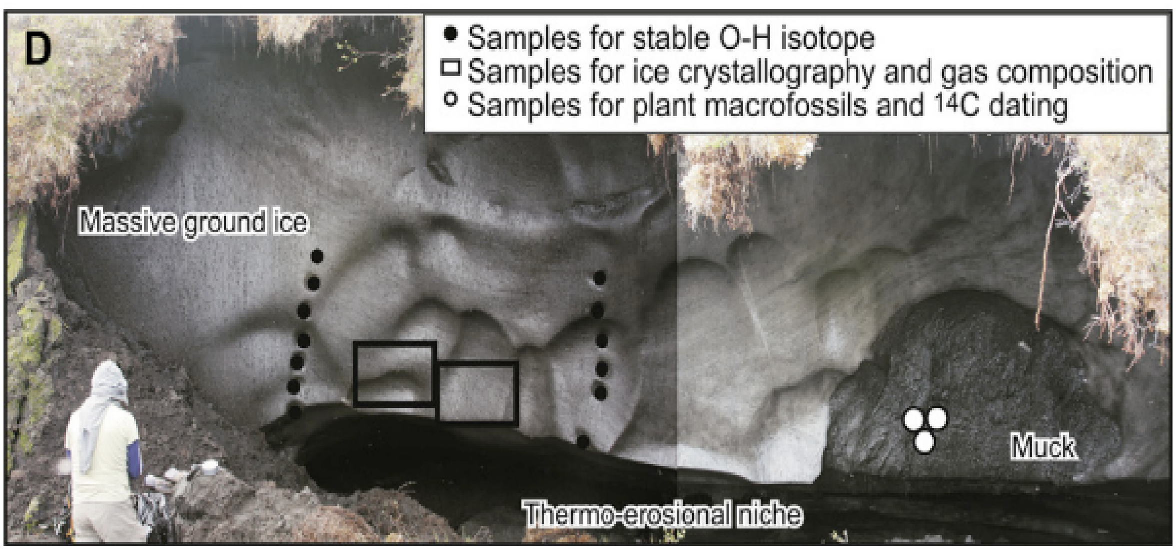

Figure 3.10: Buried Snowbank Ice. (a) Example of buried snowbank ice from a thaw slump in Red Creek, north of Dawson City, Yukon. The image highlights a 30,000 year old snowbank with a tabular appearance from Lacelle et al., (2009).

Aufeis (icings or naledi) are horizontal to sub-horizontal sheet-like masses of ice formed during spring or winter by the freezing of surface or subsurface water (Figure 3.11) (Clark and Lauriol, 1997; Crites et al., 2020). Icings have low preservation potential; however, a study by Froese et al., (2006), illustrated remnants of thin aufeis ice interbedded with Dawson tephra at Goldbottom Creek, Yukon (Figure 3.5b). Defining characteristics of buried aufeis consists of: (*i*) sheet-like masses which may encompass debris; (*iii*) CO_2 concentrations may be than atmospheric values due to biologic interactions within subsurface water (*iv)* molar ratios of O_2, N_2, and Ar gasses may different from atmospheric values, if subsurface water derived; (*v*) a wide range of isotopic values strongly dependent on age, may preserve Pleistocene or Holocene-aged isotopes; (*vi)* δD – δ^{18}O regression slope may be similar or lower than the LMWL, according to a study by Clark and Lauriol, (1997).

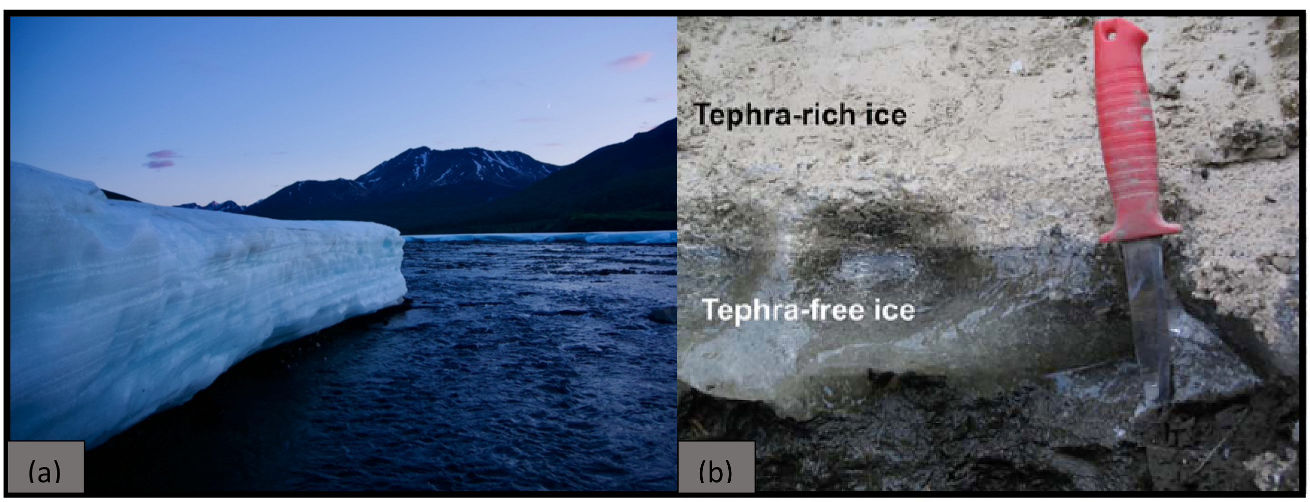

Figure 3.11: Aufeis. (a) Modern aufeis (river ice) from the North Klondike River, Yukon. **(b)** Buried aufeis with well-developed bedding, from Froese (2006)

Intrasedimental Ice Types

Segregation-Intrusive Ice is a tabular ice body with comparable morphological appearance, water isotope composition, and associated surficial materials to buried glacier ice (O'Neill et al., 2019b). Segregation-intrusive ice forms during epigenetic permafrost growth from glacial meltwater deposited between an overlying fine-grained (aquitard) unit, and an underlying coarse grained deposit (Figure 3.12) (Mackay and Dallimore, 1992).Three conceptual models to explain the formation of segregation-intrusive ice are: (1) the segregation of ice due to pore-water expulsion from the freezing of underlying saturated sand layers (Mackay, 1971); (2) hydrologically controlled injection of glacial meltwater driven towards aggrading permafrost near the ice-margin (Rampton, 1988, 1991); and (3) a more widely accepted combination of both models, glacial meltwater injection facilitated by pore-water expulsion from an underlying sand unit, Figure 3.13, (Mackay and Dallimore, 1992). Overall, segregated-intrusive ice is commonly associated with: (*i*) large bodies of banded ice, with alternating layers of ice and icy-sand and icy-clay sediments; (*ii*) may or may not be subjected to glacial deformation; (*iii*) a lower stratigraphic contact composed of coarse-grain (sand) unit; (*vi*) CO_2 concentrations likely 10 to 100 times greater than atmospheric values due to microbial activity in soils; (*v)* molar ratios of O_2, N_2, and Ar gasses may be different from atmospheric values; (*vi*) depleted Pleistocene δ^{18}O values, ~-33 to -30‰; and (*vii)* δD – δ^{18}O regression slope lower (<7) relative to the LMWL. Segregation-intrusive ice is commonly associated with hummocky topography and moraine belts formed by ice sheets, but it also may be preserved in glaciofluvial outwash, colluvium and till blanket deposits.

Figure 3.12: Segregation- Intrusive Ice (sometimes referred to as Intrasedimental Massive Ice)**.**
(a) Segregation-intrusive ice near Tuktoyaktuk, photograph by Mackay, shown in (Burn, 2017). This body of ice is within glacial outwash terrain, and it stratigraphically overlies a sandy unit.
(b) Approximately 5m of banded segregation-intrusive ice at Peninsula Point, near Tuktoyaktuk. The photograph is from Murton (2013).

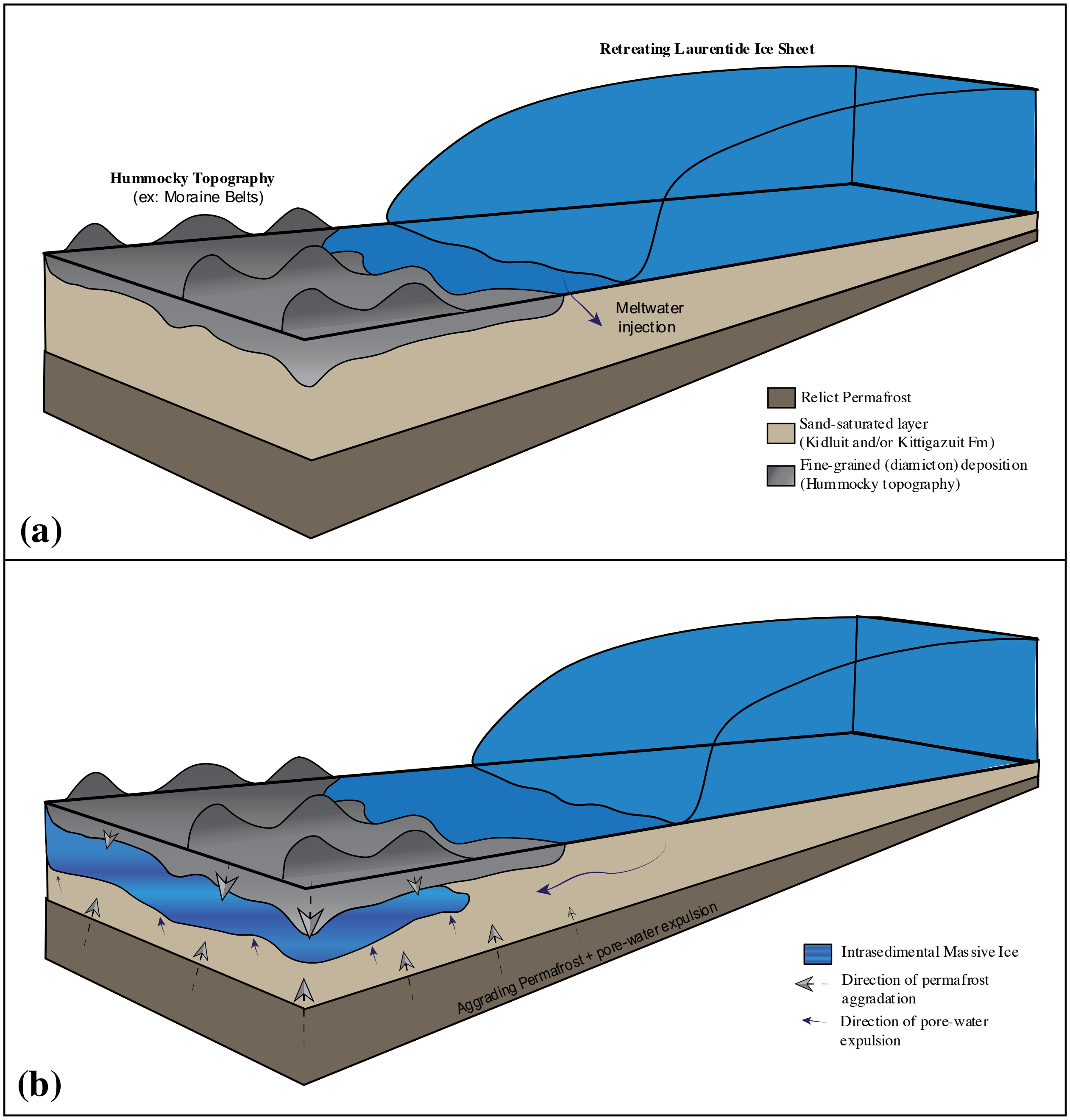

Figure 3.13: Schematic representation illustrating the formation of segregation – intrusive ice. The figure shows the Mackay and Dallimore (1992) conceptual model, modified from Lacelle et al., (2004). **(a)** The retreat of the Laurentide Ice sheet and subsequent hydrologically controlled meltwater injection into the underlying sand unit (glaciofluvial outwash deposits, Kidluit or Kittigazuit Formations). **(b)** Massive ice body forms due to (1) aquitard formed by overlying fine-grained sediments; and (2) pore-water expulsion from the underlying sand-saturated layer.

Wedge ice is the most widely distributed and most straightforward to recognize ground ice form. It is a wedge-shaped, vertical to sub-vertical foliated ice body resulting from fissure development caused by thermal cracking of permafrost at low winter temperatures (Figures 3.14a,b) (Mackay, 1990). Thermal contraction, more frequent in fine-grained soils, occurs when the ground temperature is below -13°C and a cooling rate between 0.1 and 0.6°C/d over 2 to 8 days (Mackay, 1993; Morse and Burn, 2013). Meltwater, most commonly in spring, later infills the cracks and rapidly freezes in place, forming thin ice veins, *i.e.,* vertical foliations. Repeated cracking, water infilling and refreezing, in continuous permafrost, may develop a large ice wedge capable of folding adjacent sediments and may disrupt the active layer. Ice wedges are easily identifiable by their wedge shape and vertical foliated structure (Shur et al., 2004).

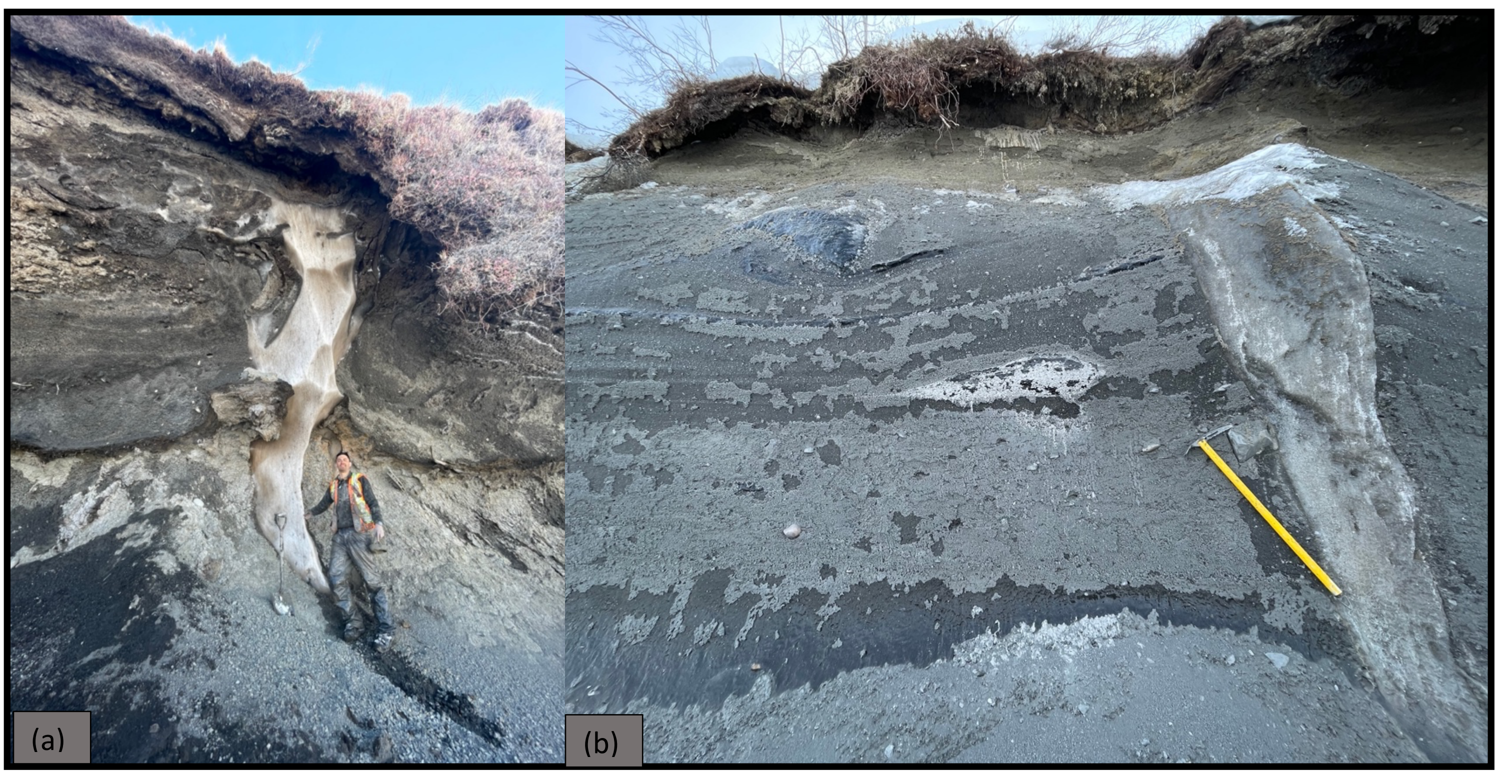

Figure 3.14: Ice Wedge. (a) Syngenetic Holocene ice wedge from the headwall of a thaw slump near Aklavik (68.113869, -135.676405). **(b)** Late Pleistocene ice wedge truncated by the early Holocene thaw. Ice wedge is located near Lantern Lake, north of Inuvik (68.527733,-133.74347) This late Pleistocene ice wedge cross cuts Pleistocene till deposits.

Segregated ice consists of ice-rich layers and lenses (centimeters to meters thick) that form due to the upward water migration towards the freezing front during downward (epigenetic) permafrost growth (Mackay 1972, ACGR, 1988). This pore water migration towards a freezing front, term cryosuction, may form thick, commonly pure, transparent ice lenses that postdate the enclosing sediments (Mackay, 1972; Murton, 2013). In epigenetic permafrost, segregated ice is concentrated near the surface, where the bottom of the active layer and the transition zone become progressively ice-rich (Figure 3.15); however, segregated ice becomes increasingly rare with depth.

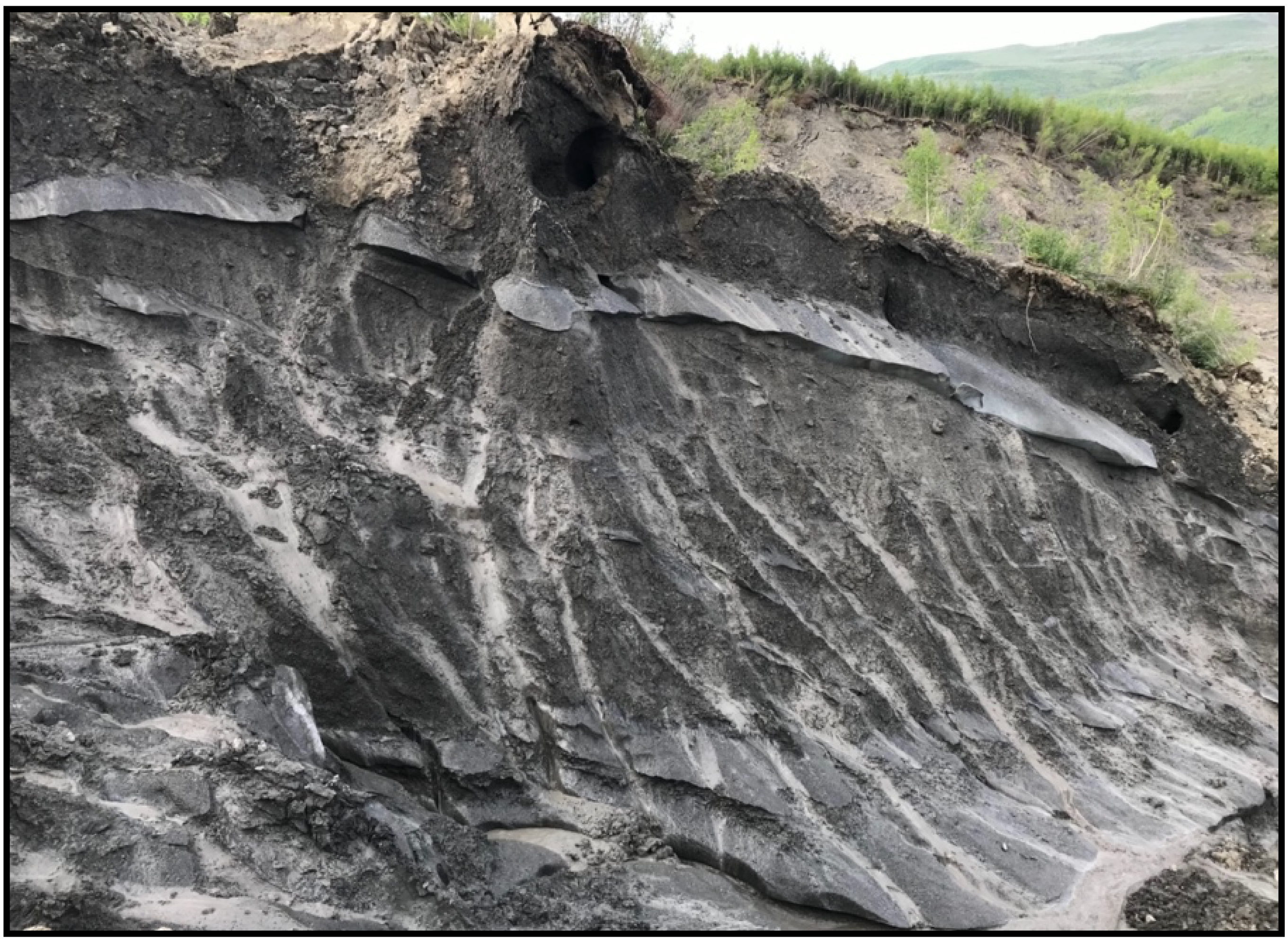

Figure 3.15 Segregated Ice. Segregated ice bodies with a massive appearance from a landslide north of the Keele River (64.290100, -125.841600).

Aggradational ice refers to ice lenses formed during syngenetic permafrost aggradation. Aggradational ice is formed by the accumulation of ice lenses at the top of permafrost from the downward migration of unfrozen water caused by annual active layer thaw and subsequently trapped by a rising permafrost table (Figure 3.16) (Mackay, 1983; O'Neill and Burn, 2012). Aggradational ice, in many areas, is responsible for near-surface ice-rich conditions.

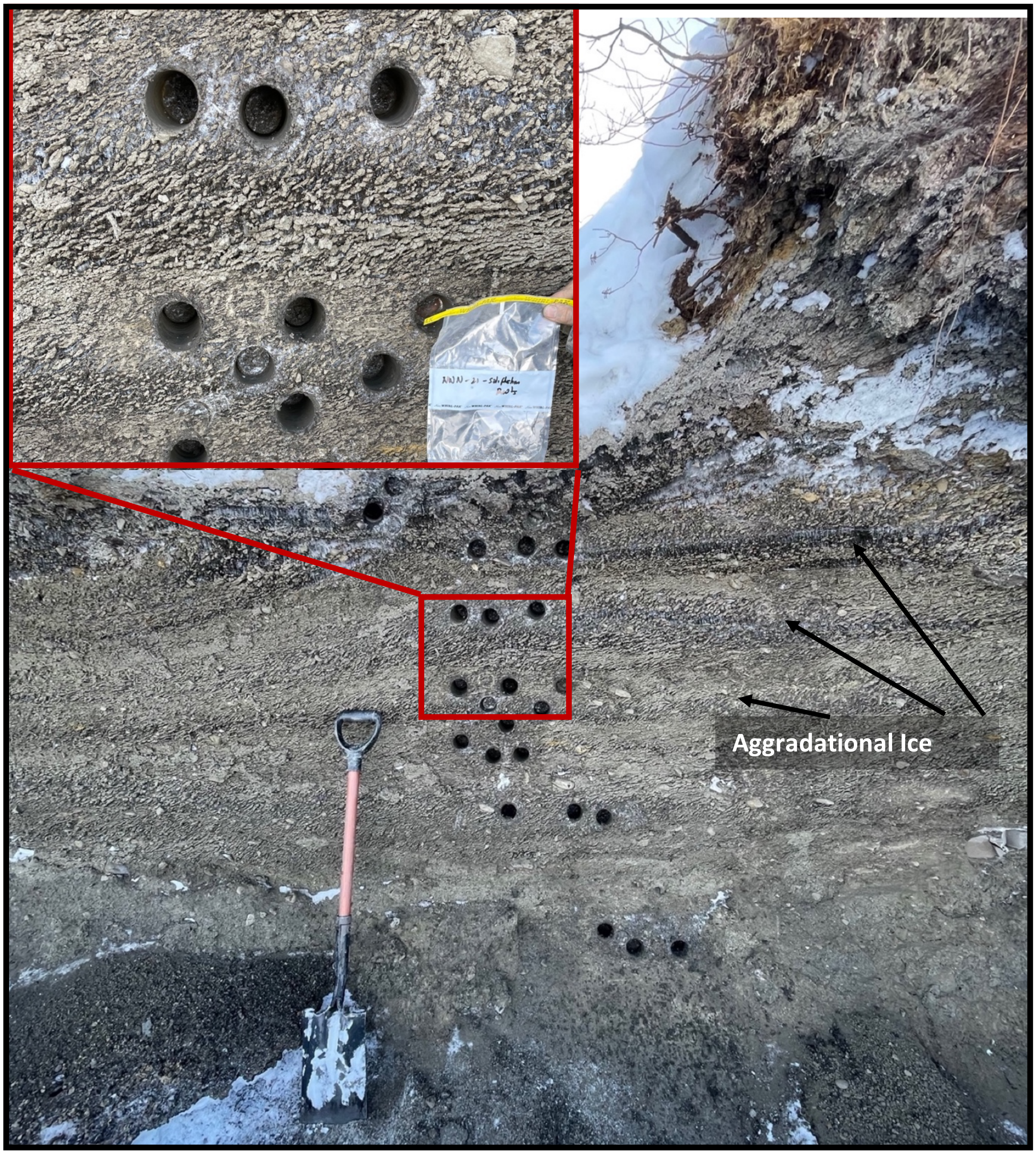

Figure 3.16 Aggradational Ice. Syngenetic aggradational ice. These ice-rich layers, concentrated at near-surface permafrost, formed as permafrost table gradually rises. This exposure illustrates a colluvial deposit progressing getting more ice-rich near the surface. Photo taken near a thaw slump northwest of Noell Lake (68.562012, -133.616487).

Injection (intrusive) ice is formed by the pressurized intrusion of water and its subsequent freezing, causing uplift of the overlying material (Mackay, 1972; Mackay and Dallimore, 1992). Injection ice is usually subject to shallow, active layer depths (Lacelle, 2002); however, injection ice has been observed deep within large ice bodies, including glacier and segregated-intrusive ice (Mackay, 1989). There are at least four different types of injection ice commonly found within ice-rich permafrost settings, pingo ice, sill ice, ice dykes, and large ice with a massive appearance (Mackay, 1989; Murton, 2013). Pingo (ice-cored hill, Figure 3.17) ice is formed where water is topographically controlled (under a hydraulic gradient), injecting into aggrading permafrost, consequently causing uplift. Similarly, large bodies of ice with a massive appearance may form at the base of permafrost within hill-sloped terrain (Figure 3.18). Sill ice forms by pressurized water intrusion into a confining material, subsequently freezing into a tabular appearance (Mackay, 1989) (Figure 3.20). An example of seasonal sill injection ice is shown in figure 3.19, a ~4-m uplift of the ground adjacent to the Inuvik – Tuktoyaktuk Highway. Lastly, ice dykes form similarly to sill ice; however, it tends to resemble igneous intrusion and typically cross-cut older sedimentary packages (Figure 3.21, 3.22) (Mackay, 1989). Typically, most injection ice types form sharp contacts with surrounding sediments and fractures conchoidally, indicative of its pressurized water formation (French, 2007)

Figure 3.17: Pingos – Example of Injection Ice and Ground ice as a landform aggradation feature. Two large pingos (ice-cored hills) form by injection ice. Photo taken south of Tuktoyaktuk, NWT.

Figure 3.18: Injection (Intrusive) Ice. Large, massive intrusive ice form at the base of permafrost. Photo taken on a Mollard-driven landslide near Johnson River, NWT (63.588253, -124.085686). Note Joe Young top left of ice body for scale.

Figure 3.19: Injection (Intrusive) Ice – Sill Ice. Uplift of ground (~4m) by injection ice adjacent to ITH near Kilometer 107. Note the conchoidal fracturing of the cores collected.

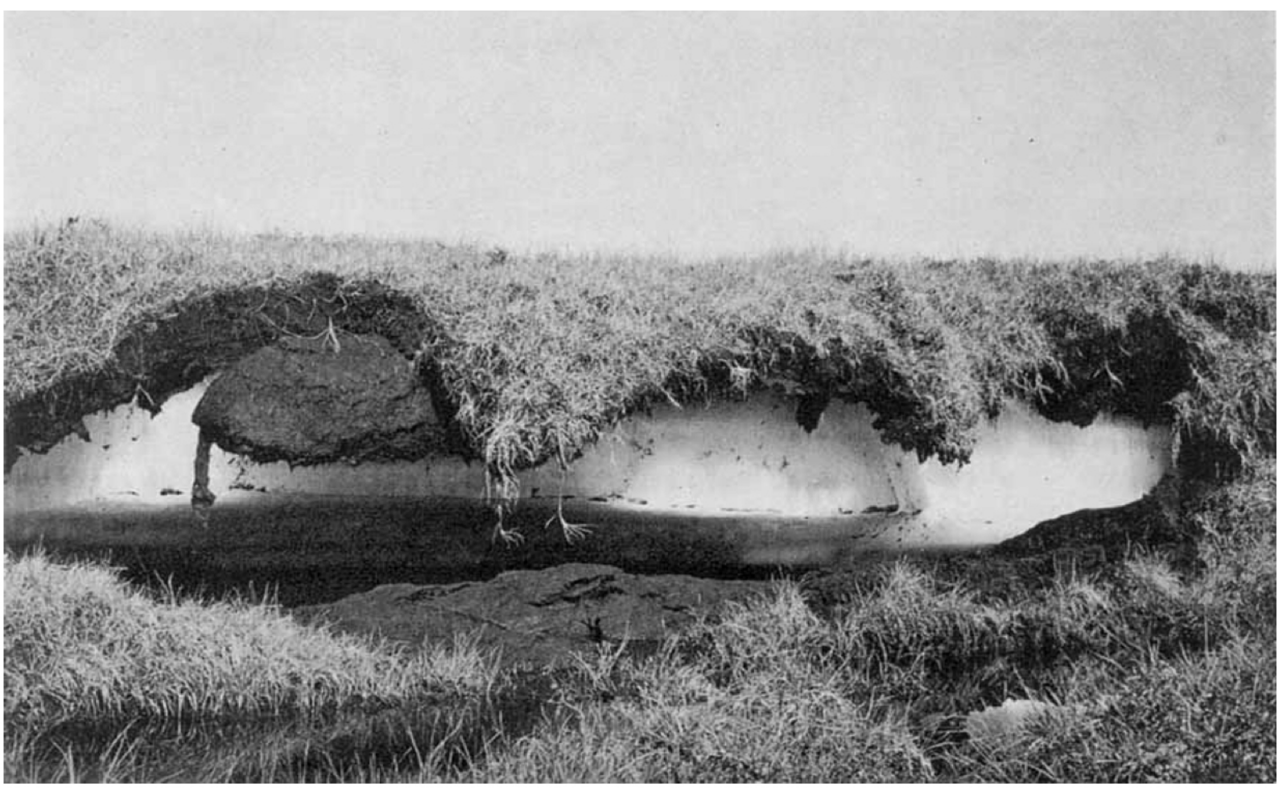

Figure 3.20: Injection (Intrusive) Ice – Sill Ice. Large, tabular sill ice body (~1.2m thick) near Brock River Delta, N.W.T. Image from Mackay (1972).

Figure 3.21: Injection (Intrusive) Ice – ice dyke. Large, tabular ice dyke roughly parallel to stratigraphy. Ice dyke is cross-cutting Pleistocene till. Photo taken near Miner River, NWT (68.630242, -131.755828).

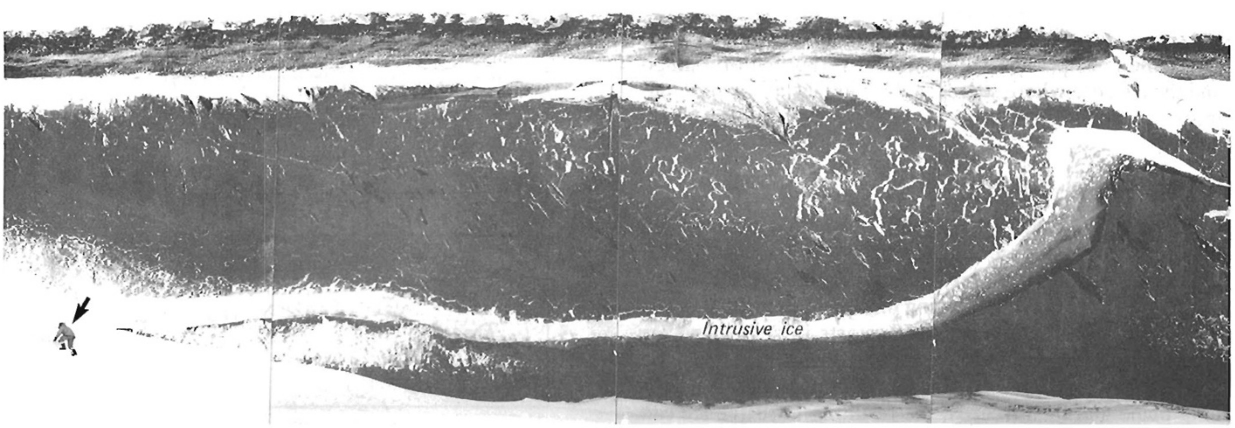

Figure 3.22: Ice Dyke. Large ice dyke body cross-cutting glacially deformed sediments in Pelly Island. Image from Dyke (1989).

Thermokarst Ice:

A proposed term to describe ice bodies that form due to thermokarst and thermal erosion processes, and subsequent permafrost re-aggradation leading to the re-freezing of trapped water.

Pool Ice consists of near-pure ice that is formed by the ponding of melting water between the gullies of ice-wedges, (Mackay, 1988). Pool ice lacks foliations and commonly occurs as horizontally banded sheets (Figure 3.23) (Murton, 2013). Pool ice is typically clear, with vertical orientation of bubble reflecting freezing direction (Shur et al., 2004). Pool ice is often used interchangeably with thermokarst cave ice, this however, is problematic since both ice forms have different structures and geneses.

Figure 3.23: Pool Ice. Multiple pool ice bodies above an ice-wedge, and a thaw contact. Photo taken on a thaw slump near Willow river, NWT (68.194038, -135.487992). The far right shows a clear, horizontally bedded pool ice truncating a vertically foliated ice wedge. A more complex geometry exits for the wedges to the left, where horizontally bedded organic deposits sits on a partially truncated wedge and may reflect either pool ice or thermokarst cave ice.

Thermokarst cave ice (also referred to as Tunnel Ice) refers to a large body of ice formed by inward freezing of trapped water within underground thermo-erosional settings, including tunnels, channels, and pipes (Fortier et al., 2008; Gilbert et al., 2016). This ice type is recognized by a columnar crystalline structure, and bubble trains suggesting inward freezing, and typically an underlying sediment-rich contact with a reticulate-chaotic cryostructure (Figure 3.19) (Fortier et al., 2008). Thermokarst cave ice typically reflects the geometry of the tunnels and cavities it infills, hence the term 'tunnel ice' (Shur et al., 2004; Gilbert et al., 2016).

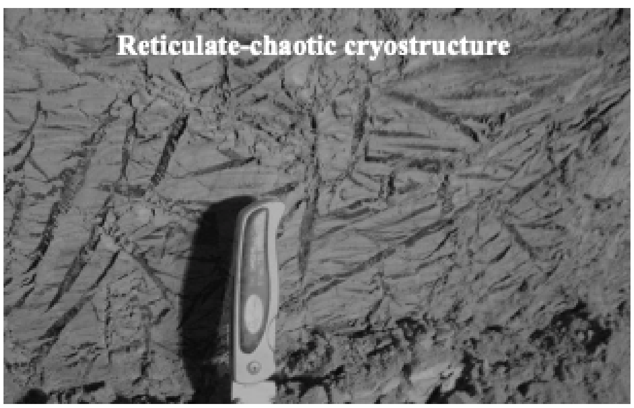

Figure 3: typical reticulate-chaotic cryostructure with multi-directional interconnected ice veins and ice lenses. The handle of the knife is about 6 cm long.

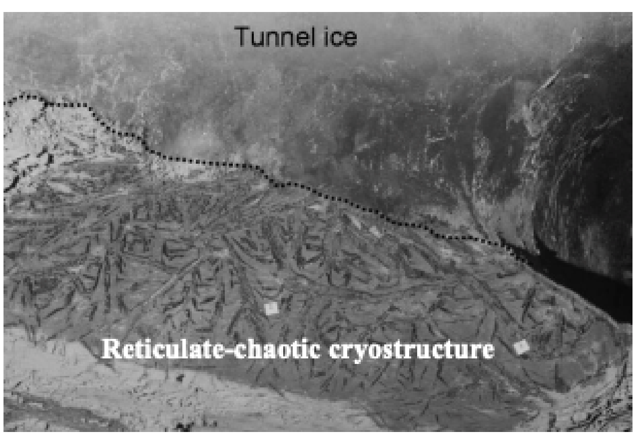

Figure 4: "tunnel ice" underlain by sediments with high-density reticulate-chaotic cryostructure. The white paper scales are 2.5 x 2.5 cm.

Figure 3.24: Thermokarst Cave Ice (Tunnel Ice). Example of thermokarst cave ice from the CRREL permafrost tunnel in Alaska. Note the diagnostic reticulate-chaotic cryostructures underlying the large ice body. Image from Fortier (2008)

References:

Associate Committee on Geotechnical Research National (ACGR), 1988, Glossary of Permafrost and Related Ground-Ice Terms: National Research Council of Canada, v. Technical, p. 156, doi:10.4224/20378888.

Burn, C.R., 2017, Mackenzie Delta: Canada's Principal Arctic Delta, *in* Springer, Cham, p. 321–334, doi:10.1007/978-3-319-44595-3_23.

Cardyn, R., Clark, I.D., Lacelle, D., Lauriol, B., Zdanowicz, C., and Calmels, F., 2007, Molar gas ratios of air entrapped in ice: A new tool to determine the origin of relict massive ground ice bodies in permafrost: Quaternary Research, v. 68, p. 239–248, doi:10.1016/j.yqres.2007.05.003.

Clark, I.D., and Lauriol, B., 1997, Aufeis of the Firth River basin, Northern Yukon, Canada: Insights into permafrost hydrogeology and karst: Arctic and Alpine Research, v. 29, p. 240–252, doi:10.2307/1552053.

Coulombe, S., Fortier, D., Lacelle, D., Kanevskiy, M., and Shur, Y., 2019, Origin, burial and preservation of late Pleistocene-age glacier ice in Arctic permafrost (Bylot Island, NU, Canada): Cryosphere, v. 13, p. 97–111, doi:10.5194/tc-13-97-2019.

Crites, H., Kokelj, S. V, and Lacelle, D., 2020, Icings and groundwater conditions in permafrost catchments of northwestern Canada: Scientific Reports, v. 10, doi:10.1038/s41598-020-60322-w.

Van Everdingen, R.O., 1998, Multi-language glossary of permafrost and related ground-ice terms (Rev. ed. 2005): International Permafrost Association, v. 1998, p. 159, https://globalcryospherewatch.org/reference/glossary_docs/Glossary_of_Permafrost_and_Ground-Ice_IPA_2005.pdf.

Fortier, D., Kanevskiy, M., and Shur, Y., 2008, Genesis of Reticulate-Chaotic Cryostructure in Permafrost:, doi:10.13140/2.1.4703.3929.

French, H., 2007, The Periglacial Environment, 3rd edn: Wiley, Chichester, 458 p.

French, H.M., and Pollard, W.H., 1986, Ground-ice investigations, Klondike District, Yukon Territory:, www.nrcresearchpress.com (accessed December 2019).

French, H., and Shur, Y., 2010, The principles of cryostratigraphy: Earth-Science Reviews, v. 101, p. 190–206, doi:10.1016/j.earscirev.2010.04.002.

Froese, D.G., Zazula, G.D., and Reyes, A. V, 2006, Seasonality of the late Pleistocene Dawson tephra and exceptional preservation of a buried riparian surface in central Yukon Territory, Canada: Quaternary Science Reviews, v. 25, p. 1542–1551, doi:10.1016/j.quascirev.2006.01.028.

Gilbert, G.L., Kanevskiy, M., and Murton, J.B., 2016, Recent Advances (2008–2015) in the Study of Ground Ice and Cryostratigraphy, *in* Permafrost and Periglacial Processes, v. 27, p. 377–389, doi:10.1002/ppp.1912.

Grosse, G., Romanovsky, V., Jorgenson, T., Anthony, K.W., Brown, J., and Overduin, P.P., 2011, Vulnerability and feedbacks of permafrost to climate change: Eos, v. 92, p. 73–74, doi:10.1029/2011EO090001.

Knight, P.G., 1997, The basal ice layer of glaciers and ice sheets: Quaternary Science Reviews, v. 16, p. 975–993, doi:10.1016/S0277-3791(97)00033-4.

Kokelj, S. V., and Burn, C.R., 2003, Ground ice and soluble cations in near-surface permafrost, Inuvik, Northwest Territories, Canada: Permafrost and Periglacial Processes, v. 14, p. 275–289, doi:10.1002/ppp.458.

Lacelle, D., 2002, Ground ice investigation in the far northwest of Canada: , p. 101.
Lacelle, D., Bjornson, J., Lauriol, B., Clark, I.D., and Troutet, Y., 2004, Segregated-intrusive ice of subglacial meltwater origin in retrogressive thaw flow headwalls, Richardson Mountains, NWT, Canada: Quaternary Science Reviews, v. 23, p. 681–696, doi:10.1016/j.quascirev.2003.09.005.
Lacelle, D., Fisher, D., Clark, I.D., and Berinstain, A., 2008, Distinguishing between vapor- and liquid-formed ground ice in the northern martian regolith and potential for biosignatures preserved in ice bodies: Icarus, v. 197, p. 458–469, doi:10.1016/j.icarus.2008.05.017.
Lacelle, D., Lauriol, B., Clark, I.D., Cardyn, R., and Zdanowicz, C., 2007, Nature and origin of a Pleistocene-age massive ground-ice body exposed in the Chapman Lake moraine complex, central Yukon Territory, Canada: Quaternary Research, v. 68, p. 249–260, doi:10.1016/j.yqres.2007.05.002.
Lacelle, D., St-Jean, M., Lauriol, B., Clark, I.D., Lewkowicz, A., Froese, D.G., Kuehn, S.C., and Zazula, G., 2009, Burial and preservation of a 30,000 year old perennial snowbank in Red Creek valley, Ogilvie Mountains, central Yukon, Canada: Quaternary Science Reviews, v. 28, p. 3401–3413, doi:10.1016/j.quascirev.2009.09.013.
Lacelle, D., and Vasil'chuk, Y.K., 2013, Recent progress (2007-2012) in permafrost isotope geochemistry: Permafrost and Periglacial Processes, v. 24, p. 138–145, doi:10.1002/ppp.1768.
Mackay, J.R., 1993, Air temperature, snow cover, creep of frozen ground, and the time of ice-wedge cracking, western Arctic coast: Canadian Journal of Earth Sciences, v. 30, p. 1720–1729, doi:10.1139/e93-151.
Mackay, J.R., 1988, Catastrophic lake drainage, Tuktoyaktuk Peninsula area, District of Mackenzie: 83–90 p., doi:10.4095/122663.
Mackay, J.R., 1983, Downward water movement into frozen ground, western arctic coast, Canada.: Canadian Journal of Earth Sciences, v. 20, p. 120–134, doi:10.1139/e83-012.
Mackay, J.R., 1989, Massive ice: some field criteria for the identification of ice types: Current Research, Part G, Geological Survey of Canada, Paper, p. 5–11.
Mackay, J.R., 1998, Pingo growth and collapse, Tuktoyaktuk Peninsula area, western arctic coast, Canada: A long-term field study: Geographie Physique et Quaternaire, v. 52, p. 271–323, doi:10.7202/004847ar.
Mackay, J.R., 1990, Some observations on the growth and deformation of epigenetic, syngenetic and anti-syngenetic ice wedges: Permafrost and Periglacial Processes, v. 1, p. 15–29, doi:10.1002/ppp.3430010104.
Mackay, J.R., 1971, The Origin of Massive Icy Beds in Permafrost, Western Arctic Coast, Canada: Canadian Journal of Earth Sciences, v. 8, p. 397–422, doi:10.1139/e71-043.
Mackay, J.R., 1972, The World Of Underground Ice: Annals of the Association of American Geographers, v. 62, p. 1–22, doi:10.1111/j.1467-8306.1972.tb00839.x.
Mackay, J.R., and Dallimore, S.R., 1992, Massive ice of the Tuktoyaktuk area, western Arctic coast, Canada: Canadian Journal of Earth Sciences, v. 29, p. 1235–1249, doi:10.1139/e92-099.
Moorman, B.J., and Michel, F.A., 2000, The burial of ice in the proglacial environment of Bylot Island, Arctic Canada: Permafrost and Periglacial Processes, v. 11, p. 161–175, doi:10.1002/1099-1530(200007/09)11:3<161::AID-PPP347>3.0.CO;2-F.
Morse, P.D., and Burn, C.R., 2013, Field observations of syngenetic ice wedge polygons, outer Mackenzie Delta, western Arctic coast, Canada: Journal of Geophysical Research: Earth

Surface, v. 118, p. 1320–1332, doi:10.1002/jgrf.20086.
Murton, J.B., 2005, Ground-ice stratigraphy and formation at North Head, Tuktoyaktuk Coastlands, western Arctic Canada: A product of glacier-permafrost interactions: Permafrost and Periglacial Processes, v. 16, p. 31–50, doi:10.1002/ppp.513.
Murton, J.B., 2013, Ground Ice and Cryostratigraphy, *in* Treatise on Geomorphology, v. 8, p. 173–201, doi:10.1016/B978-0-12-374739-6.00206-2.
Murton, J.B., and French, H.M., 1994, Cryostructures in permafrost, Tuktoyaktuk coastlands, western Arctic Canada: Canadian Journal of Earth Sciences, v. 31, p. 737–747, doi:10.1139/e94-067.
Murton, J.B., Whiteman, C.A., Waller, R.I., Pollard, W.H., Clark, I.D., and Dallimore, S.R., 2005, Basal ice facies and supraglacial melt-out till of the Laurentide Ice Sheet, Tuktoyaktuk Coastlands, western Arctic Canada: Quaternary Science Reviews, v. 24, p. 681–708, doi:10.1016/j.quascirev.2004.06.008.
Neuendorf, K.K.E., Jr, J.P.M., and Jackson, J.A., 2011, Glossary of Geology, Fifth Edition: , p. 800.
O'Neill, H.B., and Burn, C.R., 2012, Physical and temporal factors controlling the development of near-surface ground ice at Illisarvik, Western Arctic coast, Canada: Canadian Journal of Earth Sciences, v. 49, p. 1096–1110, doi:10.1139/E2012-043.
O'Neill, H.B., Wolfe, S.A., and Duchesne, C., 2019, New ground ice maps for Canada using a paleogeographic modelling approach: Cryosphere, v. 13, p. 753–773, doi:10.5194/tc-13-753-2019.
Pollard, W., 1990, The nature and origin of ground ice in the Herschel Island area, Yukon Territory: Proceedings of the fifth Canadian Conference on Permafrost, p. 23–30, http://pubs.aina.ucalgary.ca/cpc/CPC5-23.pdf (accessed March 2020).
Rampton, V.N.; Mackay, J.R., 1971, Massive ice and icy sediments throughout the Tuktoyaktuk Peninsula, Richards Island, and nearby areas, district of Mackenzie: Geol Surv Can, Pap 71-21,.
Rampton, V.N., 1991, Observations on buried glacier ice and massive segregated ice, Western Arctic Coast, Canada: Discussion: Permafrost and Periglacial Processes, v. 2, p. 163–165, doi:10.1002/ppp.3430020209.
Rampton, V.N., 1988, Quaternary Geology of the Tuktoyaktuk Coastlands, Northwest Territories: Geological Survey of Canada, p. 1–107, doi:10.1126/science.ns-6.149S.521-a.
Shumskii, P.A., 1964, Ground (subsurface) ice: Technical Translation (National Research Council of Canada), p. 118, https://doi.org/10.4224/20386780.
Shur, Y., French, H.M., Bray, M.T., and Anderson, D.A., 2004, Syngenetic permafrost growth: Cryostratigraphic observations from the CRREL tunnel near Fairbanks, Alaska: Permafrost and Periglacial Processes, v. 15, p. 339–347, doi:10.1002/ppp.486.
Shur, Y., and Jorgenson, M., 1998, Cryostructure development on the floodplain of the Colville River Delta, northern Alaska: Permafrost, Seventh International Conference, p. 993–999, http://www.arlis.org/docs/vol1/ICOP/40770716/CD-ROM/Proceedings/PDF001189/150193.pdf.
Wolfe, S.A., 2017, Ground ice in permafrost: thermokarst and hydrogeological implications: GeoOttawa 2017, p. 9.

Chapter 4: Holocene thermokarst landscape conditioning across the Pleistocene-Holocene transition: an example from the southern Inuvik-Tuktoyaktuk Highway, NW Canada.

4.1 Introduction

The sensitivity and impacts of climate change on permafrost are primarily related to the nature and abundance of ground ice in the host materials that may lose cohesion with thaw, and may develop terrain effects from subsidence, termed thermokarst. The magnitude of thermokarst development is largely a function of the presence and distribution of excess ice, or ice that exceeds the pore space of the host sediments and thickness of permafrost thawed (Mackay, 1970; Murton, 2008; Kokelj and Jorgenson, 2013; Lee et al., 2014). Since the abundance of ground ice poses a significant threat to ground stability, northern landscapes underlain by ice-rich permafrost have the potential to be dramatically transformed in response to climate change (Jorgenson et al., 2006; Lantz and Kokelj, 2008).

Thermokarst reduces soil strength due to a decrease in soil volume because of the loss of excess ice (Murton et al., 2005). These features have taken on new significance in recent years as they appear to have substantially increased in northwestern Canada (Lantz and Kokelj, 2008; Segal et al., 2016). Since the distribution and abundance of ground ice are strongly related to the geologic history of permafrost regions, understanding the geologic setting of ground ice abundance and distribution can assist in predicting future trajectories of thermokarst (Lantuit and Pollard, 2008; O'Neill et al., 2019b).

The southern section of the Inuvik – Tuktoyaktuk Highway (ITH) is part of the Anderson Plain, and its generalized Quaternary settings have been outlined by Rampton (1988) and Duk-Rodkin and Lemmen (2000). Overall, these glaciated permafrost regions are characterized by widespread past and present thermokarst activity; including thaw slumps, thermokarst lakes, and ice wedge degradation (Rampton, 1988; Murton, 2001; Kokelj et al., 2005, 2009b; O'Neill et al., 2019). Recent retrogressive thaw slump development and increases in active layer deepening are the predominant forms of thermokarst in the Mackenzie Delta region (Mackay, 1995; Kokelj and Burn, 2003; Lantz and Kokelj, 2008; Kokelj et al., 2009a; Lacelle et al., 2015).

The Early Holocene warm interval, roughly as warm as today, dates from ~7.6 – 6.6 ka BP, and is stratigraphically represented by the development of thermokarst lakes, and a regionally extensive Early Holocene thaw unconformity (Burn, 1997; Porter et al., 2019). This unconformity, representing a thickening of the active layer by ~1-3 m below the ground surface, is extensive in the western Arctic settings (Mackay, 1978; Burn et al., 1986; Murton and French, 1993b; Kokelj et al., 2002). Examples of this past widespread thermokarst include (1) paleoactive layers (Murton and French, 1993b; Burn, 1997; Kokelj et al., 2002); (2) slumping and debris-flow deposits (Murton and French, 1993a; Murton, 2001; Lacelle et al., 2004); (3) thousands of thermokarst lakes (Mackay, 1963); and (4) understanding the geologic setting of ground ice abundance and distribution ice wedge degradation (Mackay, 1990; Murton, 2001; French, 2007). Widespread thermokarst was a significant feature of the Early Holocene and strongly impacted areas in the western Arctic, leaving a mantle of sediment unconformably above Pleistocene sediments. On the contrary, some landscapes have been previously influenced by natural processes such as talik development, mass movement or fluvial processes. These landscape evolution processes likely eradicated Pleistocene ice without climate intervention and have since refrozen and re-established permafrost.

To explore the relations between permafrost and ground ice distribution in the Mackenzie Delta region, we investigated five boreholes along the ITH highway. These deep (~10m) boreholes sampled sediments ranging from organic deposits from peatlands and riparian zones, lacustrine deposits from relict thermokarst lakes and diamicts, both reworked and primary till from the Laurentide Ice sheet. The objectives of this investigation are to: (1) determine the depositional history of sediments in the five boreholes along the ITH; and (2) determine the ground ice genesis hosted within these permafrost settings. Notably, widespread thermokarst developed during the Early Holocene has resulted in many parts of the landscape inheriting properties from this past thaw initiation. Collectively, this study aims to quantify the age, ground ice setting and abundance in relation to terrain units to estimate the impacts of the Early Holocene thaw. In this study, we use stratigraphy, sediment descriptions, cryostratigraphy and water isotopes, to establish sensitivity of sedimentary and terrain units to thaw as an initial contribution to understanding regional thermokarst potential in the region.

4.2 Study Area

The study area is located along the Inuvik – Tuktoyaktuk Highway (ITH) from ~20 to 75km north of Inuvik. This highway traverses ice-rich continuous permafrost encompassing two physiographic regions, the Tuktoyaktuk Coastlands and Anderson Plain, characterized by an abundance of tundra lakes coupled with rolling hills and plains (Burn and Kokelj, 2009; Kokelj et al., 2017b). The ITH is positioned across a steep climatic gradient, with warmer and wetter conditions near Inuvik, transitioning to colder and drier towards the coast (Burn and Kokelj, 2009). The ITH crosses a region where the ecology changes from open-canopy boreal forest (near Inuvik) to dwarf-shrub tundra (near Tuktoyaktuk) that is associated with a change in annual mean ground temperatures from -3°C at Inuvik to -7°C at Tuktoyaktuk (Rampton, 1988; Kokelj et al., 2017b).

The Mackenzie Delta, Anderson Plain and the Tuktoyaktuk Coastlands are periglacial landscapes affected by the late Pleistocene glaciation (Duk-Rodkin and Lemmen, 2000). The Laurentide Ice Sheet (LIS) reached its maximum after ~18,000 ^{14}C years BP and persisted until ~13,100 ^{14}C years BP (Rampton, 1988; Hill, 1996; Duk-Rodkin and Lemmen, 2000; Lacelle and Vasil'chuk, 2013). However, the exact timing and extent of the Laurentide glaciation remain poorly constrained. The LIS reached the Mackenzie Delta region during the last glacial cycle, marked by the Toker Point Stade, and the younger Sitidgi Stade. The Toker Point Member, of the Tuktoyaktuk Formation, is a grey, pebbly clay till deposited by the northward advance of the LIS into the Tuktoyaktuk area, reaching its maximum extent ca. ~18 ka (Mackay and Dallimore, 1992; Murton et al., 2015). During the glacial maximum, ice thickness throughout western Arctic Canada reached up to ~1000m. Following retreat of the LIS, a second readvance (or stillstand), defined as the Sitidgi Stade, extended the ice sheet in the southern part of the Tuktoyaktuk Coastlands. The limit of the Sitidgi Stade, previously described by Hughes (1987) as the Tutsieta Lake glacial advance, is defined by a hummocky landform, deposited by the LIS representing the ice limit while it persisted near Inuvik (Rampton, 1988). The Sitidgi Stade dates to approximately ca. 15.3 ka cal. yr BP (Rampton, 1988; Murton et al., 2007). This area was ultimately deglaciated by ~13 ka cal year BP, based on the dating of steppe bison (*Bison priscus)* remains at Tsiigehtchic, NWT (Zazula et al., 2009). Presently, this landscape is a direct result of incomplete deglaciation, permafrost interactions and climatic variability over the last ~10,000 years. The Mackenzie Delta region has been first influenced by natural deglaciation processes, such as wetland and talik formation, fluvial networks, and mass-movement processes. These natural influences during deglaciation are the first step in either relict ice preservation or eradication. Wetland development, and fluvial networks, especially in the context of an ice-marginal environment, likely eradicated Pleistocene ice without climate intervention and have since refrozen and re-established permafrost. Subsequently, climatic cooling and warming in the Holocene have modified ground ice contents and shaped the area observed today.

This study analyzed five boreholes within the glaciated Mackenzie Delta region, recovered from hilltops, riparian, and peatland landscapes recording varying depositional environments, including hummocky, organic, and lacustrine terrains (Figure 4.1). Core BH-1 was collected from a peatland situated within polygonal terrain. Core BH-2 was collected from a hummocky hilltop. Core BH-3 was retrieved from a riparian zone. These three drilling localities (Figure 4.1c) were clustered at a site ~20 km north of Inuvik, immediately north of the treeline boundary and westward of the Sitidgi Stade limit. Core BH-4 was drilled approximately 44km northeast of Inuvik from a peatland with patterned ground near the transition zone between tall and dwarf-shrub tundra (Figure 4.1b). Lastly, BH-8 was drilled ~75km northwest of Inuvik from a peatland with patterned ground situated within dwarf-shrub tundra (Figure 4.1a). Table 1 summarizes the locations, vegetation type and surficial geology units for all five boreholes.

4.3 Methods

Drilling along the ITH was carried out in March 2017 by the Northwest Territories Geological Survey, NWT Department of Infrastructure, and other partners. This study analyzed five boreholes along the ITH intersecting different terrains and surficial geologic units. BH-1, BH-2, and BH-3 were drilled to depths of 11.2m, 19.7m, and 10.6m, respectively. BH-1 and BH-3 had a high core recovery, nearly 100 percent. However, BH-2 had a low recovery (i.e., mostly grab samples) from depths of 0m to 10m and 10.8m to 15m. The low core recovery reflects the occurrence of ice-poor, coarse (sandy and gravelly) sediments. BH-4 and BH-8, both with high core recovery, were drilled to depths of 7.7m and 11.4m, respectively. All core samples were sectioned in the field, logged, and boxed. Initial core descriptions, such as visible ice content and soil descriptions were at done at the Western Arctic Research Center located in Inuvik (Ensom et al., 2020). Cores were split lengthwise with one half used for gravimetric water content and geotechnical analyses, outlined in Ensom et al., (2020). The second half of the boreholes were transported frozen to the University of Alberta's Permafrost Archives Science (PACS) Lab.

In the laboratory, all cores were scraped to reveal textures, photographed and characterized following the cryostructure classification of Murton and French (1994) and Shur and Jorgenson (1988). Subsequently, cores were sub-sampled at ~10cm intervals for the first two meters, and at 20cm at greater depths. Subsamples were analyzed for water isotopes ($\delta^{18}O$ and δD) via a Picarro L2130-i analyzer. Two water reference materials, USGS 45 ($\delta^{18}O$ = -2.2‰ , δD = -10.3‰) and USGS 46 ($\delta^{18}O$ = -29.8‰ , δD = -235.8‰), and a laboratory reference water (QCDI), were used to calibrate measurements to the Vienna Standard Mean Ocean Water (VSMOW) – Standard Light Antarctic Precipitation (SLAP) scale and evaluate analytical precision and accuracy. We estimate the analytical precision of the Picarro analyzer is ±0.5‰ and ±0.1‰ for δD and $\delta^{18}O$, respectively, based on repeat analysis of an internal water standard.

Radiocarbon dates (^{14}C yrs BP) of organic material, including wood plant macrofossils were pretreated following a standard acid-base-acid preparation at the University of Alberta outlined in Reyes et al., (2010). Samples were analyzed with two, standards, FIRI-F and AVR07-PAL (Martinez et al., 2019), to ensure analytical precision and accuracy (Table 3). Prepared samples were shipped to the A.E Lalonde AMS Laboratory, University of Ottawa. Calibration was performed using OxCal v4.2.4 (Bronk Ramsey, 2009) and IntCal13/Bomb 13 calibration.

4.4 Results

4.4.1 Stratigraphy and Cryostructures

Five boreholes – a combination of core and grab-samples – (BH-1, BH-2, BH-3, BH-4, and BH-8) were characterized by stratigraphic units and cryostructures with respect to depth, summarized in Table 4.2 and Figure 4.2. Six cryostructures were observed through the cores, including suspended, lenticular, layered, irregular reticulate, and organic-matrix and solid. Suspended (Su), or ataxitic, is defined as individual mineral grains (clay to sand), rock clasts or aggregates suspended in ice, often associated with massive ice and ice-rich sediments (Murton and French, 1994). Lenticular (Le) is defined as a lens-shaped body of ice in sediment, often developed by ice-segregation within fine-grained sediments (Murton and French, 1994; Murton, 2013). Layered (La), or bedded, is defined as continuous layers of alternating ice and sediment, often developed by segregated or intrusive ice (French, 2007; French and Shur, 2010). Layered and Lenticular structures can have any thickness, length or orientation, and may be parallel, wavy or non-parallel relative to other layered and lenticular cryostructures (Murton and French, 1994; Shur and Jorgenson, 1998). Irregular reticulate (Ri) is a three-dimensional non-oriented web-like structure composed of ice-rich veins encompassing a sediment block, commonly associated with silt-clay or diamict units (French and Shur, 2010). Organic-matrix (O) is an ice-rich structure controlled by organic fibers in soil/peat (Kanevskiy et al., 2013; Murton, 2013). Solid (S) is defined as massive ice, and may include wedge ice, injection ice, buried ice or icy-sediments (Shur and Jorgenson, 1998; French, 2007).

BH-1: Inuvik Peatland

BH-1 consists of three stratigraphic units. At the base of the core is a dark grey, matrix-supported ice-poor diamict (depth 6.8 – 11.2m). This 4.4-meter unit has a high concentration of clasts, varying in size from pebbles to cobbles, ranging from sub-angular to angular. The cryostructures observed in the ice-poor diamict vary between lenticular and irregular reticulate (Figure 4.3a). These ice lenses vary in thickness from 1 to 5 cm. Sharply overlying the diamict is a prominent 4-meter-thick massive ice body (depth 2.2 – 6.8). The massive ice is milky-white and lacks vertical foliations (Figure 4.3b). The upper contact of the massive unit grades to a ~ 2 m thick dark-brown, organic-rich peat body (depth 0 – 2.2m). The Peat unit is predominantly composed of an organic-matrix cryostructure.

BH-2: Inuvik Hilltop

BH-2 consists of three stratigraphic units. At the base of the core is an ~8-meter thick, dark grey, matrix-supported, ice-rich diamict with a low concentration of clasts (depth 11.5 – 19.6m).

The cryostructures observed in the diamict unit vary between suspended, solid and structureless; the thickness of the ice layers/lenses varies between 1 to 30 cm (Figure 4.3d). The upper contact of the ice-rich diamict grades to a ~10-meter gravelly sand unit (depth 2 – 11.5). The gravelly sand unit is mostly ice-poor. Most of the gravelly sand unit was collected as grab samples due to a lack of cohesion, i.e., limited pore-ice. However, four key observations are illustrated from a small core retrieved at a depth of 10m to 10.8m (Figure 4.3c). (1) Strong evidence of normal grading from gravel layers to sand and layers. (2) The gravel layer is matrix-supported with sub-angular to rounded clasts. (3) The sand layer has evidence of bedding, coupled with clast imbrication, indicative of water transport. (4) Wedged between two coarse-grained layers, is a debris-free, milky-white, 15cm thick ice-lens. Overlying the gravelly sand unit, is a is a ~ 2-meter-thick peat unit. The contact between the peat and the gravelly sand was not recovered. The Peat unit is predominantly composed of organic-matrix cryostructure.

BH-3: Inuvik Riparian

BH-3 consists of two stratigraphic units. At the base of the core is an ~8-meter thick, dark grey, matrix-supported, ice-poor diamict with a moderate concentration of clasts (depth 2.4 – 10.2m). The cryostructures in the ice-poor diamict near the base exhibit lenticular lenses varying between 1-2cms, grading upwards to suspended ice, up to ~10cm thick near the upper contact (Figure 4.3f). The upper contact of the ice-poor diamict grades to a ~2.5-meter-thick organic-rich unit. The organic-rich unit is predominantly composed of large woody fragments, with minimal pore-ice at the base of the contact and grading upwards to lenticular lenses (10-15cm), and organic-matrix cryostructures (Figure 4.3e).

BH-4: Trail Valley Peatland

BH-4 consists of three stratigraphic units. At the base, a dark grey, matrix-supported ice-poor diamict with a high concentration of shield clasts varying in size from pebbles to cobbles (depth 6.2 – 7.7m). Clasts are predominantly quartzite varying from sub-angular to angular. Two predominant cryostructures are observed within the unit: (1) lenticular cryostructures with variable orientation and thickness ranging from 1-3cm, and (2) irregular reticulate cryostructures (Figure

4.3h). The upper contact of the ice-poor diamict grades to an ~ 2 m thick fine-grained unit (depth 4.1 – 6.2m). This unit is dark reddish-brown with a high abundance of lenticular cryostructures. The lenticular cryostructures are largely horizontal, non-parallel and variable in thickness ranging from 1cm to 5 cm (Figure 4.3g). Overlying the fine-grained unit with a gradual contact is a ~4.5 m thick dark-brown, organic-rich peat. The cryostructures within the peat are organic-matrix cryostructure.

BH-8: Husky Lakes Peatland

BH-8 is characterized by the presence of two stratigraphic units. At the base of the core, an ice-rich, fine-grained unit is present with thin alternating dark-brown and brownish-orange laminations (depth 4.3 – 11.4m). Three main cryostructures are observed in the unit: (1) irregular reticulate; (2) lenticular cryostructures with variable thickness (ranging from 1cm to 3cm) and orientation; and (3) layered cryostructures with variable thickness (ranging from 1cm to 7cm) and predominantly horizontal orientation, some vertically oriented (Figure 4.3j). Overlying the silt and clay unit with a gradual contact is a ~4.5 m thick dark-brown, organic-rich peat body. The peat unit is predominantly composed of organic-matrix cryostructure (Figure 4.3i).

4.4.2 Radiocarbon Dates

Five radiocarbon samples were collected from three cores within the peatlands, summarized in Table 3 and Figure 4.2. Two radiocarbon dates were obtained for BH-1. The uppermost radiocarbon sample (BH1-60) at a depth of 2.1m was selected in the peat unit above the massive-ice unit; the lowermost sample (BH1-141) at a depth of 7.0m was selected near the contact between the massive ice and ice-poor diamict units. A single radiocarbon sample was obtained for BH-4; the sample (BH4-92) was obtained in the silt and clay unit at a depth of 4.6m. Two radiocarbon samples were obtained for BH-8. The uppermost sample (BH8-75) was selected at a depth of 4.1m, near the peat and fine-grained contact; the second sample (BH8-11.3) was selected near the base of the core at a depth of 11.3m.

4.4.3 Water Isotopes and Co-Isotope Plots

BH-1: Inuvik Peatland

The $\delta^{18}O$ and δD values in BH-1 illustrate an overall enrichment with depth with a sharp isotopic discontinuity between the peat and ice-poor diamict. The uppermost unit, the peat, has an average $\delta^{18}O$ and δD values of -18.9± 0.8‰ and -152.7± 6.2‰, respectively. The underlying massive ice unit is more depleted, distinguished by an average $\delta^{18}O$ and δD values of -23.5± 3.1‰ and -189.5± 22.4‰, respectively. The lowermost ice-poor diamict unit has an average $\delta^{18}O$ and δD values of -19.8 ± 0.5‰ and -169.1± 2.3‰, respectively. Moreover, the d-excess is variable throughout the core, but tending to be negative. The d-excess in BH-1 has an average of -11± 3‰, -2 ± 4‰, and -2± 5‰ for the peat, massive ice, and ice-poor diamict units, respectively. The observed regression slopes for BH-1 vary between the units. The peat unit and the massive ice unit plot on a slope of 5.9 ($\delta D = 5.9\ \delta^{18}O - 42$ [$r^2 = 0.54$]), and 7.1 ($\delta D = 7.1\ \delta^{18}O - 23$ [$r^2 = 0.98$]), respectively. By comparison, recent work on the local meteoric water line (LMWL) at Inuvik, from Fritz et al., (2022), plots on a slope of 7.4, (Figure 4.4b, 4.4c). By contrast, the regression slope of the ice-poor diamict is much lower, at 3.3 ($\delta D = 3.3\ \delta^{18}O - 103$ [$r^2 = 0.54$]), as shown in Figure 4.4a. Lastly, as summarized in Table 4, the average gravimetric water content in BH-1 are 417%, 8500% and 33% for the peat, massive ice, and ice-poor diamict units, respectively (Figure 4.2).

BH-2: Inuvik Hilltop

The $\delta^{18}O$ and δD values in BH-2 illustrate an overall depletion with depth. This isotopic depletion is gradual, ranging from -23‰ near the surface to > -30‰ at depths exceeding 6m. The uppermost peat unit has average $\delta^{18}O$ and δD values of -22.6 ± 0.7‰ and -174.0 ± 7.2‰, respectively. The underlying gravelly sand unit is distinguished by the diffusion-dominated isotopic values, with average $\delta^{18}O$ and δD values of -28.7 ± 2.5‰ and -233.1± 11.8‰, respectively. The lowermost ice-rich diamict has average values of -29.0 ± 0.5‰ and -228.8± 2.9‰, respectively. Additionally, the d-excess is variable throughout the first 6 meters, thereafter displaying a positive trend. The d-excess in BH-2 has an average of 7.2 ± 2‰, -3.9 ± 9‰, and 2.8 ± 1‰, for the peat, gravelly sand and ice-rich diamict units, respectively. The observed regression slopes for BH-2 plots on a shallow slope, much lower than the LMWL. The gravelly sand unit and the ice-rich diamict unit plot on a slope of 4.6 ($\delta D = 4.6\ \delta^{18}O - 102$ [$r^2 = 0.97$]), and 5.8 ($\delta D = 5.8\ \delta^{18}O - 61$ [$r^2 = 0.93$]), respectively (Figure 4.4b). Insufficient samples precluded, a co-isotope plot for the peat unit in BH-2. Lastly, the average gravimetric water content in BH-2 are 54%, 318% and 611% for the peat, gravelly sand, and ice-rich diamict units, respectively (Figure 4.2).

BH-3: Inuvik Riparian

The $\delta^{18}O$ and δD values in BH-2 illustrate an overall depletion with depth. This isotopic depletion is gradual, over ~10 meters, ranging from -18‰ to -24‰. The uppermost peat unit has average $\delta^{18}O$ and δD values of -17.5 ± 0.5‰ and -148.3± 2.0‰, respectively. The underlying ice-poor diamict is distinguished by the diffusion-dominated isotopic values, with average $\delta^{18}O$ and δD values of -19.8 ± 1.2‰ and -164.7± 9.5‰, respectively. Moreover, the d-excess displays an overall negative trend with depth. The d-excess in BH-3 has an average of -8± 2‰, and -6± 1‰ for the peat, and the ice-poor diamict, respectively. The observed regression slope for the peat unit is 4.1 ($\delta D = 4.1\ \delta^{18}O - 77$ [$r^2 = 0.77$]), Figure 4.4c. By contrast, the ice-poor diamict plots on a regression slope of 7.5 ($\delta D = 7.5\ \delta^{18}O - 15$ [$r^2 = 0.98$]), Figure 4.4a. Lastly, the average gravimetric water content in BH-3 are 600% and 38% for the peat and ice-poor diamict units, respectively (Figure 4.2).

BH-4: Trail Valley Peatland

BH-4 shows a strong enrichment of δD and $\delta^{18}O$ values, and a progressive negative d-excess trend with depth. The uppermost unit, the peat, has average $\delta^{18}O$ and δD values of -20.5± 0.4‰ and -163.0± 1.3‰, respectively. The underlying silt and clay unit is relatively more enriched, with average $\delta^{18}O$ and δD values of -19.6 ± 0.2‰ and -166.2± 2.2‰, respectively. Lastly, the lowermost ice-poor diamict, illustrates the most enriched waters with average $\delta^{18}O$ and δD values of -18.9 ± 0.4‰ and -164.8± 1.6‰, respectively. The d-excess in BH-4 is somewhat variable, with a general negative trend with depth. The d-excess in BH-4 has an average of 1± 2‰, -10± 3‰, and -14± 2‰ for the peat, silt and clay, and ice-poor diamict, respectively. The regression slopes for the units in BH-4 are similar, with the peat and ice-poor diamict plotting with a slope of 3.0 ($\delta D = 3.0\ \delta^{18}O - 101$ [$r^2 = 0.76$]) and 3.9 ($\delta D = 3.9\ \delta^{18}O - 92$ [$r^2 = 0.82$]), respectively (Figure 4.4a, 4.4c). The regression slope for the silt and clay unit was not determined since all values were tightly clustered. Lastly, the average gravimetric water content in BH-4 are 541%, 98% and 24% for the peat, silt and clay, and ice-poor diamict units, respectively (Figure 4.2).

BH-8: Husky Lakes Peatland

The δ^{18}O and δD values in BH-8 illustrate a strong isotopic enrichment with depth. The uppermost unit, the peat, has average δ^{18}O and δD values of -19.9± 0.2‰ and -161.1± 1.4‰, respectively. The underlying silt and clay unit has average δ^{18}O and δD values of -17.1 ± 0.2‰ and -151.2± 0.7‰, respectively. Additionally, BH-8 has an increasingly negative d-excess trend with depth. The d-excess has an average of -1 ± 4 ‰, and -14 ± 4‰ for the peat and silt and clay unit, respectively. The regression slopes between the two units are distinct. The peat unit has a regression slope of 8.0 (δD = 8.0 δ^{18}O –103[r^2 = 0.96]), Figure 4.4c. By contrast, the regression slope of the silt and clay unit is much lower, at 4.6 (δD = 4.6 δ^{18}O –72 [r^2 = 0.98]), Figure 4.4b. Lastly, the average gravimetric water content in BH-8 are 168% and 63% for the peat, gravelly sand, and ice-rich diamict units, respectively (Figure 4.2).

4.5 Discussion

4.5.1. Interpretation of Ground Ice and Stratigraphic Units within the boreholes

Ice marginal glaciated settings characteristic of western Arctic Canada have a complex history of deposition and post-glacial modification that gives rise to heterogenous ground ice distribution, including (1) epigenetic wedge ice commonly associated with rolling uplands underlain by fine-grained soils (Pollard and French, 1980; Holland et al., 2020); and syngenetic wedge ice found within lacustrine and alluvial lowland settings (Kokelj et al., 2007, 2014; Morse and Burn, 2013). (2) Relict ice, or buried glacier ice, forming as a result of incomplete deglaciation, and is typically associated with hummocky topography and moraine belts formed by ice sheets (Rampton, 1988; Murton, 2005; Kokelj et al., 2017a). (3) Segregated ice consisting of ice-rich layers and lenses (centimeters to meters thick) that form due to the migration of unfrozen pore water towards a freezing front typically found within the uppermost meters within permafrost settings (Mackay, 1983; ACGR, 1988); or found within refreezing of lacustrine and taliks as post-glacial drainage creates environments for permafrost aggradation in fine-grained and diamict deposits (Mackay, 1989). Lastly, (4) injection ice, or intrusive ice, found within the bounds of shallow permafrost, is formed by the pressurized intrusion of water and its subsequent freezing, causing uplift of overlying material (Mackay, 1972; Mackay and Dallimore, 1992).

Interpretation of the Ice-Poor Diamict Units in BH-1, BH-3 and BH-4:

The ice-poor diamicts present in BH-1, BH-3 and BH-4, at depths greater than of 6.8, 2.4 and 6.2m, have an average δ^{18}O values of -19.8 ± 0.5‰, -19.8 ± 0.5‰, and -18.9 ± 0.4‰, respectively. The co-isotope slopes of BH-1 and BH-4 are 3.2 and 3.9, respectively (Figure 4.4a). These isotope values are typical of Holocene waters that have undergone some evaporative enrichment, given the low co-isotope slope and negative average d-excess values of -11 and -6 for BH-1 and BH-4, respectively. These diamicts, isotopic values, and their observed reticulate cryostructures are indicative of refreezing of taliks as post-glacial drainage creates an environment for permafrost aggradation.

BH-3, on the other hand, has a regression slope of 7.5 (Figure 4.4a), similar to the LMWL. Moreover, BH-3 displays a gradual δ^{18}O depletion, at depths between 1 and 10m, ranging from -18‰ to -24‰, suggestive of a diffusion-dominated δ^{18}O profile (Figure 4.2). This diffusion-dominated δ^{18}O profile, coupled with an average d-excess value of -6 suggests a formation of a residual talik and the transport of water between young and older sediment packages. A ~ 9m diffusion-dominated δ^{18}O profile likely reflects BH-3 being located on a riparian zone within a local talik connected with the stream. The primary cryostructures in these ice-poor diamicts have been disturbed, and now include lenticular, layered and reticulate structures, which exemplify ice-poor epigenetic permafrost conditions (Shur and Jorgenson, 1998; French and Shur, 2010). Therefore, these ice-poor diamicts are interpreted as a redeposited melt-out till following the early Holocene thaw. This is strongly supported by the enriched isotope values similar to Lacelle et al., (2004), where the authors interpreted ice-poor diamicts being formed the thawing and redeposition of Pleistocene melt-out till affected by the early Holocene.

Interpretation of the Ice-rich Diamict Unit in BH-2

The ice-rich diamict in BH-2, situated at a depth greater than 11.5m, has an average $\delta^{18}O$ value of -29.0 ± 0.4‰, a co-isotope slope of 5.8 (Figure 4.4b) and an average d-excess of 3 ± 1‰ suggesting little evidence of evaporative enrichment. This ice-rich diamict exhibits significant excess ice, with gravimetric water content exceeding 600% in suspended, solid (massive ice) and reticulate cryostructures hosted within fine-grained texture with some clasts. Therefore, this dark-gray till is interpreted as a primary Pleistocene till with relict ice due to: (1) isotopic values indicative of Pleistocene water. (2) This ice-rich diamict is interpreted as deformation till due to massive structure and fine-grained homogenized texture (Benn and Evans, 2010). (3) Suspended, and reticulate cryostructures throughout the unit suggest a basal glacier ice origin, similar to basal glacier ice noted by Murton et al., (2005). (4) Situated within a glaciofluvial deposit, just northwest of the Sitidgi Stade stillstand, which acted as rapid burial mechanisms, similarly to the buried glacier ice in Coulombe et al., (2019). Lastly, (4) a co-isotope slope of 5.8 (lower than the LMWL), similar to a slope of 6.3 by Lacelle et al., (2004), suggests a basal glacier sediment package undergoing frequent melting and refreezing as the glacier advances.

Interpretation of Gravelly sand Unit in BH-2

The gravelly sand unit, overlying the relict basal till, has average $\delta^{18}O$ values of -28.7 ± 2.5‰, and a regression slope of 4.6. The average gravimetric water content of this unit is ~300%. The sediments illustrate normal grading coupled with laminations within the sandy layers, and imbricate pebbles indicate traction currents (Figure 4.3c). The d-excess values range between 5 near the base of the unit and -20 near the uppermost contact. This positive d-excess trend with depth suggests a diffusion-dominated $\delta^{18}O$ profile between a depth of 3.5 and 7.5 m (Figure 4.2) suggesting little evaporative enrichment near the base. Comparable to Lacelle et al., (2004), as the paleo-active layer deepened, and relict Pleistocene material thawed out, Holocene $\delta^{18}O$ values mixed with the Pleistocene water within the diffusion zone. Overall, this $\delta^{18}O$ diffusion-profile suggests the formation of a residual talik, promoting diffusion within this unit, during the early Holocene warming. Therefore, the plausible interpretation for the gravelly sand unit is that an ice-marginal outwash channel deposited it with LIS Pleistocene waters due to: (1) isotopic Pleistocene values near the lower contact with little evidence of evaporative enrichment and (2) stratigraphic evidence of water involvement. Subsequent warming in the early Holocene, thawed the upper meters of this unit, consequently forming a residual talik with Holocene waters expressed by the diffusion-dominated δ^{18}O profile and negative d-excess values.

Interpretation of the Massive Ice Unit in BH-1

The four-meter-thick massive ice unit, situated 4m below the ground surface in BH-1 is milky-white, and massive in appearance, lacking debris or vertical foliations. Radiocarbon dates near the upper and lower contacts of the massive ice are 3,780 ^{14}C yr BP and 13,866 ^{14}C yr BP, respectively. This massive ice unit has an average δ^{18}O value of -23.5 ± 3.1‰, and d-excess average of -2 ± 4‰. These values are more enriched than typical Pleistocene glacier ice values in the region and typical of Holocene waters with minor evaporative enrichment. Further, the regression line plots on a slope of 7.1, similar to the LMWL, suggesting a meteoric water source with minimal transformation (Figure 4.4b). This atmospheric water source, coupled with δ^{18}O values as depleted as -27‰ suggests winter precipitation. This massive ice unit is interpreted as injection ice due to lack of vertical foliations and presence of horizontal layering, ruling out familiar sources of massive ice typically observed within the northwestern Arctic. Secondly, isotopic values with a co-isotope slope of 7.1, and minor evaporative enrichment suggest a winter meteoric water source. Third, this massive ice body has a sharp lower and upper contact, coupled with winter meteoric water and absence of foliations suggests the formation of injection ice between organic materials and underlying fine-grained diamict (Kokelj, personal communication, 2022). Lastly, radiocarbon dates above on the upper contact suggest Holocene peat deposition, meanwhile, lower diamict unit has Holocene-aged water, suggestive of a tabular injection ice, similar to tabular ice bodies mentioned by Mackay (1979), between the bedding plane of the peat and fine-grained diamict.

Interpretation of the Silt and Clay Units in BH-4 and BH-8

The silt and clay unit in BH-4 and BH-8 has average δ^{18}O values of 19.6± 0.2‰, and -17.1± 1.2‰, respectively. The regression slope of BH-8 is 4.6, with d-excess values for both BH-4 and BH-8 displaying a sharply decreasing d-excess values (Figure 4.4b). These isotopes values Holocene waters with strong evaporative enrichment. The stratigraphic presence of fine-grained clay and silt foliations in the cores coupled with surficial deposits, indicate the deposit represent lacustrine or glaciolacustrine sediments for BH-4 and BH-8, respectively. The cryostructures within these fine-grained units are predominantly horizontal layered and lenticular, which tend to follow the laminations present within the lacustrine and glaciolacustrine units. These cryostructures are commonly found in fine-grained lacustrine and glaciolacustrine sediments indicative of ice-rich epigenetic permafrost (French and Shur, 2010; Kanevskiy et al., 2014; Gilbert et al., 2016). Radiocarbon dates from the lacustrine unit in BH-4 indicates sediment accumulation in a local thermokarst lake from ~15,800 to 12,600 cal yr BP. This lake subsequently drained and developed epigenetic permafrost. In the case of BH-8, since it lies within glaciolacustrine Husky Lake sediments, the radiocarbon date suggests continuous deposition from Husky Lakes between ~11,500 to 9,000 cal yr BP. Thereafter, Husky Lake level lowered, permafrost aggraded, followed by peat growth ~9000 cal yr BP.

4.5.2 Conceptual models for thaw degradation

5.2.1 Conceptual Model for BH-1 and BH-3 - A localized wetland and deep taliks

The BH-1 and BH-3 cores have a reworked till hosting ice-poor Holocene waters, overlain by extensive peat bodies. Additionally, BH-1 has a ~4m thick massive ice body, with Holocene $\delta^{18}O$ winter precipitation values. The observations suggest a depositional model where these lowlands have been significantly influenced by wetlands or localized lakes (and subsequent talik formation) as a product of landscape evolution and subsequently influenced by the early Holocene warm interval. These redeposited melt-out diamicts represent till composed of material deposited from the LIS with minimal ice. This extensive talik formation (due to deglaciation processes, which may have been coupled with extensive warming) led to the reworking of primary ice-rich tills, thus losing their original Pleistocene waters and cryostructures. Subsequent drainage of these shallow talks, followed by cooling, results in the reestablishment of epigenetic permafrost to aggrade, leading to refreezing of Holocene-aged waters with lower ice content, and reticulate and structureless cryostructures. Lastly, Holocene conditions favoured rapid syngenetic peat growth with wedge ice formation. Today, BH-1 is located in polygonal-terrain peatland where wedge ice is likely present.

5.2.2 Conceptual Model for BH-2 - A glaciofluvial hilltop hosting buried glacier ice

The BH-2 core has a lowermost till unit hosting Pleistocene ice (based upon isotopic water values), overlain by a gravelly sand diamict likely representing an ice-marginal outwash channel that is overlain by peat. These observations suggest a conceptual model where the lowermost till and buried glacier ice unit directly results from rapid burial from an outwash channel. This hilltop, located ~4km north of the Sitidgi Stade limit, is a remnant outwash channel within an ice-marginal landsystem. This ice-marginal deglaciation process deposited the gravelly sand unit, with evidence of water transport and hosting a Pleistocene ice lens near the bottom contact, likely resulted from an outwash channel deposit. Proglacial processes likely fed this outwash channel from the nearby Sitidgi Stade ice margin, ~15,300 cal yr BP (Rampton, 1988; Murton et al., 2007). Later, the early Holocene warm interval led to widespread thermokarst development. Consequently, warming promoted thermokarst slope instability within this hummocky terrain. Slope truncation led to the thawing and reworking of relict Pleistocene material within the upper ~5 meters. Holocene warming promoted organic accumulation and re-aggradation of permafrost. Today, the thick organic deposits serve as a critical thermal conductivity shield for the underlying permafrost, especially in ice-cored hummocky terrain prone to hosting ice-rich Pleistocene ice at depth. This conceptual model is shown in Figure 4.6.

5.2.3 Conceptual Model for BH-4 and BH-8 – A lacustrine deposit with large taliks

The BH-4 core shows a redeposited till hosting Holocene ice, overlain by a lacustrine deposit and peat. BH-8, located within glaciolacustrine sediments of the Husky Lakes, shows a thick lacustrine sequence, overlain by peat. These observations suggest a conceptual model where the lowermost redeposited diamict, similar to BH-1 and BH-3, have been significantly affected by talik development promoted by the early Holocene warming in conjunction with processes of post-glacial landscape evolution. This thaw led to widespread thermokarst and ground ice thaw. This extensive thermokarst consequently formed a thermokarst lake in the slope concavity where BH-4 is located. In contrast, BH-8 was part of the proglacial Husky Lakes. Following the localized thermokarst lake drainage near BH-4 and receding lake levels of the Husky Lake in BH-8, permafrost would have epigenetically been aggraded first as soon as materials were exposed.

Followed by rapid aggradation of syngenetic peat and permafrost with the inclusion of Holocene-aged waters. Additionally, these terrain units today are locations of ice wedge development. This conceptual model is shown in Figure 4.5.

4.5.3 Landscape Conditioning following the early Holocene thaw

Following the Laurentide Ice Sheet's retreat and subsequent permafrost formation in the study region, our data shows that the early Holocene warm interval led to widespread thermokarst development. The early Holocene warm interval (7.6 – 6.6 ka PB) was perhaps ~1 – 2°C cooler than today, but marginally warmer than the early 20th century (Porter et al., 2019). Yet, this warming interval led to widespread thermokarst development including, thermokarst lake initiation (and subsequent talik formation) and the development of a deep thaw unconformity recorded within the western Canadian Arctic (Burn et al., 1986; Burn, 1997; Kokelj et al., 2002; Kokelj and Burn, 2003; Lacelle et al., 2004; Murton et al., 2004). The variability in landscape evolution across the Mackenzie Delta region has led to heterogeneity in ground ice conditions. This variability is highlighted by the preservation potential of Pleistocene ice within ice-cored and glaciofluvial deposit terrains, in addition to the development of Holocene ice within peatlands and lacustrine environments. Today, ground ice hosted within these arctic settings is dictated by landscape preconditioning. The geologic history highlights expansive talik developments that were promoted by the early Holocene warming in conjunction with processes of post-glacial landscape evolution.

Our observations in boreholes BH-1, BH-3, BH-4, and BH-8 indicate that low-lying areas, such as lacustrine, peatland and riparian environments, have more modest ice content at depth. These environments, which favor talik formation in the early Holocene, show ice-poor epigenetic cryostructures, and relatively low visible ice and low gravimetric water contents. Conversely, areas prone to hosting basal ice, such as hummocky terrain (BH-2), tend to store ice-rich Pleistocene material. These Pleistocene deposits have ice-rich suspended cryostructures, and massive ice bodies, highlighted by the high gravimetric water content at depths underlying the early Holocene thaw unconformity.

The early Holocene warming modified the landscape significantly. Yet, modern temperatures likely exceed the Early Holocene warm interval (Porter et al., 2019). Subsequently, this previous warming has led to a decrease in excess-ice, and ice-rich sediments in the upper meters of permafrost, and hence, decreased landscape sensitivity from future warming. This decrease in ice abundance is observed near the surface (i.e., upper 4-5m) on hilltops, where Pleistocene ice and ice-rich sediments are found past the thaw unconformity. On the contrary, the widespread Early Holocene thaw, coupled with landscape evolution, has resulted in less abundant ground ice in terrains such as peatlands, lacustrine, and glaciolacustrine since waterbodies and subsequent talik development occupied these terrains.

Overall, the stratigraphy, cryostructure and water isotope analysis, coupled with geologic history, collectively suggest that this landscape has been extensively preconditioned by post-glacial landscape evolution and subsequent widespread thermokarst in the early Holocene warm interval that has reduced the abundance of ground ice. This study explores the key relations between landscape preconditioning during the early Holocene relative to excess-ice hosted within ice-rich deglaciated and periglacial landscapes. We would argue that landscapes were more vulnerable to widespread early Holocene thaw, exacerbated by thermokarst lake initiation in flat-lying areas, has resulted in less abundant ground ice. Overall, the lacustrine, glaciolacustrine, and organic deposits within this deglaciated and periglacial settings experienced significant thaw in the early Holocene, resulting in a landscape that hosts less ice and thus is protected from further thaw.

In the study area today, hilltops of hummocky and rolling terrain units are more likely to host ground ice bodies and ice-rich sediments, such as buried glacier ice and relict till. These locations, which were less likely to be influenced by thermokarst processes associated with standing water and from incomplete drainage, resulted in a landscape more likely to host Pleistocene ice. Today, where relict basal ice is preserved at depth, it is inherently more sensitive to future thermokarst trajectories (Lacelle et al., 2010; Lantuit et al., 2012; Kokelj et al., 2015). In addition, due to landscape evolution as a result of thaw lake development or fluvial incisions, through ice-cored terrain, increases the potential for destabilization and thaw of relict ice in these settings.

Further, this study has implications for future thaw trajectories. Future thermokarst is more likely to occur in areas with abundant excess ice. From our study this is most likely where relict Pleistocene deposits are near the surface, including moraine belts and hilltops in the study region.

In contrast, lowlands/flat-lying regions such as, peatlands, riparian and lacustrine terrain are likely protected from future thaw.

6. Conclusions

The study region has been generally considered to be an area of abundant ground ice, including relict, segregated and wedge ice. However, results from stratigraphy, cryostructure and water isotope analyses indicate that the excess ice landscape has considerable heterogeneity related to its geology history. This heterogeneity is primarily a function of landscape geologic history, including, first and foremost, the preservation or eradication of relict ice by natural deglaciation processes (i.e., talik development, fluvial networks, mass-wasting processes) and subsequent climatic warming during the early Holocene. Low relief zones (i.e., lacustrine, peatlands riparian zones) have sediments at depth that tend to host ice-poor, Holocene-aged sediments. On the contrary, hilltops, at depths surpassing the early Holocene thaw unconformity, likely store ice-rich, materials, including original ice-rich cryostructures and relict Laurentide ice sheet till. The diamicts in BH-1, BH-3 and BH-4 are interpreted as melt-out till modified by thawing and refreezing with Holocene pore waters. A preliminary ice-rich – dominated with massive ice – Pleistocene landscape was subsequently disrupted by the post-glacial landscape evolution and the Holocene Thermal Maximum, causing thaw degradation. This original material was reworked and lost the original Pleistocene ice, by talik or thermokarst lake formation. Once the landscape stabilized, it allowed for vegetation and permafrost to aggrade. These ice-poor diamicts have since highly become ice-poor with Holocene waters.

The early Holocene warming in the northwestern Arctic was extensive and modified the landscape resulting in much of the area being less ice rich. Overall, the association between excess-ice in hilltops and relatively less ground ice within flat-lying terrain indicates the early Holocene warming has been a significant preconditioning mechanism. Much of the landscape observed today is likely less ice-rich, and less susceptible to future thaw relative to present warming conditions. This is highlighted in our data, where at least 10m of early Holocene thaw occurred in low relief terrains, while perhaps half that amount occurred in high relief areas, such as hummocky terrain.

Results from this study indicate the role of past landscape histories and their impacts may influence thaw trajectories at a local scale. We suggest low relief and flat terrains, with thick organic cover coupled with permafrost hosting minimal excess ice, may not be as severely impacted by near-future warming relative to landscape positions where Pleistocene ice-rich material is prevalent. Unalike, hilltops, especially ice-cored hilltops, storing primary tills and vast quantities of excess ice, may become hot spots for future thermokarst degradation. Future work will use surficial geology mapping, and site investigations to evaluate stratigraphy, geochemistry to understand the distribution of ground ice its future thermokarst implications across the Mackenzie Delta region and similar landscapes.

References:

Associate Committee on Geotechnical Research National (ACGR), 1988, Glossary of Permafrost and Related Ground-Ice Terms: National Research Council of Canada, v. Technical, p. 156, doi:10.4224/20378888.

Benn, D.I., and Evans, D.J.A., 2010, Glaciers and Glaciation, 2nd edition: Hodder Arnold Publication, 816 p., doi:https://doi.org/10.4324/9780203785010.

Boaretto, E. et al., 2002, Summary findings of the fourth international radiocarbon intercomparison (FIRI)(1998–2001): Journal of Quaternary Science, v. 17, p. 633–637, doi:10.1002/JQS.702.

Bronk Ramsey, C., 2009, Bayesian Analysis of Radiocarbon Dates: Radiocarbon, v. 51, p. 337–360, doi:10.1017/s0033822200033865.

Burn, C.R., 1997, Cryostratigraphy, paleogeography, and climate change during the early Holocene warm interval, western Arctic coast, Canada: Canadian Journal of Earth Sciences, v. 34, p. 912–925, doi:10.1139/e17-076.

Burn, C.R., and Kokelj, S. V., 2009, The environment and permafrost of the Mackenzie Delta area: Permafrost and Periglacial Processes, v. 20, p. 83–105, doi:10.1002/ppp.655.

Burn, C.R., Michel, F.A., and Smith, M.W., 1986, Stratigraphic, isotopic, and mineralogical evidence for an early Holocene thaw unconformity at Mayo, Yukon Territory.: Canadian Journal of Earth Sciences, v. 23, p. 794–803, doi:10.1139/e86-081.

Duk-Rodkin, A., and Lemmen, D.S., 2000, Glacial history of the Mackenzie region: Bulletin of the Geological Survey of Canada, p. 11–20, doi:10.4095/211903.

Dyke, A.S., and Evans, D.J.A., 2003, Ice-marginal terrestrial landsystems: Northern laurentide and innuitian ice sheet margins, *in* London, A. ed., Glacial Landsystems, p. 143–165, doi:10.4324/9780203784976.

Ensom, T., Morse, P.D., Kokelj, S. V, Macdonald, E., Young, J., Tank, S., Grozic, E., and Castagner, A., 2020, Permafrost geotechnical borehole data synthesis: 2013‒2017 Inuvik-Tuktoyaktuk region, Northwest Territories; Northwest Territories Geological Survey, NWT Open Report 2019-012; Geological Survey of Canada, Open File 8652.:

French, H., 2007, The Periglacial Environment, 3rd edn: Wiley, Chichester, 458 p.

French, H., and Shur, Y., 2010, The principles of cryostratigraphy: Earth-Science Reviews, v. 101, p. 190–206, doi:10.1016/j.earscirev.2010.04.002.

Fritz, M., Wetterich, S., Mcalister, J., and Meyer, H., 2022, A new local meteoric water line for Inuvik (NT, Canada): Earth System Science Data, v. 14, p. 57–63, doi:10.5194/essd-14-57-2022.

Gilbert, G.L., Kanevskiy, M., and Murton, J.B., 2016, Recent Advances (2008–2015) in the Study of Ground Ice and Cryostratigraphy, *in* Permafrost and Periglacial Processes, v. 27, p. 377–389, doi:10.1002/ppp.1912.

Harry, D.G., French, H.M., and Pollard, W.H., 1988, Massive ground ice and ice-cored terrain near Sabine Point, Yukon coastal plain: Canadian Journal of Earth Sciences, v. 25, p. 1846–1856, doi:10.1139/e88-174.

Hill, P.R., 1996, Late Quaternary sequence stratigraphy of the Mackenzie Delta: Canadian Journal of Earth Sciences, v. 33, p. 1064–1074, doi:10.1139/e96-081.

Holland, K.M., Porter, T.J., Froese, D.G., Kokelj, S. V., and Buchanan, C.A., 2020, Ice-Wedge Evidence of Holocene Winter Warming in the Canadian Arctic: Geophysical Research Letters, v. 47, p. e2020GL087942, doi:10.1029/2020GL087942.

Hughes, O.L., 1987, Late Wisconsinan Laurentide glacial limits of northwestern Canada: the Tutsieta Lake and Kelly Lake phases: Geological Survery of Canada, p. 25, doi:10.4095/122385.

Jorgenson, M.T., Shur, Y.L., and Pullman, E.R., 2006, Abrupt increase in permafrost degradation in Arctic Alaska: Geophysical Research Letters, v. 33, p. 2–5, doi:10.1029/2005GL024960.

Kanevskiy, M., Jorgenson, T., Shur, Y., O'Donnell, J.A., Harden, J.W., Zhuang, Q., and Fortier, D., 2014, Cryostratigraphy and Permafrost Evolution in the Lacustrine Lowlands of West-Central Alaska: Permafrost and Periglacial Processes, v. 25, p. 14–34, doi:10.1002/ppp.1800.

Kanevskiy, M., Shur, Y., Jorgenson, M.T., Ping, C.L., Michaelson, G.J., Fortier, D., Stephani, E., Dillon, M., and Tumskoy, V., 2013, Ground ice in the upper permafrost of the Beaufort Sea coast of Alaska: Cold Regions Science and Technology, v. 85, p. 56–70, doi:10.1016/j.coldregions.2012.08.002.

Kokelj, S. V., and Burn, C.R., 2003, Ground ice and soluble cations in near-surface permafrost, Inuvik, Northwest Territories, Canada: Permafrost and Periglacial Processes, v. 14, p. 275–289, doi:10.1002/ppp.458.

Kokelj, S. V., Jenkins, R.E., Milburn, D., Burn, C.R., and Snow, N., 2005, The influence of thermokarst disturbance on the water quality of small upland lakes, Mackenzie Delta region, Northwest Territories, Canada: Permafrost and Periglacial Processes, v. 16, p. 343–353, doi:10.1002/ppp.536.

Kokelj, S. V., Lantz, T.C., Kanigan, J., Smith, S.L., and Coutts, R., 2009a, Origin and polycyclic behaviour of tundra thaw slumps, Mackenzie Delta region, Northwest Territories, Canada: Permafrost and Periglacial Processes, v. 20, p. 173–184, doi:10.1002/ppp.642.

Kokelj, S. V., Lantz, T.C., Wolfe, S.A., Kanigan, J.C., Morse, P.D., Coutts, R., Molina-Giraldo, N., and Burn, C.R., 2014, Distribution and activity of ice wedges across the forest-tundra transition, western arctic Canada: Journal of Geophysical Research: Earth Surface, v. 119, p. 2032–2047, doi:10.1002/2014JF003085.

Kokelj, S. V., Palmer, M.J., Lantz, T.C., and Burn, C.R., 2017, Ground Temperatures and Permafrost Warming from Forest to Tundra, Tuktoyaktuk Coastlands and Anderson Plain, NWT, Canada: Permafrost and Periglacial Processes, v. 28, p. 543–551, doi:10.1002/PPP.1934.

Kokelj, S. V, Pisaric, M.F.J., and Burn, C.R., 2007, Cessation of ice-wedge development during the 20th century in spruce forests of eastern Mackenzie Delta, Northwest Territories, Canada: Canadian Journal of Earth Sciences, v. 44, p. 1503–1515, doi:10.1139/E07-035.

Kokelj, S. V., Smith, C.A.S., and Burn, C.R., 2002, Physical and chemical characteristics of the active layer and permafrost, Herschel Island, western Arctic Coast, Canada: Permafrost and Periglacial Processes, v. 13, p. 171–185, doi:10.1002/ppp.417.

Kokelj, S. V., Tunnicliffe, J., Lacelle, D., Lantz, T.C., Chin, K.S., and Fraser, R., 2015, Increased precipitation drives mega slump development and destabilization of ice-rich permafrost terrain, northwestern Canada: Global and Planetary Change, v. 129, p. 56–68, doi:10.1016/j.gloplacha.2015.02.008.

Kokelj, S. V., Zajdlik, B., and Thompson, M.S., 2009b, The impacts of Thawing permafrost on the chemistry of lakes across the subarctic boreal-tundra transition, Mackenzie Delta region, Canada: Permafrost and Periglacial Processes, v. 20, p. 185–199, doi:10.1002/ppp.641.

Lacelle, D., Bjornson, J., and Lauriol, B., 2010, Climatic and geomorphic factors affecting contemporary (1950-2004) activity of retrogressive thaw slumps on the Aklavik plateau, Richardson mountains, NWT, Canada: Permafrost and Periglacial Processes, v. 21, p. 1–15, doi:10.1002/ppp.666.

Lacelle, D., Bjornson, J., Lauriol, B., Clark, I.D., and Troutet, Y., 2004, Segregated-intrusive ice of subglacial meltwater origin in retrogressive thaw flow headwalls, Richardson Mountains, NWT, Canada: Quaternary Science Reviews, v. 23, p. 681–696, doi:10.1016/j.quascirev.2003.09.005.

Lacelle, D., Brooker, A., Fraser, R.H., and Kokelj, S. V., 2015, Distribution and growth of thaw slumps in the Richardson Mountains-Peel Plateau region, northwestern Canada: Geomorphology, v. 235, p. 40–51, doi:10.1016/j.geomorph.2015.01.024.

Lacelle, D., and Vasil'chuk, Y.K., 2013, Recent progress (2007-2012) in permafrost isotope geochemistry: Permafrost and Periglacial Processes, v. 24, p. 138–145, doi:10.1002/ppp.1768.

Lantuit, H., and Pollard, W.H., 2008, Fifty years of coastal erosion and retrogressive thaw slump activity on Herschel Island, southern Beaufort Sea, Yukon Territory, Canada: Geomorphology, v. 95, p. 84–102, doi:10.1016/j.geomorph.2006.07.040.

Lantuit, H., Pollard, W.H., Couture, N., Fritz, M., Schirrmeister, L., Meyer, H., and Hubberten, H.W., 2012, Modern and Late Holocene Retrogressive Thaw Slump Activity on the Yukon Coastal Plain and Herschel Island, Yukon Territory, Canada: Permafrost and Periglacial Processes, v. 23, p. 39–51, doi:10.1002/ppp.1731.

Lantz, T.C., and Kokelj, S. V., 2008, Increasing rates of retrogressive thaw slump activity in the Mackenzie Delta region, N.W.T., Canada: Geophysical Research Letters, v. 35, p. 1–5, doi:10.1029/2007GL032433.

Lee, H., Swenson, S.C., Slater, A.G., and Lawrence, D.M., 2014, Effects of excess ground ice on projections of permafrost in a warming climate: Environmental Research Letters, v. 9, p. 124006, doi:10.1088/1748-9326/9/12/124006.

Mackay, J.R., 1995, Active layer changes (1968 to 1993) following the forest-tundra fire near Inuvik, NWT, Canada: Arctic and Alpine Research, v. 27, p. 323–336, doi:10.2307/1552025.

Mackay, R.J., 1970, Disturbances to the tundra and forest tundra environment of the western Arctic: Canadian Geotechnical Journal, v. 7, p. 420–432, doi:10.1139/t70-054.

Mackay, J.R., 1983, Downward water movement into frozen ground, western arctic coast, Canada.: Canadian Journal of Earth Sciences, v. 20, p. 120–134, doi:10.1139/e83-012.

Mackay, J.R., 1978, Freshwater shelled invertebrate indicators of paleoclimate in northwestern Canada during late glacial times: Discussion: Canadian Journal of Earth Sciences, v. 15, p. 461–462.

Mackay, J.R., 1979, Pingos of the Tuktoyaktuk Peninsula area, Northwest Territories.: Geographie Physique et Quaternaire, v. 33, p. 3–62, doi:10.7202/1000322ar.

Mackay, J.R., 1990, Some observations on the growth and deformation of epigenetic, syngenetic and anti-syngenetic ice wedges: Permafrost and Periglacial Processes, v. 1, p. 15–29, doi:10.1002/ppp.3430010104.

Mackay, J.R., 1963, The Mackenzie delta area, Northwestern Territories: 202 p., https://books.google.ca/books/about/The_Mackenzie_Delta_Area_N_W_T.html?id=Zzr-vgEACAAJ&redir_esc=y (accessed July 2022).

Mackay, J.R., 1972, The World Of Underground Ice: Annals of the Association of American Geographers, v. 62, p. 1–22, doi:10.1111/j.1467-8306.1972.tb00839.x.

Mackay, J.R., and Dallimore, S.R., 1992, Massive ice of the Tuktoyaktuk area, western Arctic coast, Canada: Canadian Journal of Earth Sciences, v. 29, p. 1235–1249, doi:10.1139/e92-099.
Morse, P.D., and Burn, C.R., 2013, Field observations of syngenetic ice wedge polygons, outer Mackenzie Delta, western Arctic coast, Canada: Journal of Geophysical Research: Earth Surface, v. 118, p. 1320–1332, doi:10.1002/jgrf.20086.
Murton, J.B., 2008, Global Warming and Thermokarst, *in* Permafrost Soils, Springer, Berlin, Heidelberg, p. 185–203, doi:10.1007/978-3-540-69371-0_13.
Murton, J.B., 2005, Ground-ice stratigraphy and formation at North Head, Tuktoyaktuk Coastlands, western Arctic Canada: A product of glacier-permafrost interactions: Permafrost and Periglacial Processes, v. 16, p. 31–50, doi:10.1002/ppp.513.
Murton, J.B., 2013, Ground Ice and Cryostratigraphy, *in* Treatise on Geomorphology, v. 8, p. 173–201, doi:10.1016/B978-0-12-374739-6.00206-2.
Murton, J.B., 2001, Thermokarst sediments and sedimentary structures, Tuktoyaktuk Coastlands, western Arctic Canada: Global and Planetary Change, v. 28, p. 175–192, doi:10.1016/S0921-8181(00)00072-2.
Murton, J.B., Bateman, M.D., Waller, R.I., Sciences, G., and Whiteman, C.A., 2015, Late Wisconsin glaciation of Hadwen and Summer islands , Tuktoyaktuk Coastlands ,: 68e Conférence Canadienne de Géotechnique et 7e Conférence Canadienne sur le Pergélisol, 20 au 23 septembre 2015, Québec, Québec.,.
Murton, J.B., Frechen, M., and Maddy, D., 2007, Luminescence dating of mid- to Late Wisconsinan aeolian sand as a constraint on the last advance of the Laurentide Ice Sheet across the Tuktoyaktuk Coastlands, western Arctic Canada: Canadian Journal of Earth Sciences, v. 44, p. 857–869, doi:10.1139/E07-015.
Murton, J.B., and French, H.M., 1994, Cryostructures in permafrost, Tuktoyaktuk coastlands, western Arctic Canada: Canadian Journal of Earth Sciences, v. 31, p. 737–747, doi:10.1139/e94-067.
Murton, J.B., and French, H.M., 1993a, Thaw modification of frost-fissure wedges, Richards Island, Pleistocene Mackenzie Delta, Western Arctic Canada: Journal of Quaternary Science, v. 8, p. 185–196, doi:10.1002/jqs.3390080302.
Murton, J.B., and French, H.M., 1993b, Thermokarst involutions, summer island, pleistocene mackenzie delta, Western Canadian arctic: Permafrost and Periglacial Processes, v. 4, p. 217–229, doi:10.1002/ppp.3430040304.
Murton, J.B., Waller, R.I., Hart, J.K., Whiteman, C.A., Pollard, W.H., and Clark, I.D., 2004, Stratigraphy and glaciotectonic structures of permafrost deformed beneath the northeast margin of the Laurentide ice sheet, Tuktoyaktuk Coastlands, Canada: Journal of Glaciology, v. 50, p. 399–412.
Murton, J.B., Whiteman, C.A., Waller, R.I., Pollard, W.H., Clark, I.D., and Dallimore, S.R., 2005, Basal ice facies and supraglacial melt-out till of the Laurentide Ice Sheet, Tuktoyaktuk Coastlands, western Arctic Canada: Quaternary Science Reviews, v. 24, p. 681–708, doi:10.1016/j.quascirev.2004.06.008.
O'Neill, H.B. et al., 2020, Permafrost thaw and northern development: Nature Climate Change, v. 10, p. 722–723, doi:10.1038/s41558-020-0862-5.
O'Neill, H.B., Smith, S.L., and Duchesne, C., 2019a, Long-Term Permafrost Degradation and Thermokarst Subsidence in the Mackenzie Delta Area Indicated by Thaw Tube Measurements, *in* American Society of Civil Engineers (ASCE), p. 643–651,

doi:10.1061/9780784482599.074.
O'Neill, H.B., Wolfe, S.A., and Duchesne, C., 2019b, New ground ice maps for Canada using a paleogeographic modelling approach: Cryosphere, v. 13, p. 753–773, doi:10.5194/tc-13-753-2019.
Pollard, W.H., and French, H.M., 1980, A first approximation of the volume of ground ice, Richards Island, Pleistocene Mackenzie delta, Northwest Territories, Canada.: Canadian Geotechnical Journal, v. 17, p. 509–516, doi:10.1139/t80-059.
Porter, T.J., Schoenemann, S.W., Davies, L.J., Steig, E.J., Bandara, S., and Froese, D.G., 2019, Recent summer warming in northwestern Canada exceeds the Holocene thermal maximum: Nature Communications, v. 10, doi:10.1038/s41467-019-09622-y.
Rampton, V.N., 1988, Quaternary Geology of the Tuktoyaktuk Coastlands, Northwest Territories: Geological Survey of Canada, p. 1–107, doi:10.1126/science.ns-6.149S.521-a.
Reyes, A. V, Jensen, B.J.L., Zazula, G.D., Ager, T.A., Kuzmina, S., La Farge, C., and Froese, D.G., 2010, A late-Middle Pleistocene (Marine Isotope Stage 6) vegetated surface buried by Old Crow tephra at the Palisades, interior Alaska: Quaternary Science Reviews, v. 29, p. 801–811, doi:10.1016/j.quascirev.2009.12.003.
Segal, R.A., Lantz, T.C., and Kokelj, S. V., 2016, Acceleration of thaw slump activity in glaciated landscapes of the Western Canadian Arctic: Environmental Research Letters, v. 11, doi:10.1088/1748-9326/11/3/034025.
Shur, Y., and Jorgenson, M., 1998, Cryostructure development on the floodplain of the Colville River Delta, northern Alaska: Permafrost, Seventh International Conference, p. 993–999, http://www.arlis.org/docs/vol1/ICOP/40770716/CD-ROM/Proceedings/PDF001189/150193.pdf.
Zazula, G.D., MacKay, G., Andrews, T.D., Shapiro, B., Letts, B., and Brock, F., 2009, A late Pleistocene steppe bison (Bison priscus) partial carcass from Tsiigehtchic, Northwest Territories, Canada: Quaternary Science Reviews, v. 28, p. 2734–2742, doi:10.1016/j.quascirev.2009.06.012.

Table 4.1: Summary of location and elevation of BH-1, BH-2, BH-3, BH-4 and BH-8. Additionally, the terrain and surrounding vegetation, and surficial geologic units, modified from (Rampton, 1988)

Borehole	GPS Coordinates	Elevation (m)	Terrain	Vegetation	Surficial Geology Unit
BH-1	68° 32′ 18.25″N, 133° 46′ 22.94″W	92	Patterned ground Peatland	Tall-shrub tundra	Organic overlying hummocky till
BH-2	68° 32′ 16.3″N, 133° 45′ 44.24″W	106	Hummocky hilltop	Tall-shrub tundra	Hummocky till
BH-3	68° 32′ 16.0"N, 133° 45′ 46.32″W	96	Riparian zone	Tall and Dwarf shrub tundra	Organic overlying hummocky till
BH-4	68° 44′ 52.8″N, 133° 32′ 28.61″W	88	Patterned ground Peatland	Tall and Dwarf shrub tundra	Organic overlying hummocky till
BH-8	69° 0′ 49.1″N, 133° 16′ 22.83″W	14	Patterned ground Peatland	Dwarf-shrub tundra	Organic overlying Glaciolacustrine

Table 4.2: Summary of Units, average gravimetric water content (GWC) and Cryostructures within the Boreholes

Site	*Unit*	*Depth Interval (m)*	*Average GWC (%)*	*n*	*Cryostructures*	*Thickness of ice (cm)*
BH-1	Peat	0.0 – 2.2	417	4	Organic-Matrix	-
	Massive Ice	2.2 – 6.8	8500	8	Solid (Massive Ice)	-
	Ice-poor Diamict	6.8 – 11.2	33	10	Lenticular, Layered, Reticulate	1 - 5
BH-2	Peat	0.0 – 2.0	54	5	Organic-Matrix	-
	Gravelly Sand	2.0 – 11.5	318	19	-	-
	Ice-rich Diamict	11.5 – 19.6	611	17	Lenticular, Layered, Structureless	1 - 30
BH-3	Woody Organic	0.0 – 2.4	600	5	Crustal	1 - 5
	Ice-poor Diamict	2.4 – 10.3	38	16	Lenticular, Suspended	1 - 10
BH-4	Peat	0 – 4.1	541	10	Organic-Matrix	-
	Silt and Clay	4.1 – 6.2	98	4	Lenticular	1 - 5
	Ice-poor Diamict	6.2 – 7.7	24	7	Lenticular, Layered, Reticulate	1 - 5
BH-8	Peat	0 – 4.3	168	9	Organic-Matrix	-
	Silt and Clay	4.3 – 11.4	63	14	Lenticular, Layered, Reticulate	1 - 7

Table 4.3: Radiocarbon dates for three boreholes.

Analysis done by A.E Lalonde AMS Laboratory, University of Ottawa. Dates calibrated using OxCal v4.2.4 (Bronk Ramsey, 2009) and IntCal13/Bomb 13 calibration. Last two samples, FIRI F and AVR-PAL, are two radiocarbon standards used in this study. FIRI F is a wood sample with a consensus age estimate of ca 4565 ^{14}C yr BP (Boaretto et al., 2002). AVR-PAL is a wood sample with a non-finite consensus age (Reyes et al., 2010b).

Lab ID	Depth (m)	Unit	Material	Location	Age (^{14}C yr BP)	Sample ID
UOC-5201	2.1	Peat	Mixed Plant Macrofossils	BH-1 (Peatland)	3778 ± 26	BH1-60
UOC-5202	7.0	Ice-poor diamict	Mixed Plant Macrofossils	BH-1 (Peatland)	13866 ± 41	BH1-141
UOC-5204	4.6	Clay and Silt	Mixed Plant Macrofossils	BH-4 (Peatland)	10887 ± 50	BH4-92
UOC-5203	4.1	Peat	Wood	BH-8 (Peatland)	8074 ± 25	BH8-75
UOC-5206	11.3	Clay and Silt	Wood	BH-8 (Peatland)	10003 ± 32	BH8-11.3
UOC-5199	-	Standard	Wood		4565 ± 25	FIRI F
UOC-5200	-	Standard	Wood		Non-finite	AVR07-PAL

Table 4.4: Summary of and water isotopes for all five boreholes.

Site	***Unit***	***δD (±1σ) ‰***	***δ¹⁸O (±1σ) ‰***	***d-excess (±1σ) ‰***	***δD-δ¹⁸O***		
					Slope	Intercept	R^2
BH-1	Peat	-152.7 ± 6.2	-18.9 ± 0.9	-2 ± 5	5.9	– 42	0.54
	Massive Ice	-189.5 ± 22.4	-23.5± 3.1	-2 ± 4	7.1	– 23	0.98
	Ice-poor Diamict	-169.1 ± 2.3	-19.8 ± 0.5	-11 ± 3	3.2	– 106	0.57
BH-2	Peat	-174.2 ± 7.2	-22.6 ± 0.7	7.2 ± 2	-	-	-
	Gravelly Sand	-233.1± 11.8	-28.7 ± 2.5	-3.9 ± 9	4.6	– 102	0.97
	Ice-rich Diamict	-228.8± 2.9	29.0 ± 0.5	2.8 ± 1	5.8	– 61	0.93
BH-3	Peat	-148.3± 2.0	-17.5 ± 0.5	-8± 2	4.1	– 76	0.77
	Ice-poor Diamict	-164.7± 9.5	-19.8 ± 1.2	-6± 1	7.5	– 15	0.98
BH-4	Peat	-163.0 ± 1.3	-20.5± 0.4	1 ± 2	7.2	– 13	0.76
	Clay and Silt	-166.2 ± 2.2	-19.6 ± 0.2	-10 ± 3	-	-	-
	Ice-poor Diamict	-164.8 ± 1.6	-18.9 ± 0.4	-14 ± 2	3.9	– 92	0.82
BH-8	Peat	-157.9 ± 12.4	-19.96± 1.5	-1 ± 4	8.0	–1	0.96
	Clay and Silt	-151.2 ± 5.4	-17.1 ± 1.2	-14 ± 4	4.6	– 72	0.98

Figure 4.1: Location of the Inuvik-Tuktoyaktuk Highway transecting the five boreholes analyzed in this study., BH-1, BH-2, BH-3, BH-4 and BH-8. Figures 4.1a-c shows the 1m resolution Lidar, provided by the GNWT Geomatics, to highlight topography across these boreholes.

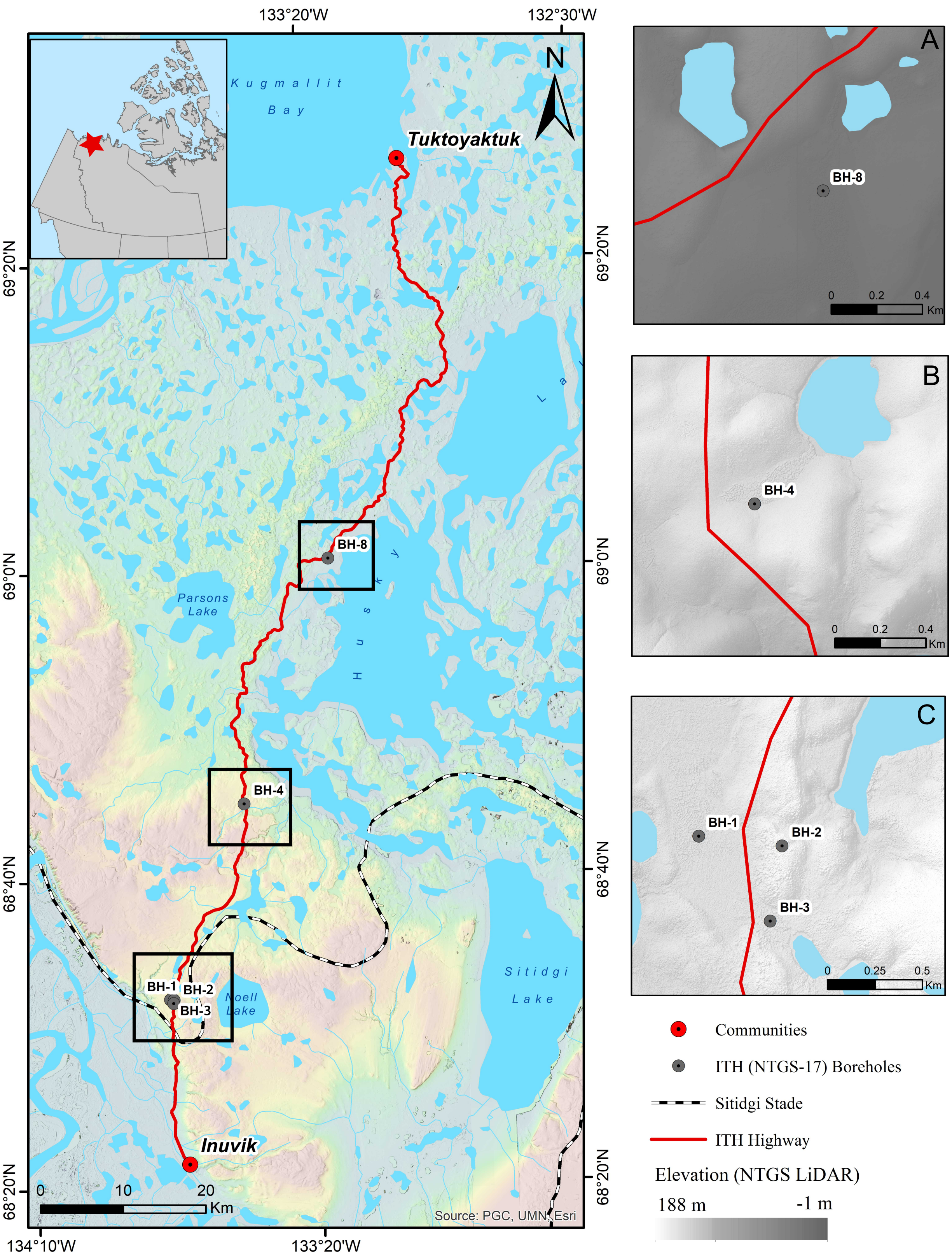

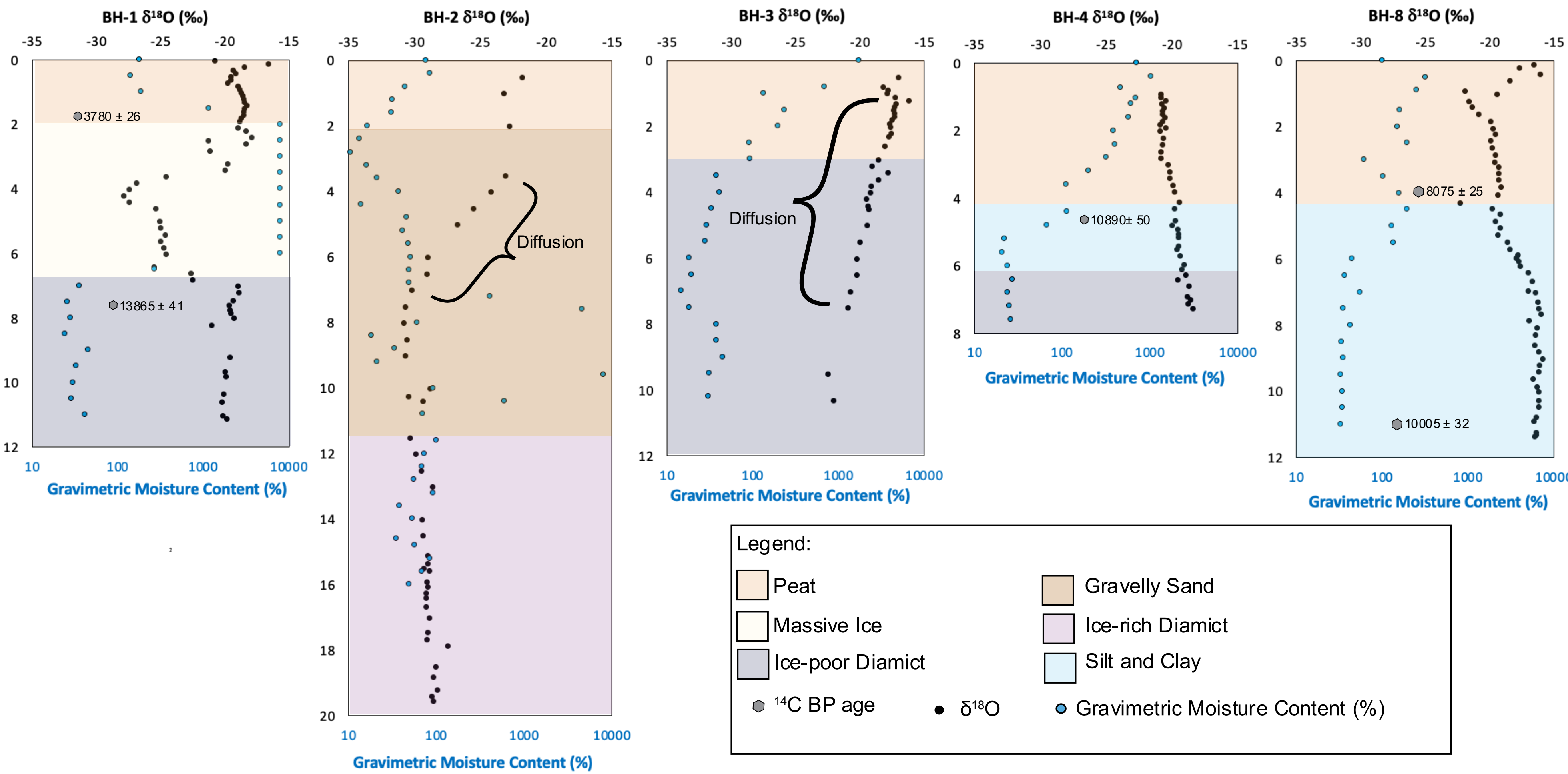

Figure 4.2: Summary of Boreholes: δ^{18}O profiles and ^{14}C dates from BH-1, BH-2, BH-3, BH-4 and BH-8

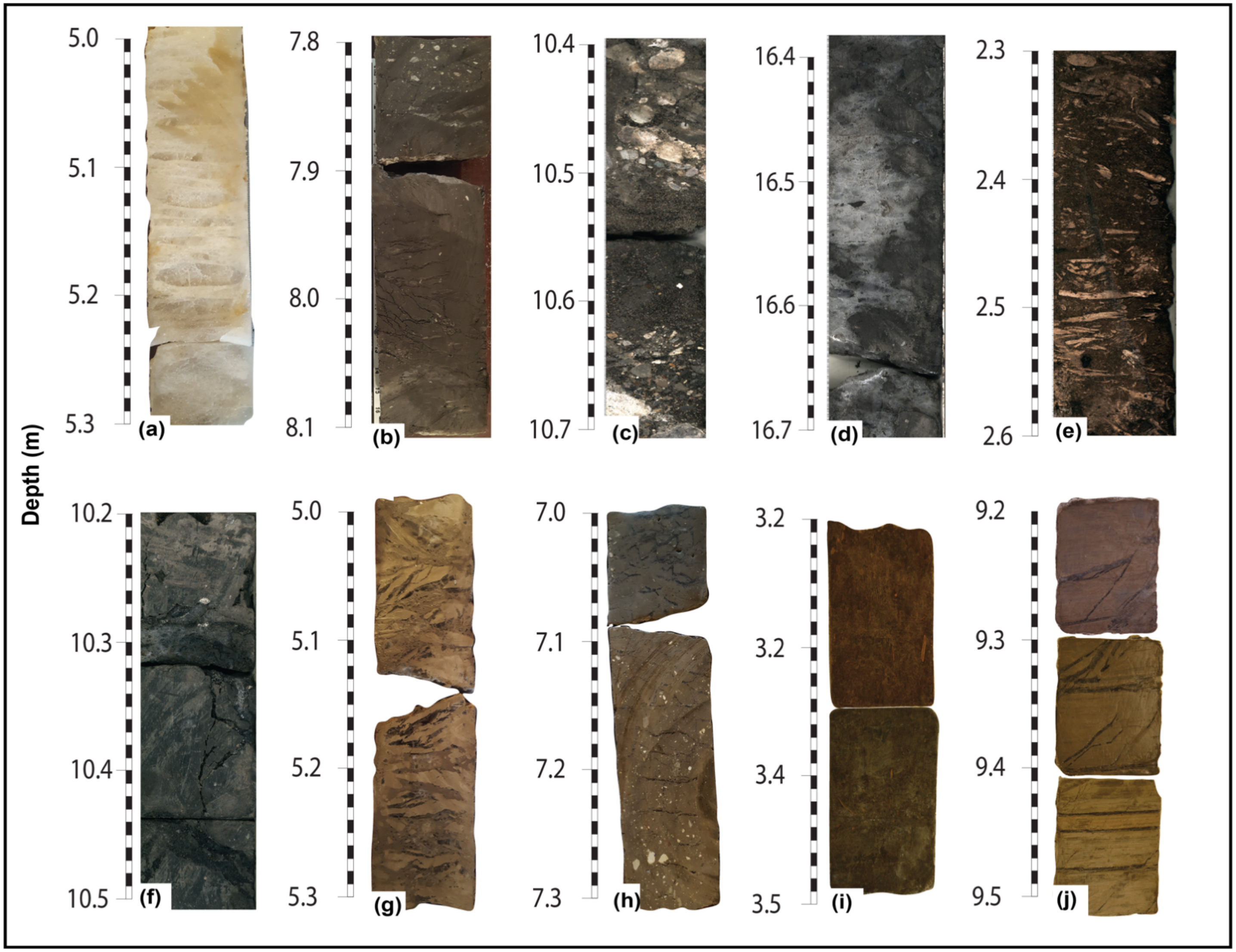

Figure 4.3: Representative core segments highlining different stratigraphic units and cryostructures. (a) Massive Ice unit in BH-1. (b) Ice-poor diamict with lenticular cryostructures in BH-1. **(c)** Gravelly sand unit in BH-2 showcasing normal grading with almost no pore-ice. **(d)** Ice-rich diamict in BH-2 highlighting suspended ice. **(e)** Organic-rich unit in BH-3. **(f)** ice-poor diamict with vertical lenses in BH-3. **(g)** Silt and clay unit in BH-4 with lenticular cryostructures. **(h)** Ice-poor diamict in BH-4 highlighting small lenticular and reticulate cryostructures. **(i)** peat unit in BH-8**.** **(j)** Silt and clay unit in BH-8 illustrating parallel layered cryostructures, both horizontal following bedding plane, and vertical layers.

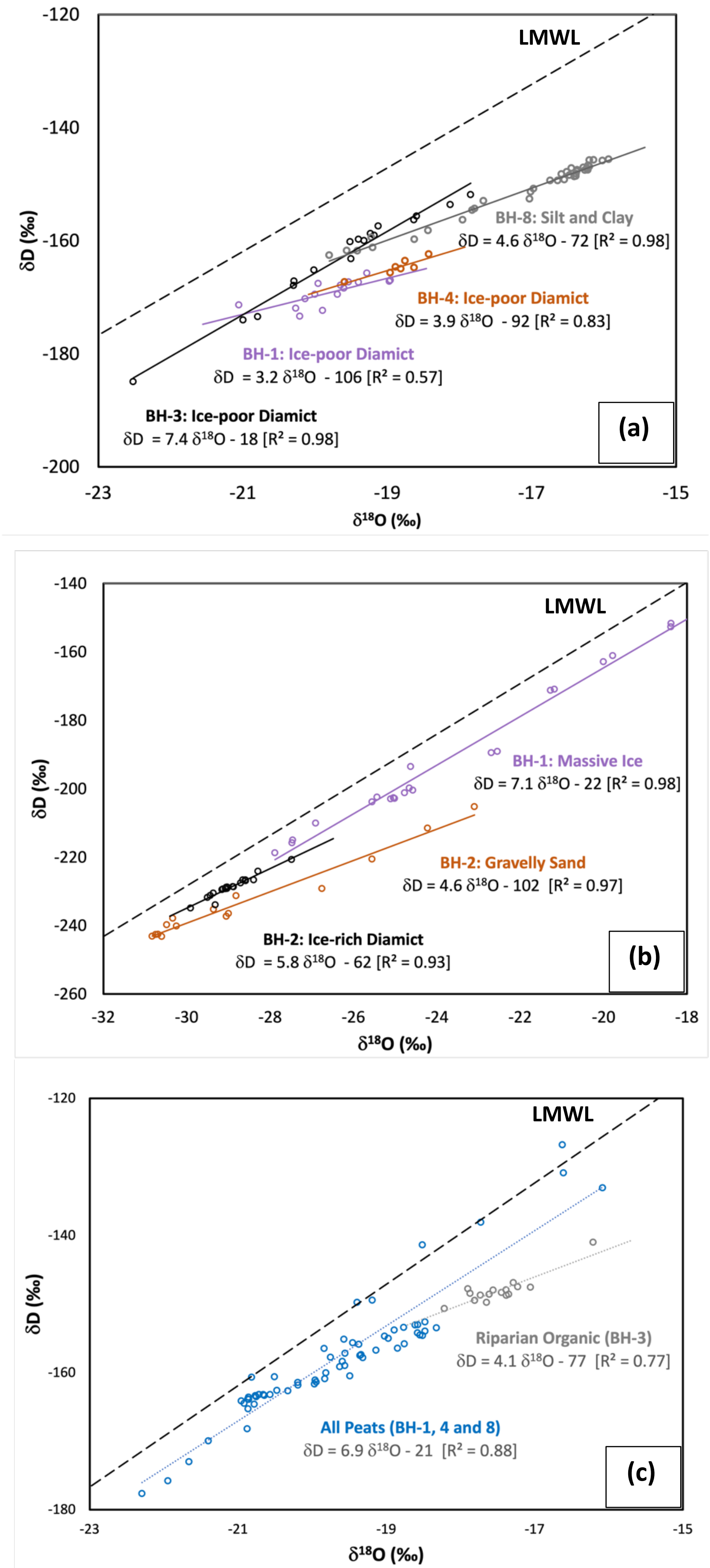

LMWL
BH-8: Silt and Clay
$\delta D = 4.6\ \delta^{18}O - 72$ [$R^2 = 0.98$]
BH-4: Ice-poor Diamict
$\delta D = 3.9\ \delta^{18}O - 92$ [$R^2 = 0.83$]
BH-1: Ice-poor Diamict
$\delta D = 3.2\ \delta^{18}O - 106$ [$R^2 = 0.57$]
BH-3: Ice-poor Diamict
$\delta D = 7.4\ \delta^{18}O - 18$ [$R^2 = 0.98$]
(a)
δD (‰)
$\delta^{18}O$ (‰)
LMWL
BH-1: Massive Ice
$\delta D = 7.1\ \delta^{18}O - 22$ [$R^2 = 0.98$]
BH-2: Gravelly Sand
$\delta D = 4.6\ \delta^{18}O - 102$ [$R^2 = 0.97$]
BH-2: Ice-rich Diamict
$\delta D = 5.8\ \delta^{18}O - 62$ [$R^2 = 0.93$]
(b)
δD (‰)
$\delta^{18}O$ (‰)
LMWL
Riparian Organic (BH-3)
$\delta D = 4.1\ \delta^{18}O - 77$ [$R^2 = 0.77$]
All Peats (BH-1, 4 and 8)
$\delta D = 6.9\ \delta^{18}O - 21$ [$R^2 = 0.88$]
(c)
δD (‰)
$\delta^{18}O$ (‰)

Figure 4.4 : Co-isotopes illustrating regression slopes ($S_{D\text{-}18O}$) from all the units within all five boreholes. **(a)** Co-isotopes plots for the isotopically enriched silt and clay, and ice-poor diamicts in BH-1, BH-3, BH-4 and BH-8. **(b)** Co-isotopes plots for the isotopically depleted massive ice, gravelly sand, and ice-rich diamicts in BH-1 and BH-2. **(c)** Co-isotopes plots for the peat units within BH-1, BH-4 and BH-8, and organic-rich unit in BH-3.

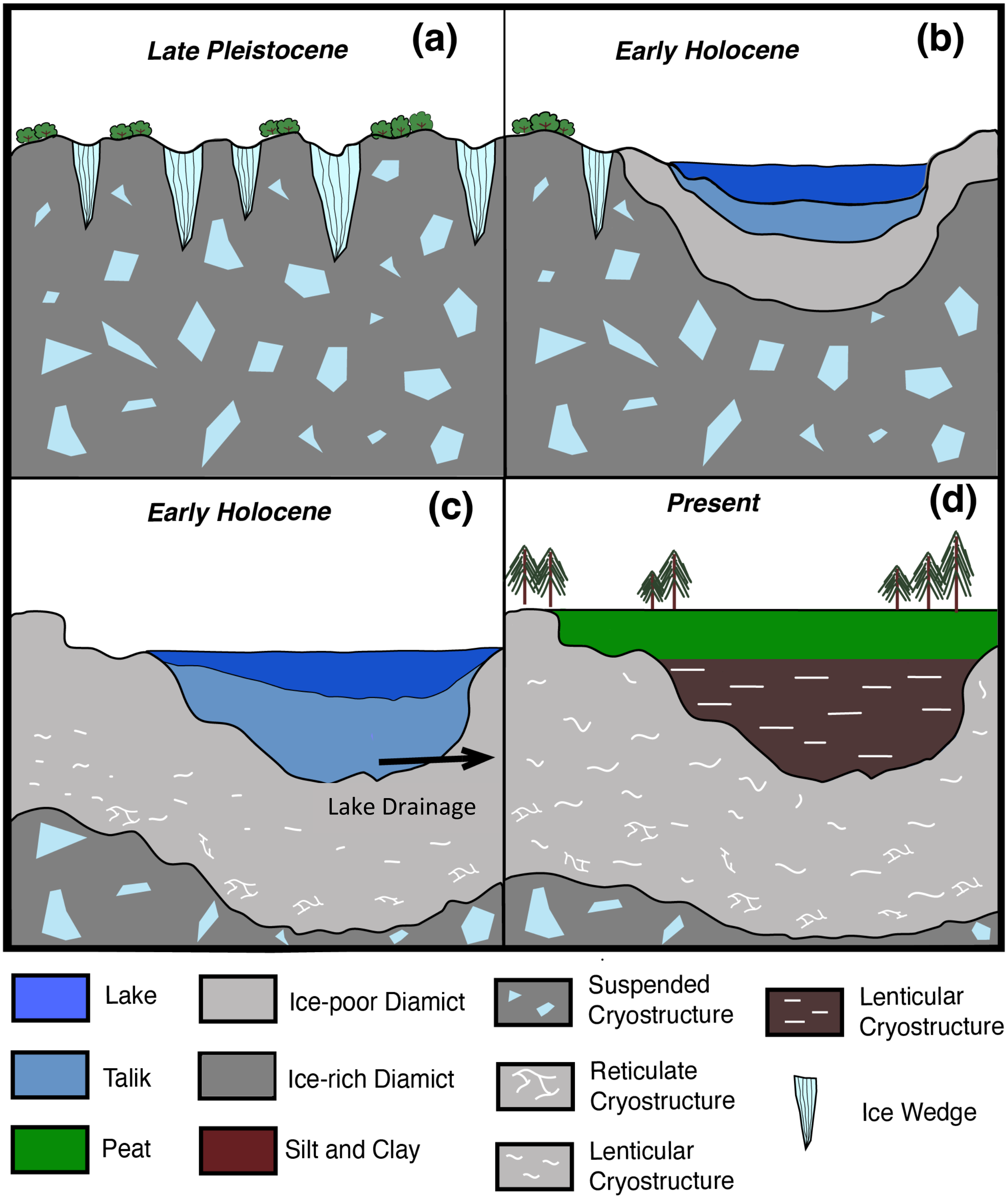

Figure 4.5: Schematic representation of Low relief areas: BH-1, BH-3, BH-4 and BH-8

(a) Massive Pleistocene ice wedges underwent permafrost degradation, forming a hummocky surface; **(b)** a thermokarst lake is formed due to coalescence of small pods, subsequent talik develops beneath thermokarst lake and relict ice-rich Pleistocene material thaws; **(c)** Deepening of active layer, initiation of thermokarst lake drainage and continuous deposition of lake sediments; **(d)** fully drained thermokarst lake promotes the rapid infilling of syngenetic peat , permafrost regrades with ice-poor reticulate and layered within redeposited tills and lacustrine sediments, respectively.

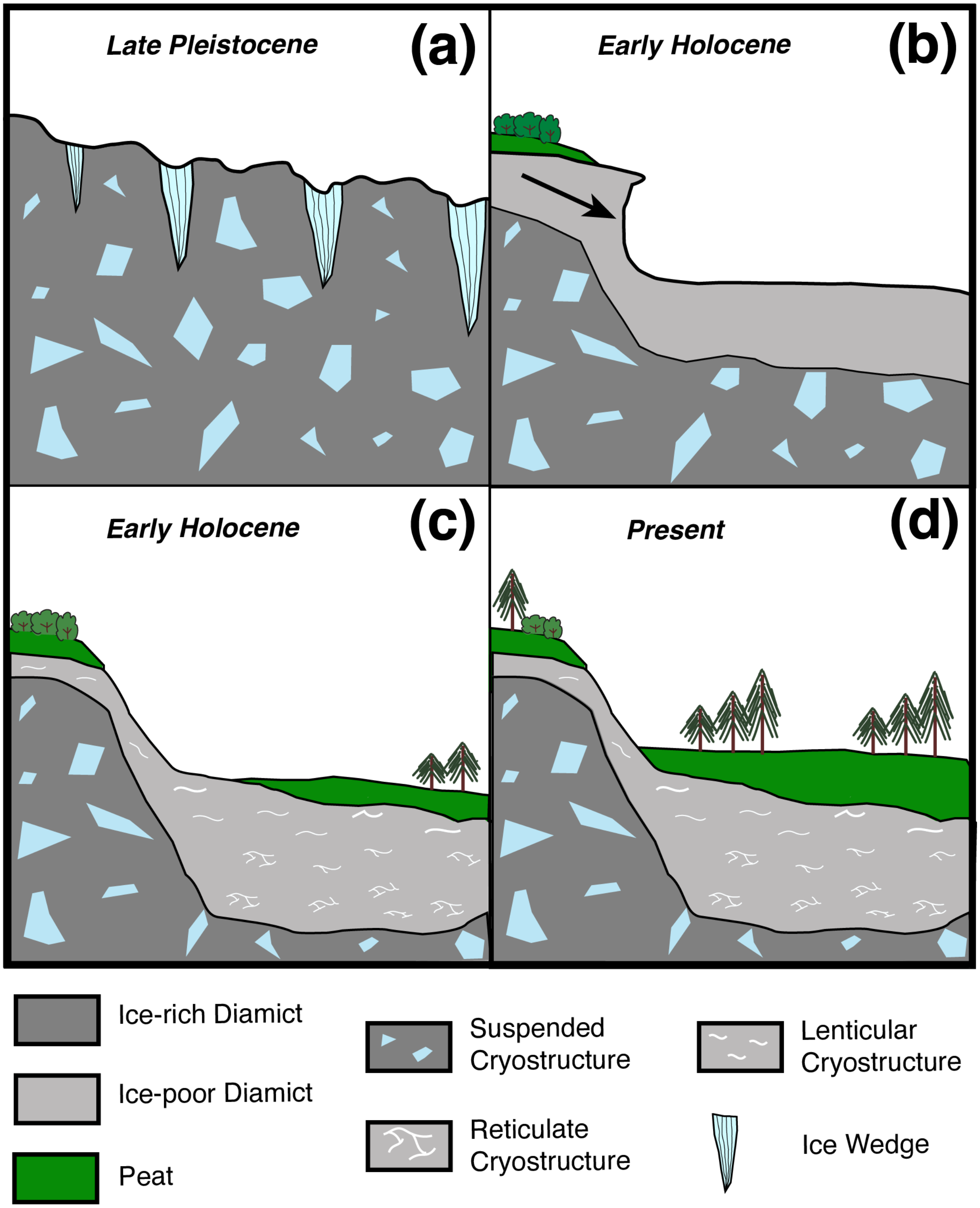

Figure 4.6: Schematic representation of high relief areas (BH-2) relative to low relief areas (BH-1).

(a) Massive Pleistocene ice wedges, overlying hillslope terrain, underwent permafrost degradation; **(b)** deepening of active layer, and slope instability results in a thermokarst induced mass wasting and thawing of ice-rich Pleistocene material; **(c)** colluvium sediments, i.e., redeposited primary till, are deposited; **(d)** slope instability is mitigated by colluvial deposition, permafrost regrades with ice-poor reticulate and layered within redeposited tills.

Chapter 5: Conclusion and Future Work

The sensitivity and impacts of climate change on permafrost (perennially frozen ground) are primarily related to the nature and abundance of ground ice in the host materials that may lose cohesion with thaw. Ground ice plays a vital role in landscape modification, potentially resulting in land degradation, primarily due to the presence and distribution of ground ice once permafrost thaws (Mackay 1970, French, 2007). The Mackenzie Delta region has been generally considered an ice-rich landscape. This landscape has been preconditioned since the late Pleistocene by natural deglaciation processes and subsequent climatic warming. This landscape was first influenced by natural processes, such as hydrological networks, mass movements, or the formation of lakes and wetlands in an ice-marginal, recently deglaciated environment. Without a climatic intervention, these natural influences during deglaciation were the first step between relict ice preservation or eradication before subsequent permafrost aggradation. Later, the early Holocene warming in the northwestern Arctic modified certain landscapes, which inherited relict ice, resulting in much of the area being less ice-rich. Overall, the association between excess-ice on hilltops and relatively less ground ice within flat-lying terrain indicates that the early Holocene warming has been an effective preconditioning mechanism. Much of the landscape observed today is likely less ice-rich, and less susceptible to future thaw relative to present warming conditions.

This work aimed to improve understanding of the Quaternary history of ground ice and its host sediments within boreholes obtained adjacent to the Inuvik – Tuktoyaktuk corridor. The main objectives of this theses are to: (1) provide a literature review on ground ice found within northwestern arctic settings; (2) determine the depositional history of sediments in the five boreholes along the ITH; (3) determine the ground ice genesis hosted within these permafrost settings; (4) introduce the precondition landscape hypothesis, in which the landscape today is less ice-rich (and therefore less susceptible to future thaw) than previous warm periods due to natural landscape evolution and previous climatic warming.

Summary of Work:

Chapter 1 introduced the quaternary, environmental and permafrost settings of the Mackenzie Delta Region. Chapter 2 of this thesis presents a technical communication on laboratory methods used in this study. Additionally, it provides introductory information on the techniques utilized, including Geotek Density scanning, stratigraphy, cryostratigraphy, till and diamict classification, water isotope analysis, and radiocarbon dating. Chapter 3 of this thesis presents a literature review of ground ice and ground ice forms typically hosted within the Mackenzie Delta region. This review includes commonly used ground ice definitions and examples of different ground ice forms typically found within the Mackenzie Delta Region, Klondike, and central Mackenzie Valley. Chapter 4 of this thesis presents a manuscript titled "Holocene thermokarst landscape conditioning across the Pleistocene-Holocene transition: an example from the southern Inuvik-Tuktoyaktuk Highway, NW Canada," detailing the stratigraphy and ground-ice evolution of five boreholes along the Inuvik-Tuktoyaktuk Highway.

Depositional history of the five boreholes

Five boreholes – a combination of core and grab-samples – (BH-1, BH-2, BH-3, BH-4, and BH-8) were characterized by stratigraphic units and cryostructures with respect to depth to determine their depositional history. These sites recorded various depositional histories. BH-1, located in a peatland environment, consisted of three stratigraphic units. An ice-poor reworked till, a massive ice unit, likely injection ice, and a peat body with reticulate, solid and organic-matrix cryostructures, respectively. BH-2, located in a hilltop environment, consisted of three stratigraphic units. An ice-rich primary till, a glaciofluvial outwash deposit, and a peat unit with suspended, structureless and organic-matrix cryostructures, respectively. BH-3 is situated within a riparian environment consisting of two stratigraphic units. An ice-poor reworked till and an organic-rich unit with structureless and organic-matrix cryostructures, respectively. BH-4 is located within a peatland and consists of three stratigraphic units. An ice-poor reworked melt-out till, a lacustrine deposit, and a peat unit with layered and organic-matrix cryostructures, respectively. BH-8 is situated within a peatland consisting of two stratigraphic units. A glaciolacustrine unit and a peat deposit with layered and organic-matrix cryostructures, respectively.

Ground Ice Genesis and Water Isotope Geochemistry:

The Five boreholes (BH-1, BH-2, BH-3, BH-4 and BH-8) subdivided by their stratigraphic units were analyzed using water isotope (δ18O and δD) geochemistry. These sites recorded various ground ice contents, ages, and forms, including pore ice, segregated ice, and injection ice. Apart from the organic-rich units observed within the top 2 – 4 meters of all five sites, which all had exceptionally high gravimetric water contents ranging between 200 – 2000%, the following conclusions are made. BH-1 was characterized as having relatively low ground ice within the melt-out till and a massive ice unit, likely injection ice, formed between the peat and the diamict units. All three stratigraphic units within BH-1 are classified as having Holocene-aged ice. BH-2 constitutes an ice-rich primary till hosting Pleistocene-age ice, while the overlying outwash sediments are characterized by mainly storing Pleistocene-aged pore ice and segregated ice. BH-3, BH-4 and BH-8 are all characterized by ice-poor deposits, including reworked till, lacustrine, and glaciolacustrine sediments with Holocene-aged ice.

Landscape Preconditioning:

The Mackenzie Delta region has been generally considered an area of abundant ground ice, including relict, segregated and wedge ice. However, results from stratigraphy, cryostructure and water isotope analyses indicate that the excess ice landscape has considerable heterogeneity related to its geology history. This geologic history includes preserving or eradicating relict ice by natural processes (such as hydrological and talik developments) and subsequent warming in the early Holocene. Today, Lacustrine, peatlands and riparian environments, such as BH-1, BH-3, BH-4 and BH-8 (i.e., low relief zones), have sediments at depth that tend to host ice-poor, Holocene-aged sediments. On the contrary, BH-2, situated on a hilltop at depths surpassing the early Holocene thaw unconformity, stores ice-rich materials, including original ice-rich cryostructures and relict Laurentide ice sheet till. In addition, ice-cored hilltops, due to landscape evolution as a result of thermokarst of fluvial incisions, increases the potential for slope destabilization and further thaw of relict ice in these settings. Overall, episodes of warming (such as today or the early Holocene) coupled with landscape evolution creates a unique landscape where it slowly becomes less and less ice-rich with time.

Future Work:

The ground ice review highlighted in Chapter 3, coupled with this idea of landscape pre-conditioning in Chapter 4, raises several questions. Firstly, is there a way to predict ground ice within specific geologic settings? Secondly, can we use geophysical surveys to map permafrost settings, especially in areas where ground ice is not visible? Lastly, this thesis highlights how valuable near-surface permafrost community mapping and excess-ice contents are for future landscape conditioning.

Using a landsystem model coupled with boreholes, surficial geology mapping, and geophysical surveys is a new approach to understanding the patterns and processes of thaw at landscape scales, i.e., predicting ground ice within specific geological units. A Landsystems is defined as an area with typical terrain attributes different from adjacent areas (Evans, 2014). A glacial landsystem uses a recurring topology pattern, soil, and vegetation to define specific areas (Evans, 2014). Similarly, a permafrost landsystem could be based upon the recognition of surficial geology, landform assembles, vegetation, nature of permafrost, type of host sediments, glacial and paleoenvironmental history, source of moisture, and freezing mechanism to predict ground ice within each landsystem. Future work will utilize deep permafrost cores (collected by the NWT government and the University of Alberta's PACS Lab in 2017 and stored at the University of Alberta), which will be supplemented by shallow coring (collected in the 2021 and 2022) within permafrost induced mass-movements, and geophysical analysis to characterize the vertical ice content and distribution. These permafrost samples will undergo Computed-Tomography (CT) imaging, geochemical and geotechnical analyses. Collectively, these data will refine the depositional models that inform the processes and history of permafrost development and its associated ground ice constraints of the underlying sediments. Results from this study will increase our understanding of climate change and future landform degradation in northern Canada and develop a set of tools that can be used in other regions to evaluate future thaw trajectories for northern landscapes. Ultimately, the results will establish a geologic map illustrating underlying features susceptible to thaw along the Mackenzie Delta Region, which will aid the NWT Geological Survey and Highways in planning for future thaw-related impacts of climate change.

References:

Evans, D.J.A., 2014, Glacial landsystems: Glacial Landsystems, p. 1–531, doi:10.4324/9780203784976.

French, H., 2007, The Periglacial Environment, 3rd edn: Wiley, Chichester, 458 p.

Mackay, R.J., 1970, Disturbances to the tundra and forest tundra environment of the western Arctic: Canadian Geotechnical Journal, v. 7, p. 420–432, doi:10.1139/t70-054.

Bibliography:

Associate Committee on Geotechnical Research National (ACGR), 1988, Glossary of Permafrost and Related Ground-Ice Terms: National Research Council of Canada, v. Technical, p. 156, doi:10.4224/20378888.

Aylsworth, J.M., Burgess, M.M., Desrochers, D.T., Duk-Rodkin, A., Robertson, T., and Traunor, J.A., 2001, Surficial geology, subsurface materials, and thaw sentivity of sediments: Bulletin of the Geological Survey of Canada, p. 41–48.

Bandara, S., 2017, Records of atmospheric mercury deposition and post-depositional mobility in peat permafrost archives from central and northern Yukon, Canada: 119 p., https://doi.org/10.7939/R3KD1R04P.

Benn, D.I., and Evans, D.J.A., 2010, Glaciers and Glaciation, 2nd edition: Hodder Arnold Publication, 816 p., doi:https://doi.org/10.4324/9780203785010.

Boaretto, E. et al., 2002, Summary findings of the fourth international radiocarbon intercomparison (FIRI)(1998–2001): Journal of Quaternary Science, v. 17, p. 633–637, doi:10.1002/JQS.702.

Bray, M.T., French, H.M., and Shur, Y., 2006, Further cryostratigraphic observations in the CRREL permafrost tunnel, Fox, Alaska: Permafrost and Periglacial Processes, v. 17, p. 233–243, doi:10.1002/ppp.558.

Bronk Ramsey, C., 2009, Bayesian Analysis of Radiocarbon Dates: Radiocarbon, v. 51, p. 337–360, doi:10.1017/s0033822200033865.

Burn, C.R., 1997, Cryostratigraphy, paleogeography, and climate change during the early Holocene warm interval, western Arctic coast, Canada: Canadian Journal of Earth Sciences, v. 34, p. 912–925, doi:10.1139/e17-076.

Burn, C.R., 2017, Mackenzie Delta: Canada's Principal Arctic Delta, *in* Springer, Cham, p. 321–334, doi:10.1007/978-3-319-44595-3_23.

Burn, C.R., and Kokelj, S. V., 2009, The environment and permafrost of the Mackenzie Delta area: Permafrost and Periglacial Processes, v. 20, p. 83–105, doi:10.1002/ppp.655.

Burn, C.R., Michel, F.A., and Smith, M.W., 1986, Stratigraphic, isotopic, and mineralogical evidence for an early Holocene thaw unconformity at Mayo, Yukon Territory.: Canadian Journal of Earth Sciences, v. 23, p. 794–803, doi:10.1139/e86-081.

Calmels, F., Froese, D.G., and Clavano, W.R., 2012, Cryostratigraphic record of permafrost degradation and recovery following historic (1898-1992) surface disturbances in the klondike region, central yukon territory 1,2: Canadian Journal of Earth Sciences, v. 49, p. 938–952, doi:10.1139/E2012-023.

Cardyn, R., Clark, I.D., Lacelle, D., Lauriol, B., Zdanowicz, C., and Calmels, F., 2007, Molar gas ratios of air entrapped in ice: A new tool to determine the origin of relict massive ground ice bodies in permafrost: Quaternary Research, v. 68, p. 239–248, doi:10.1016/j.yqres.2007.05.003.

Clark, I.D., and Lauriol, B., 1997, Aufeis of the Firth River basin, Northern Yukon, Canada: Insights into permafrost hydrogeology and karst: Arctic and Alpine Research, v. 29, p. 240–252, doi:10.2307/1552053.

Coulombe, S., Fortier, D., Lacelle, D., Kanevskiy, M., and Shur, Y., 2019, Origin, burial and preservation of late Pleistocene-age glacier ice in Arctic permafrost (Bylot Island, NU, Canada): Cryosphere, v. 13, p. 97–111, doi:10.5194/tc-13-97-2019.

Craig, H., 1961, Standard for reporting concentrations of deuterium and oxygen-18 in natural

waters: Science, v. 133, p. 1833–1834, doi:10.1126/science.133.3467.1833.
Crites, H., Kokelj, S. V, and Lacelle, D., 2020, Icings and groundwater conditions in permafrost catchments of northwestern Canada: Scientific Reports, v. 10, doi:10.1038/s41598-020-60322-w.
Dansgaard, W., 1964, Stable isotopes in precipitation: Tellus, v. 16, p. 436–468, doi:10.3402/tellusa.v16i4.8993.
Duk-Rodkin, A., and Hughes, O.L., 1992, Pleistocene montane glaciations in the Mackenzie Mountains, Northwest Territories: Geographie Physique et Quaternaire, v. 46, p. 69–83, doi:10.7202/032889ar.
Duk-Rodkin, A., and Lemmen, D.S., 2000, Glacial history of the Mackenzie region: Bulletin of the Geological Survey of Canada, p. 11–20, doi:10.4095/211903.
Dyke, A.S., and Evans, D.J.A., 2003, Ice-marginal terrestrial landsystems: Northern laurentide and innuitian ice sheet margins, *in* London, A. ed., Glacial Landsystems, p. 143–165, doi:10.4324/9780203784976.
E.L, H., 1970, SOUND VELOCITY AND RELATED PROPERTIES OF MARINE SEDIMENTS, NORTH PACIFIC: J Geophys Res, v. 75, p. 4423–4446, doi:10.1029/jb075i023p04423.
Ensom, T., Morse, P.D., Kokelj, S. V, Macdonald, E., Young, J., Tank, S., Grozic, E., and Castagner, A., 2020, Permafrost geotechnical borehole data synthesis: 2013–2017 Inuvik-Tuktoyaktuk region, Northwest Territories; Northwest Territories Geological Survey, NWT Open Report 2019-012; Geological Survey of Canada, Open File 8652.:
Evans, D.J.A., 2014, Glacial landsystems: Glacial Landsystems, p. 1–531, doi:10.4324/9780203784976.
Evans, D.J.A., Phillips, E.R., Hiemstra, J.F., and Auton, C.A., 2006, Subglacial till: Formation, sedimentary characteristics and classification: Earth-Science Reviews, v. 78, p. 115–176, doi:10.1016/j.earscirev.2006.04.001.
Van Everdingen, R.O., 1998, Multi-language glossary of permafrost and related ground-ice terms (Rev. ed. 2005): International Permafrost Association, v. 1998, p. 159, https://globalcryospherewatch.org/reference/glossary_docs/Glossary_of_Permafrost_and_Ground-Ice_IPA_2005.pdf.
Fortier, D., Kanevskiy, M., and Shur, Y., 2008, Genesis of Reticulate-Chaotic Cryostructure in Permafrost:, doi:10.13140/2.1.4703.3929.
French, H., 2011, Frozen sediments and previously-frozen sediments: Geological Society Special Publication, v. 354, p. 153–166, doi:10.1144/SP354.9.
French, H., 2007, The Periglacial Environment, 3rd edn: Wiley, Chichester, 458 p.
French, H.M., and Pollard, W.H., 1986, Ground-ice investigations, Klondike District, Yukon Territory:, www.nrcresearchpress.com (accessed December 2019).
French, H., and Shur, Y., 2010, The principles of cryostratigraphy: Earth-Science Reviews, v. 101, p. 190–206, doi:10.1016/j.earscirev.2010.04.002.
Fritz, M., Wetterich, S., Mcalister, J., and Meyer, H., 2022, A new local meteoric water line for Inuvik (NT, Canada): Earth System Science Data, v. 14, p. 57–63, doi:10.5194/essd-14-57-2022.
Froese, D.G., Zazula, G.D., and Reyes, A. V, 2006, Seasonality of the late Pleistocene Dawson tephra and exceptional preservation of a buried riparian surface in central Yukon Territory, Canada: Quaternary Science Reviews, v. 25, p. 1542–1551, doi:10.1016/j.quascirev.2006.01.028.

Geotek, 2008, Multi-Sensor Core Logger Manual:, www.geotek.co.uk (accessed May 2021).
Gilbert, G.L., Kanevskiy, M., and Murton, J.B., 2016, Recent Advances (2008–2015) in the Study of Ground Ice and Cryostratigraphy, *in* Permafrost and Periglacial Processes, v. 27, p. 377–389, doi:10.1002/ppp.1912.
Grosse, G., Romanovsky, V., Jorgenson, T., Anthony, K.W., Brown, J., and Overduin, P.P., 2011, Vulnerability and feedbacks of permafrost to climate change: Eos, v. 92, p. 73–74, doi:10.1029/2011EO090001.
Harry, D.G., French, H.M., and Pollard, W.H., 1988, Massive ground ice and ice-cored terrain near Sabine Point, Yukon coastal plain: Canadian Journal of Earth Sciences, v. 25, p. 1846–1856, doi:10.1139/e88-174.
Hill, P.R., 1996, Late Quaternary sequence stratigraphy of the Mackenzie Delta: Canadian Journal of Earth Sciences, v. 33, p. 1064–1074, doi:10.1139/e96-081.
Holland, K.M., Porter, T.J., Froese, D.G., Kokelj, S. V., and Buchanan, C.A., 2020, Ice-Wedge Evidence of Holocene Winter Warming in the Canadian Arctic: Geophysical Research Letters, v. 47, p. e2020GL087942, doi:10.1029/2020GL087942.
Hughes, O.L., 1987, Late Wisconsinan Laurentide glacial limits of northwestern Canada: the Tutsieta Lake and Kelly Lake phases: Geological Survery of Canada, p. 25, doi:10.4095/122385.
Jorgenson, M.T., Shur, Y.L., and Pullman, E.R., 2006, Abrupt increase in permafrost degradation in Arctic Alaska: Geophysical Research Letters, v. 33, p. 2–5, doi:10.1029/2005GL024960.
Kanevskiy, M., Jorgenson, T., Shur, Y., O'Donnell, J.A., Harden, J.W., Zhuang, Q., and Fortier, D., 2014, Cryostratigraphy and Permafrost Evolution in the Lacustrine Lowlands of West-Central Alaska: Permafrost and Periglacial Processes, v. 25, p. 14–34, doi:10.1002/ppp.1800.
Kanevskiy, M., Shur, Y., Jorgenson, M.T., Ping, C.L., Michaelson, G.J., Fortier, D., Stephani, E., Dillon, M., and Tumskoy, V., 2013, Ground ice in the upper permafrost of the Beaufort Sea coast of Alaska: Cold Regions Science and Technology, v. 85, p. 56–70, doi:10.1016/j.coldregions.2012.08.002.
Knight, P.G., 1997, The basal ice layer of glaciers and ice sheets: Quaternary Science Reviews, v. 16, p. 975–993, doi:10.1016/S0277-3791(97)00033-4.
Kokelj, S. V., and Burn, C.R., 2003, Ground ice and soluble cations in near-surface permafrost, Inuvik, Northwest Territories, Canada: Permafrost and Periglacial Processes, v. 14, p. 275–289, doi:10.1002/ppp.458.
Kokelj, S. V., Jenkins, R.E., Milburn, D., Burn, C.R., and Snow, N., 2005, The influence of thermokarst disturbance on the water quality of small upland lakes, Mackenzie Delta region, Northwest Territories, Canada: Permafrost and Periglacial Processes, v. 16, p. 343–353, doi:10.1002/ppp.536.
Kokelj, S. V., and Jorgenson, M.T., 2013, Advances in thermokarst research: Permafrost and Periglacial Processes, v. 24, p. 108–119, doi:10.1002/ppp.1779.
Kokelj, S. V., Lantz, T.C., Kanigan, J., Smith, S.L., and Coutts, R., 2009a, Origin and polycyclic behaviour of tundra thaw slumps, Mackenzie Delta region, Northwest Territories, Canada: Permafrost and Periglacial Processes, v. 20, p. 173–184, doi:10.1002/ppp.642.
Kokelj, S. V, Lantz, T.C., Tunnicliffe, J., Segal, R., and Lacelle, D., 2017a, Climate-driven thaw of permafrost preserved glacial landscapes, northwestern Canada: GEOLOGY, v. 45, doi:10.1130/G38626.1.

Kokelj, S. V., Lantz, T.C., Wolfe, S.A., Kanigan, J.C., Morse, P.D., Coutts, R., Molina-Giraldo, N., and Burn, C.R., 2014, Distribution and activity of ice wedges across the forest-tundra transition, western arctic Canada: Journal of Geophysical Research: Earth Surface, v. 119, p. 2032–2047, doi:10.1002/2014JF003085.

Kokelj, S. V., Palmer, M.J., Lantz, T.C., and Burn, C.R., 2017b, Ground Temperatures and Permafrost Warming from Forest to Tundra, Tuktoyaktuk Coastlands and Anderson Plain, NWT, Canada: Permafrost and Periglacial Processes, v. 28, p. 543–551, doi:10.1002/PPP.1934.

Kokelj, S. V, Pisaric, M.F.J., and Burn, C.R., 2007, Cessation of ice-wedge development during the 20th century in spruce forests of eastern Mackenzie Delta, Northwest Territories, Canada: Canadian Journal of Earth Sciences, v. 44, p. 1503–1515, doi:10.1139/E07-035.

Kokelj, S. V., Smith, C.A.S., and Burn, C.R., 2002, Physical and chemical characteristics of the active layer and permafrost, Herschel Island, western Arctic Coast, Canada: Permafrost and Periglacial Processes, v. 13, p. 171–185, doi:10.1002/ppp.417.

Kokelj, S. V., Tunnicliffe, J., Lacelle, D., Lantz, T.C., Chin, K.S., and Fraser, R., 2015, Increased precipitation drives mega slump development and destabilization of ice-rich permafrost terrain, northwestern Canada: Global and Planetary Change, v. 129, p. 56–68, doi:10.1016/j.gloplacha.2015.02.008.

Kokelj, S. V., Zajdlik, B., and Thompson, M.S., 2009b, The impacts of Thawing permafrost on the chemistry of lakes across the subarctic boreal-tundra transition, Mackenzie Delta region, Canada: Permafrost and Periglacial Processes, v. 20, p. 185–199, doi:10.1002/ppp.641.

Lacelle, D., 2002, Ground ice investigation in the far northwest of Canada: , p. 101.

Lacelle, D., 2011, On the δ18O, δD and D-excess relations in meteoric precipitation and during equilibrium freezing: Theoretical approach and field examples: Permafrost and Periglacial Processes, v. 22, p. 13–25, doi:10.1002/ppp.712.

Lacelle, D., Bjornson, J., and Lauriol, B., 2010, Climatic and geomorphic factors affecting contemporary (1950-2004) activity of retrogressive thaw slumps on the Aklavik plateau, Richardson mountains, NWT, Canada: Permafrost and Periglacial Processes, v. 21, p. 1–15, doi:10.1002/ppp.666.

Lacelle, D., Bjornson, J., Lauriol, B., Clark, I.D., and Troutet, Y., 2004, Segregated-intrusive ice of subglacial meltwater origin in retrogressive thaw flow headwalls, Richardson Mountains, NWT, Canada: Quaternary Science Reviews, v. 23, p. 681–696, doi:10.1016/j.quascirev.2003.09.005.

Lacelle, D., Brooker, A., Fraser, R.H., and Kokelj, S. V., 2015, Distribution and growth of thaw slumps in the Richardson Mountains-Peel Plateau region, northwestern Canada: Geomorphology, v. 235, p. 40–51, doi:10.1016/j.geomorph.2015.01.024.

Lacelle, D., Fisher, D., Clark, I.D., and Berinstain, A., 2008, Distinguishing between vapor- and liquid-formed ground ice in the northern martian regolith and potential for biosignatures preserved in ice bodies: Icarus, v. 197, p. 458–469, doi:10.1016/j.icarus.2008.05.017.

Lacelle, D., Fisher, D.A., Coulombe, S., Fortier, D., and Frappier, R., 2018, Buried remnants of the Laurentide Ice Sheet and connections to its surface elevation: Scientific Reports, v. 8, doi:10.1038/s41598-018-31166-2.

Lacelle, D., Lauriol, B., Clark, I.D., Cardyn, R., and Zdanowicz, C., 2007, Nature and origin of a Pleistocene-age massive ground-ice body exposed in the Chapman Lake moraine complex, central Yukon Territory, Canada: Quaternary Research, v. 68, p. 249–260, doi:10.1016/j.yqres.2007.05.002.

Lacelle, D., St-Jean, M., Lauriol, B., Clark, I.D., Lewkowicz, A., Froese, D.G., Kuehn, S.C., and Zazula, G., 2009, Burial and preservation of a 30,000 year old perennial snowbank in Red Creek valley, Ogilvie Mountains, central Yukon, Canada: Quaternary Science Reviews, v. 28, p. 3401–3413, doi:10.1016/j.quascirev.2009.09.013.
Lacelle, D., and Vasil'chuk, Y.K., 2013, Recent progress (2007-2012) in permafrost isotope geochemistry: Permafrost and Periglacial Processes, v. 24, p. 138–145, doi:10.1002/ppp.1768.
Lantuit, H., and Pollard, W.H., 2008, Fifty years of coastal erosion and retrogressive thaw slump activity on Herschel Island, southern Beaufort Sea, Yukon Territory, Canada: Geomorphology, v. 95, p. 84–102, doi:10.1016/j.geomorph.2006.07.040.
Lantuit, H., Pollard, W.H., Couture, N., Fritz, M., Schirrmeister, L., Meyer, H., and Hubberten, H.W., 2012, Modern and Late Holocene Retrogressive Thaw Slump Activity on the Yukon Coastal Plain and Herschel Island, Yukon Territory, Canada: Permafrost and Periglacial Processes, v. 23, p. 39–51, doi:10.1002/ppp.1731.
Lantz, T.C., and Kokelj, S. V., 2008, Increasing rates of retrogressive thaw slump activity in the Mackenzie Delta region, N.W.T., Canada: Geophysical Research Letters, v. 35, p. 1–5, doi:10.1029/2007GL032433.
Lantz, T.C., Kokelj, S. V., Gergel, S.E., and Henry, G.H.R., 2009, Relative impacts of disturbance and temperature: Persistent changes in microenvironment and vegetation in retrogressive thaw slumps: Global Change Biology, v. 15, p. 1664–1675, doi:10.1111/j.1365-2486.2009.01917.x.
Lee, H., Swenson, S.C., Slater, A.G., and Lawrence, D.M., 2014, Effects of excess ground ice on projections of permafrost in a warming climate: Environmental Research Letters, v. 9, p. 124006, doi:10.1088/1748-9326/9/12/124006.
Lewkowicz, A.G., and Way, R.G., 2019, Extremes of summer climate trigger thousands of thermokarst landslides in a High Arctic environment: Nature Communications, v. 10, p. 1–11, doi:10.1038/s41467-019-09314-7.
Mackay, J.R., 1995, Active layer changes (1968 to 1993) following the forest-tundra fire near Inuvik, NWT, Canada: Arctic and Alpine Research, v. 27, p. 323–336, doi:10.2307/1552025.
Mackay, J.R., 1993, Air temperature, snow cover, creep of frozen ground, and the time of ice-wedge cracking, western Arctic coast: Canadian Journal of Earth Sciences, v. 30, p. 1720–1729, doi:10.1139/e93-151.
Mackay, J.R., 1988, Catastrophic lake drainage, Tuktoyaktuk Peninsula area, District of Mackenzie: 83–90 p., doi:10.4095/122663.
Mackay, R.J., 1970, Disturbances to the tundra and forest tundra environment of the western Arctic: Canadian Geotechnical Journal, v. 7, p. 420–432, doi:10.1139/t70-054.
Mackay, J.R., 1983, Downward water movement into frozen ground, western arctic coast, Canada.: Canadian Journal of Earth Sciences, v. 20, p. 120–134, doi:10.1139/e83-012.
Mackay, J.R., 1978, Freshwater shelled invertebrate indicators of paleoclimate in northwestern Canada during late glacial times: Discussion: Canadian Journal of Earth Sciences, v. 15, p. 461–462.
Mackay, J.R., 1989, Massive ice: some field criteria for the identification of ice types: Current Research, Part G, Geological Survey of Canada, Paper, p. 5–11.
Mackay, J.R., 1998, Pingo growth and collapse, Tuktoyaktuk Peninsula area, western arctic coast, Canada: A long-term field study: Geographie Physique et Quaternaire, v. 52, p. 271–

323, doi:10.7202/004847ar.
Mackay, J.R., 1979, Pingos of the Tuktoyaktuk Peninsula area, Northwest Territories.: Geographie Physique et Quaternaire, v. 33, p. 3–62, doi:10.7202/1000322ar.
Mackay, J.R., 1990, Some observations on the growth and deformation of epigenetic, syngenetic and anti-syngenetic ice wedges: Permafrost and Periglacial Processes, v. 1, p. 15–29, doi:10.1002/ppp.3430010104.
Mackay, J.R., 1963, The Mackenzie delta area, Northwestern Territories: 202 p., https://books.google.ca/books/about/The_Mackenzie_Delta_Area_N_W_T.html?id=Zzr-vgEACAAJ&redir_esc=y (accessed July 2022).
Mackay, J.R., 1971, The Origin of Massive Icy Beds in Permafrost, Western Arctic Coast, Canada: Canadian Journal of Earth Sciences, v. 8, p. 397–422, doi:10.1139/e71-043.
Mackay, J.R., 1972, The World Of Underground Ice: Annals of the Association of American Geographers, v. 62, p. 1–22, doi:10.1111/j.1467-8306.1972.tb00839.x.
Mackay, J.R., and Dallimore, S.R., 1992, Massive ice of the Tuktoyaktuk area, western Arctic coast, Canada: Canadian Journal of Earth Sciences, v. 29, p. 1235–1249, doi:10.1139/e92-099.
Moorman, B.J., and Michel, F.A., 2000, The burial of ice in the proglacial environment of Bylot Island, Arctic Canada: Permafrost and Periglacial Processes, v. 11, p. 161–175, doi:10.1002/1099-1530(200007/09)11:3<161::AID-PPP347>3.0.CO;2-F.
Morse, P.D., and Burn, C.R., 2013, Field observations of syngenetic ice wedge polygons, outer Mackenzie Delta, western Arctic coast, Canada: Journal of Geophysical Research: Earth Surface, v. 118, p. 1320–1332, doi:10.1002/jgrf.20086.
Murton, J.B., 2008, Global Warming and Thermokarst, *in* Permafrost Soils, Springer, Berlin, Heidelberg, p. 185–203, doi:10.1007/978-3-540-69371-0_13.
Murton, J.B., 2005, Ground-ice stratigraphy and formation at North Head, Tuktoyaktuk Coastlands, western Arctic Canada: A product of glacier-permafrost interactions: Permafrost and Periglacial Processes, v. 16, p. 31–50, doi:10.1002/ppp.513.
Murton, J.B., 2013, Ground Ice and Cryostratigraphy, *in* Treatise on Geomorphology, v. 8, p. 173–201, doi:10.1016/B978-0-12-374739-6.00206-2.
Murton, J.B., 2001, Thermokarst sediments and sedimentary structures, Tuktoyaktuk Coastlands, western Arctic Canada: Global and Planetary Change, v. 28, p. 175–192, doi:10.1016/S0921-8181(00)00072-2.
Murton, J.B., and Ballantyne, C.K., 2017, Periglacial and permafrost ground models for Great Britain, *in* Geological Society Engineering Geology Special Publication, v. 28, p. 501–579, doi:10.1144/EGSP28.5.
Murton, J.B., Bateman, M.D., Telka, A.M., Waller, R., Whiteman, C., and Kuzmina, S., 2017, Early to mid Wisconsin Fluvial Deposits and Palaeoenvironment of the Kidluit Formation, Tuktoyaktuk Coastlands, Western Arctic Canada: Permafrost and Periglacial Processes, v. 28, p. 523–533, doi:10.1002/ppp.1946.
Murton, J.B., Bateman, M.D., Waller, R.I., Sciences, G., and Whiteman, C.A., 2015, Late Wisconsin glaciation of Hadwen and Summer islands , Tuktoyaktuk Coastlands ,: 68e Conférence Canadienne de Géotechnique et 7e Conférence Canadienne sur le Pergélisol, 20 au 23 septembre 2015, Québec, Québec.,.
Murton, J.B., Frechen, M., and Maddy, D., 2007, Luminescence dating of mid- to Late Wisconsinan aeolian sand as a constraint on the last advance of the Laurentide Ice Sheet across the Tuktoyaktuk Coastlands, western Arctic Canada: Canadian Journal of Earth

Sciences, v. 44, p. 857–869, doi:10.1139/E07-015.
Murton, J.B., and French, H.M., 1994, Cryostructures in permafrost, Tuktoyaktuk coastlands, western Arctic Canada: Canadian Journal of Earth Sciences, v. 31, p. 737–747, doi:10.1139/e94-067.
Murton, J.B., and French, H.M., 1993a, Thaw modification of frost-fissure wedges, Richards Island, Pleistocene Mackenzie Delta, Western Arctic Canada: Journal of Quaternary Science, v. 8, p. 185–196, doi:10.1002/jqs.3390080302.
Murton, J.B., and French, H.M., 1993b, Thermokarst involutions, summer island, pleistocene mackenzie delta, Western Canadian arctic: Permafrost and Periglacial Processes, v. 4, p. 217–229, doi:10.1002/ppp.3430040304.
Murton, J.B., Waller, R.I., Hart, J.K., Whiteman, C.A., Pollard, W.H., and Clark, I.D., 2004, Stratigraphy and glaciotectonic structures of permafrost deformed beneath the northeast margin of the Laurentide ice sheet, Tuktoyaktuk Coastlands, Canada: Journal of Glaciology, v. 50, p. 399–412.
Murton, J.B., Whiteman, C.A., Waller, R.I., Pollard, W.H., Clark, I.D., and Dallimore, S.R., 2005, Basal ice facies and supraglacial melt-out till of the Laurentide Ice Sheet, Tuktoyaktuk Coastlands, western Arctic Canada: Quaternary Science Reviews, v. 24, p. 681–708, doi:10.1016/j.quascirev.2004.06.008.
Neuendorf, K.K.E., Jr, J.P.M., and Jackson, J.A., 2011, Glossary of Geology, Fifth Edition: , p. 800.
O'Neill, H.B. et al., 2020, Permafrost thaw and northern development: Nature Climate Change, v. 10, p. 722–723, doi:10.1038/s41558-020-0862-5.
O'Neill, H.B., and Burn, C.R., 2012, Physical and temporal factors controlling the development of near-surface ground ice at Illisarvik, Western Arctic coast, Canada: Canadian Journal of Earth Sciences, v. 49, p. 1096–1110, doi:10.1139/E2012-043.
O'Neill, H.B., Smith, S.L., and Duchesne, C., 2019a, Long-Term Permafrost Degradation and Thermokarst Subsidence in the Mackenzie Delta Area Indicated by Thaw Tube Measurements, *in* American Society of Civil Engineers (ASCE), p. 643–651, doi:10.1061/9780784482599.074.
O'Neill, H.B., Wolfe, S.A., and Duchesne, C., 2019b, New ground ice maps for Canada using a paleogeographic modelling approach: Cryosphere, v. 13, p. 753–773, doi:10.5194/tc-13-753-2019.
O'Neill, H.B., Wolfe, S.A., and Duchesne, C., 2019c, New ground ice maps for Canada using a paleogeographic modelling approach: Cryosphere, v. 13, p. 753–773, doi:10.5194/tc-13-753-2019.
Opel, T., Dereviagin, A.Y., Meyer, H., Schirrmeister, L., and Wetterich, S., 2011, Palaeoclimatic information from stable water isotopes of Holocene ice wedges on the Dmitrii Laptev Strait, northeast Siberia, Russia: Permafrost and Periglacial Processes, v. 22, p. 84–100, doi:10.1002/ppp.667.
Pollard, W., 1990, The nature and origin of ground ice in the Herschel Island area, Yukon Territory: Proceedings of the fifth Canadian Conference on Permafrost, p. 23–30, http://pubs.aina.ucalgary.ca/cpc/CPC5-23.pdf (accessed March 2020).
Pollard, W.H., and French, H.M., 1980, A first approximation of the volume of ground ice, Richards Island, Pleistocene Mackenzie delta, Northwest Territories, Canada.: Canadian Geotechnical Journal, v. 17, p. 509–516, doi:10.1139/t80-059.
Porter, T.J., Schoenemann, S.W., Davies, L.J., Steig, E.J., Bandara, S., and Froese, D.G., 2019,

Recent summer warming in northwestern Canada exceeds the Holocene thermal maximum: Nature Communications, v. 10, doi:10.1038/s41467-019-09622-y.
Rampton, V.N.; Mackay, J.R., 1971, Massive ice and icy sediments throughout the Tuktoyaktuk Peninsula, Richards Island, and nearby areas, district of Mackenzie: Geol Surv Can, Pap 71-21,.
Rampton, V.N., 1991, Observations on buried glacier ice and massive segregated ice, Western Arctic Coast, Canada: Discussion: Permafrost and Periglacial Processes, v. 2, p. 163–165, doi:10.1002/ppp.3430020209.
Rampton, V.N., 1988, Quaternary Geology of the Tuktoyaktuk Coastlands, Northwest Territories: Geological Survey of Canada, p. 1–107, doi:10.1126/science.ns-6.149S.521-a.
Reyes, A. V., Froese, D.G., and Jensen, B.J.L., 2010a, Permafrost response to last interglacial warming: Field evidence from non-glaciated Yukon and Alaska: Quaternary Science Reviews, v. 29, p. 3256–3274, doi:10.1016/j.quascirev.2010.07.013.
Reyes, A. V, Jensen, B.J.L., Zazula, G.D., Ager, T.A., Kuzmina, S., La Farge, C., and Froese, D.G., 2010b, A late-Middle Pleistocene (Marine Isotope Stage 6) vegetated surface buried by Old Crow tephra at the Palisades, interior Alaska: Quaternary Science Reviews, v. 29, p. 801–811, doi:10.1016/j.quascirev.2009.12.003.
Ross Mackay, J., 1974, RETICULATE ICE VEINS IN PERMAFROST, NORTHERN CANADA.: Canadian Geotechnical Journal, v. 11, p. 230–237, doi:10.1139/t74-019.
Rudy, A.C.A., Morse, P.D., Kokelj, S. V, Sladen, W.E., and Smith, S.L., 2019, A New Protocol to Map Permafrost Geomorphic Features and Advance Thaw-Susceptibility Modelling, *in* p. 661–669, doi:10.1061/9780784482599.076.
Segal, R.A., Lantz, T.C., and Kokelj, S. V., 2016, Acceleration of thaw slump activity in glaciated landscapes of the Western Canadian Arctic: Environmental Research Letters, v. 11, doi:10.1088/1748-9326/11/3/034025.
Shumskii, P.A., 1964, Ground (subsurface) ice: Technical Translation (National Research Council of Canada), p. 118, https://doi.org/10.4224/20386780.
Shur, Y., French, H.M., Bray, M.T., and Anderson, D.A., 2004, Syngenetic permafrost growth: Cryostratigraphic observations from the CRREL tunnel near Fairbanks, Alaska: Permafrost and Periglacial Processes, v. 15, p. 339–347, doi:10.1002/ppp.486.
Shur, Y., and Jorgenson, M., 1998, Cryostructure development on the floodplain of the Colville River Delta, northern Alaska: Permafrost, Seventh International Conference, p. 993–999, http://www.arlis.org/docs/vol1/ICOP/40770716/CD-ROM/Proceedings/PDF001189/150193.pdf.
Steedman, A.E., Lantz, T.C., and Kokelj, S. V., 2017, Spatio-Temporal Variation in High-Centre Polygons and Ice-Wedge Melt Ponds, Tuktoyaktuk Coastlands, Northwest Territories: Permafrost and Periglacial Processes, v. 28, p. 66–78, doi:10.1002/ppp.1880.
Wolfe, S.A., 2017, Ground ice in permafrost: thermokarst and hydrogeological implications: GeoOttawa 2017, p. 9.
Wolfe, S., Murton, J., Bateman, M., and Barlow, J., 2020, Oriented-lake development in the context of late Quaternary landscape evolution, McKinley Bay Coastal Plain, western Arctic Canada: Quaternary Science Reviews, v. 242, p. 106414, doi:10.1016/j.quascirev.2020.106414.
Zazula, G.D., MacKay, G., Andrews, T.D., Shapiro, B., Letts, B., and Brock, F., 2009, A late Pleistocene steppe bison (Bison priscus) partial carcass from Tsiigehtchic, Northwest Territories, Canada: Quaternary Science Reviews, v. 28, p. 2734–2742,

doi:10.1016/j.quascirev.2009.06.012.

Appendix 1a: BH-1 Water Isotopes ($\delta^{18}O$ and $\delta^{2}H$) Results

Unit	***Depth (m)***	***δ18O (‰)***	***δD (‰)***	***d-excess (‰)***
Peat	0.00	-20.82	-160.69	5.8
	0.10	-16.61	-130.89	2.0
	0.20	-18.51	-141.37	6.7
	0.30	-19.39	-149.76	5.4
	0.40	-19.19	-149.45	4.1
	0.50	-19.57	-155.16	1.4
	0.60	-19.56	-157.20	-0.7
	0.70	-19.84	-156.49	2.2
	0.80	-19.02	-154.69	-2.5
	0.90	-18.89	-153.82	-2.7
	1.00	-18.77	-153.42	-3.3
	1.10	-18.61	-153.05	-4.2
	1.20	-18.57	-153.04	-4.4
	1.30	-18.51	-154.61	-6.5
	1.40	-18.32	-153.47	-6.9
	1.50	-18.48	-153.95	-6.1
	1.60	-18.58	-154.23	-5.6
	1.70	-18.55	-154.55	-6.2
	1.80	-18.76	-155.81	-5.8
	1.90	-18.85	-156.46	-5.7
	2.10	-18.97	-155.02	-3.2
Massive Ice	2.20	-18.38	-151.72	-4.7
	2.40	-17.94	-149.08	-5.5
	2.50	-21.27	-171.24	-1.1
	2.60	-18.39	-152.72	-5.6
	2.80	-21.18	-170.96	-1.5
	3.20	-19.78	-161.13	-2.9
	3.40	-20.00	-162.91	-2.9
	3.60	-24.63	-193.59	3.4
	3.80	-26.91	-210.09	5.2
	4.00	-27.48	-215.86	3.9
	4.20	-27.88	-218.77	4.3
	4.40	-27.46	-215.00	4.7
	4.60	-25.44	-202.50	1.0
	5.00	-25.10	-202.99	-2.2

	5.20	-25.01	-202.83	-2.7
	5.40	-24.66	-199.83	-2.5
	5.60	-25.04	-202.67	-2.3
	5.80	-24.78	-201.21	-3.0
	6.00	-24.57	-200.45	-3.8
	6.40	-25.56	-203.85	0.6
	6.60	-22.69	-189.50	-8.0
	6.80	-22.55	-189.13	-8.7
Ice-poor Diamict	7.00	-18.97	-167.19	-15.4
	7.20	-18.96	-166.99	-15.3
	7.45	-19.40	-167.33	-12.2
	7.60	-19.69	-169.50	-12.0
	7.75	-19.65	-167.91	-10.7
	7.85	-19.53	-167.31	-11.0
	8.00	-19.28	-165.76	-11.5
	8.20	-21.05	-171.39	-3.0
	9.20	-19.60	-168.41	-11.6
	9.65	-20.00	-169.50	-9.5
	9.80	-19.96	-167.60	-8.0
	10.35	-20.14	-170.29	-9.2
	10.60	-20.26	-171.95	-9.8
	11.00	-20.21	-173.35	-11.7
	11.10	-19.90	-172.33	-13.2

Appendix 1b: BH-2 Water Isotopes ($\delta^{18}O$ and $\delta^{2}H$) Results

Unit	*Depth (m)*	*δ18O (‰)*	*δD (‰)*	*d-excess (‰)*
Peat	0.5	-21.83	-165.79	8.8
	1	-23.27	-179.40	6.8
	2	-22.83	-176.76	5.9
Gravelly Sand	3.5	-23.10	-205.27	-20.5
	4	-24.22	-211.54	-17.8
	4.5	-25.55	-220.56	-16.1
	5	-26.76	-229.18	-15.1
	6	-29.00	-236.46	-4.5
	6.5	-29.05	-237.29	-4.9
	7	-30.25	-240.14	1.8
	7.5	-30.74	-242.60	3.4
	8	-30.83	-243.11	3.5
	8.5	-30.60	-243.22	1.6
	9	-30.69	-242.58	2.9
	10.00	-28.81	-231.32	-0.8
	10.25	-30.48	-239.78	4.1
	10.40	-29.35	-235.25	-0.4
	11.5	-30.34	-237.90	4.8
Ice-rich Diamict	12.0	-29.91	-234.87	4.4
	12.5	-29.50	-231.77	4.3
	13.0	-28.66	-226.65	2.6
	14.0	-29.44	-231.23	4.3
	14.5	-29.36	-230.53	4.3
	15.10	-29.02	-228.95	3.2
	15.35	-29.03	-229.20	3.1
	15.50	-29.32	-233.95	0.6
	15.55	-28.89	-228.62	2.5
	15.90	-29.07	-229.29	3.3
	16.05	-29.03	-228.75	3.5
	16.25	-29.15	-229.45	3.7
	16.40	-29.15	-229.51	3.7
	16.65	-29.13	-229.31	3.7
	17.00	-28.88	-228.72	2.3
	17.45	-29.05	-228.95	3.4

	17.65	-29.05	-228.82	3.6
	17.85	-27.48	-220.74	-0.9
	18.50	-28.39	-226.64	0.5
	18.80	-28.59	-226.93	1.8
	19.20	-28.29	-224.14	2.2
	19.40	-28.71	-227.52	2.1
	19.55	-28.59	-226.64	2.1

Appendix 1c: BH-3 Water Isotopes ($\delta^{18}O$ and $\delta^{2}H$) Results

Unit	*Depth (m)*	*δ18O (‰)*	*δD (‰)*	*d-excess (‰)*
Woody Organic (Riparian)	0.5	-17.06	-147.55	-11.1
	0.8	-18.22	-150.67	-4.9
	0.9	-17.87	-148.46	-5.5
	1	-17.90	-147.78	-4.6
	1.1	-17.29	-146.89	-8.6
	1.2	-16.21	-141.00	-11.3
	1.3	-17.23	-147.50	-9.7
	1.4	-17.38	-147.95	-8.9
	1.5	-17.45	-148.32	-8.7
	1.6	-17.35	-148.57	-9.8
	1.7	-17.38	-148.74	-9.7
	1.8	-17.56	-147.99	-7.5
	1.9	-17.73	-148.71	-6.9
	2	-17.65	-149.77	-8.6
	2.2	-17.61	-148.59	-7.7
	2.3	-17.81	-149.49	-7.0
ice-poor diamict	2.6	-18.13	-153.61	-8.6
	3	-18.59	-155.64	-6.9
	3.2	-19.12	-157.41	-4.4
	3.4	-17.84	-151.86	-9.1
	3.6	-18.63	-156.33	-7.3
	3.8	-19.18	-159.07	-5.6
	4	-19.23	-158.76	-4.9
	4.2	-19.51	-160.20	-4.1
	4.4	-19.40	-159.76	-4.6
	4.5	-19.32	-160.00	-5.4
	5	-19.50	-163.19	-7.2
	5.5	-20.01	-165.19	-5.1
	6	-20.29	-167.15	-4.8
	6.5	-20.30	-167.92	-5.6
	7	-20.79	-173.44	-7.1
	7.5	-21.00	-174.04	-6.1
	9.5	-22.52	-184.94	-4.8
	10.3	-22.11	-183.08	-6.1

Appendix 1d: BH-4 Water Isotopes ($\delta^{18}O$ and $\delta^{2}H$) Results

Unit	***Depth (m)***	***δ18O (‰)***	***δD (‰)***	***d-excess (‰)***
Peat	0.90	-20.86	-163.92	3.0
	1.00	-20.86	-165.30	1.6
	1.10	-20.48	-162.60	1.2
	1.20	-20.78	-164.63	1.6
	1.30	-20.64	-163.34	1.8
	1.40	-20.72	-163.21	2.5
	1.50	-20.77	-163.39	2.8
	1.60	-20.57	-163.20	1.4
	1.70	-20.75	-163.54	2.5
	1.80	-20.92	-164.51	2.9
	1.90	-20.51	-160.64	3.4
	2.00	-20.96	-164.14	3.5
	2.20	-20.66	-163.23	2.1
	2.40	-20.72	-163.23	2.5
	2.60	-20.86	-163.58	3.3
	2.80	-20.87	-163.87	3.1
	3.00	-20.33	-162.69	-0.1
	3.20	-20.19	-161.47	0.1
	3.40	-20.19	-161.84	-0.3
	3.60	-19.96	-161.11	-1.4
	3.80	-19.83	-160.90	-2.3
	4.10	-19.49	-160.49	-4.6
Silt and Clay	4.30	-19.85	-160.72	-1.9
	4.65	-19.78	-164.01	-5.8
	4.80	-20.00	-167.34	-7.3
	4.90	-19.57	-166.48	-9.9
	5.05	-19.54	-166.44	-10.1
	5.15	-19.55	-167.11	-10.7
	5.40	-19.53	-167.24	-11.0
	5.50	-19.67	-168.89	-11.5
	5.70	-19.44	-167.41	-11.9
	5.95	-19.13	-166.68	-13.6
	6.10	-19.30	-166.25	-11.9
	6.25	-18.96	-165.68	-14.0

Ice-poor diamict	6.40	-19.59	-167.31	-10.6
	6.60	-18.75	-163.57	-13.6
	6.90	-18.88	-164.63	-13.6
	7.00	-18.63	-164.78	-15.7
	7.10	-18.81	-164.97	-14.5
	7.25	-18.42	-162.37	-15.0

Appendix 1e: BH-8 Water Isotopes ($\delta^{18}O$ and $\delta^{2}H$) Results

Unit	*Depth (m)*	*δ18O (‰)*	*δD (‰)*	*d-excess (‰)*
Peat	0.10	-16.63	-126.76	6.2
	0.20	-17.72	-138.07	3.7
	0.40	-16.08	-133.06	-4.4
	0.60	-18.48	-152.60	-4.8
	0.90	-21.94	-175.81	-0.3
	1.00	-19.45	-155.65	0.0
	1.23	-21.66	-173.02	0.3
	1.40	-21.40	-169.98	1.2
	1.60	-20.87	-168.22	-1.2
	1.83	-19.94	-161.39	-1.8
	2.03	-19.75	-157.78	0.2
	2.20	-19.56	-159.00	-2.5
	2.40	-19.97	-161.67	-1.9
	2.62	-19.81	-160.04	-1.5
	2.84	-19.59	-158.37	-1.6
	3.05	-19.63	-159.14	-2.1
	3.21	-19.34	-157.40	-2.7
	3.40	-19.32	-157.84	-3.3
	3.60	-19.36	-157.50	-2.7
	3.81	-19.14	-156.74	-3.6
	4.05	-19.37	-155.88	-0.9
	4.28	-22.29	-177.65	0.7
Silt and Clay	4.45	-19.80	-162.59	-4.2
	4.64	-19.22	-159.41	-5.7
	4.85	-19.56	-161.74	-5.3
	5.05	-19.20	-161.20	-7.6
	5.25	-19.41	-161.80	-6.5
	5.47	-18.62	-159.76	-10.8
	5.68	-18.43	-158.21	-10.7
	5.87	-17.82	-154.59	-12.0
	5.95	-17.95	-156.32	-12.7
	6.05	-17.79	-154.32	-12.0
	6.20	-17.67	-152.97	-11.6

	6.40	-17.03	-152.59	-16.4
	6.65	-16.74	-149.36	-15.4
	6.94	-17.01	-151.35	-15.3
	7.00	-16.47	-148.41	-16.6
	7.28	-16.28	-147.04	-16.8
	7.48	-16.20	-146.88	-17.3
	7.66	-16.02	-145.85	-17.7
	7.85	-16.97	-150.80	-15.0
	8.05	-16.37	-147.73	-16.8
	8.29	-16.45	-147.18	-15.6
	8.60	-16.51	-147.83	-15.7
	8.79	-16.20	-145.77	-16.2
	9.00	-15.93	-145.59	-18.1
	9.20	-16.14	-145.71	-16.6
	9.40	-16.22	-146.66	-16.9
	9.60	-16.64	-149.35	-16.3
	9.85	-16.37	-147.48	-16.5
	10.00	-16.23	-147.19	-17.3
	10.26	-16.26	-147.52	-17.5
	10.46	-16.22	-147.50	-17.7
	10.78	-16.38	-148.13	-17.1
	10.90	-16.58	-148.22	-15.5
	11.23	-16.39	-148.59	-17.5
	11.29	-16.41	-148.66	-17.4
	11.34	-16.54	-149.21	-16.9

Appendix 2a: BH-1 Gravimetric Water Content (GWC%)

Unit	***Depth***	***GWC (%)***
Peat	0.00	178.6
	0.50	141.3
	1.00	189.8
	1.50	1159.2
Massive Ice	2.00	9500.0
	2.50	9500.0
	3.00	9500.0
	3.50	9500.0
	4.00	9500.0
	4.50	9500.0
	5.00	9500.0
	5.50	9500.0
	6.00	9500.0
	6.50	269.9
Ice-poor Diamict	7.00	35.9
	7.50	26.0
	8.00	28.1
	8.50	24.4
	9.00	45.7
	9.50	33.3
	10.00	30.1
	10.50	28.9
	11.00	42.1

Appendix 2b: BH-2 Gravimetric Water Content (GWC%)

Unit	***Depth***	***GWC (%)***
Peat	0.00	76.1
	0.50	84.4
	1.00	44.8
	1.50	31.4
	2.00	31.3
Gravelly Sand	2.50	16.7
	3.00	13.5
	3.50	10.6
	4.00	16.1
	4.50	21.1
	5.00	37.3
	5.50	14.0
	6.00	46.6
	6.50	41.3
	7.00	47.9
	7.50	51.5
	8.00	49.1
	8.50	49.3
	9.00	412.2
	9.50	4528.1
	11.00	33.9
	11.50	21.4
	10.00	61.4
	10.50	18.4
Ice-rich diamict	12.00	8000.0
	12.50	92.8
	13.00	592.3
	13.50	70.3
	14.00	1.8
	14.50	100.5
	19.00	85.7
	19.50	69.6
	20.00	49.8
	15.00	73.9
	15.50	68.5
	16.00	55.5

	16.50	93.3
	17.00	38.3
	17.50	53.5
	18.25	34.9
	18.50	56.5

Appendix 2c: BH-3 Gravimetric Water Content (GWC%)

Unit	***Depth***	***GWC (%)***
Peat	0.00	1734.7
	0.80	691.4
	1.00	135.9
	1.50	237.0
	2.00	197.6
Ice-poor diamict	2.50	92.3
	3.00	93.5
	3.50	38.2
	4.00	41.0
	4.50	33.4
	5.00	29.5
	5.50	28.1
	6.00	18.1
	6.50	19.3
	7.00	14.6
	7.50	18.4
	8.00	38.0
	8.50	37.8
	9.00	44.9
	9.50	31.3
	10.20	30.6

Appendix 2d: BH-4 Gravimetric Water Content (GWC%)

Unit	***Depth***	***GWC (%)***
Peat	0.00	715.8
	0.50	1039.3
	0.90	466.8
	1.30	696.5
	1.50	613.1
	2.00	571.2
	2.50	387.9
	3.00	398.8
	3.50	320.1
	4.00	200.8
Clay and Silt	4.50	111.4
	5.50	113.5
	6.00	67.2
Ice-poor diamict	6.50	22.2
	7.00	20.6
	7.50	24.0
	8.00	27.1
	8.50	24.2
	9.00	25.0
	9.50	26.0

Appendix 2e: BH-8 Gravimetric Water Content (GWC%)

Unit	*Depth*	*GWC (%)*
Peat	0.00	100.4
	0.50	324.5
	0.90	255.0
	1.50	161.2
	2.00	152.9
	2.50	196.0
	3.00	62.0
	3.50	102.3
	4.00	159.0
Clay and Silt	4.50	196.8
	5.00	130.0
	5.50	136.2
	6.00	44.4
	6.50	36.6
	7.00	55.4
	7.50	35.3
	8.00	42.8
	8.50	34.0
	9.00	34.9
	9.50	33.1
	10.00	34.4
	10.50	34.5
	11.00	33.1

Appendix 3a: BH-2 Geotek Scanner Density and Magnetic Susceptibility

Core Depth (cm)	**Section Number**	**Core Thickness (cm)**	**Density (g/cm^3)**	**Magnetic Susceptibility ($x10^{-5}$)**
1002	1	4.294	1.7124	14.15
1003	1	4.151	1.6632	14.88
1004	1	4.281	1.6742	27.11
1005	1	4.075	1.6231	21.3
1006	1	4.191	1.5916	14.95
1007	1	4.14	1.5788	17.99
1008	1	4.263	1.5756	25.59
1009	1	4.147	1.6254	24.93
1010	1	4.151	1.6075	16.27
1011	1	4.057	1.5033	26.19
1012	1	4.074	1.5101	16.53
1013	1	4.126	1.5642	21.96
1014	1	4.131	1.5217	42.92
1015	1	4.163	1.5911	15.08
1016	1	4.171	1.791	17.86
1017	1	4.195	1.7868	37.56
1018	1	4.158	1.7714	20.17
1019	1	4.181	1.769	32.87
1020	1	4.168	1.6036	24.94
1023	1	3.734	1.313	10.59
1024	1	3.799	1.4697	17.73
1025	1	3.818	1.2639	0.4
1026	1	3.898	0.9862	-0.33
1027	1	3.555	0.9228	-0.92
1028	1	3.727	0.893	-1.45
1029	1	3.72	0.8927	-1.39
1030	1	3.835	0.8735	-0.92
1031	1	3.665	0.93	-1.52
1032	1	4.044	0.9033	-1.58
1033	1	4.136	0.8707	-1.39
1034	1	4.221	0.9331	-1.59
1035	1	4.242	0.951	-1.65
1036	1	4.109	0.8879	-1.91
1039	1	4.044	0.9303	-1.58

1040	1	4.015	1.5949	1.78
1041	1	4.056	1.9268	69.97
1042	1	4.014	2.1226	375.43
1043	1	4.008	2.0339	185.9
1044	1	4.084	2.0577	12.04
1045	1	4.1	2.2927	11.71
1046	1	4.112	2.2645	2.52
1047	1	4.129	2.3887	13.36
1048	1	4.154	2.3302	23.21
1049	1	4.179	2.369	22.82
1050	1	4.165	2.4873	30.09
1051	1	4.237	2.2949	38.75
1052	1	4.243	2.2887	16.93
1053	1	4.211	2.4107	28.83
1054	1	4.253	2.3167	50.33
1055	1	4.314	2.1192	40.87
1056	1	4.296	2.0575	57.73
1057	1	4.266	1.9719	37.77
1058	1	4.304	1.9006	12.83
1059	1	4.204	1.8768	98.67
1063	1	4.349	2.0354	24.94
1064	1	4.332	1.93	21.63
1065	1	4.318	1.9338	13.16
1066	1	4.31	2.0494	24.14
1067	1	4.298	2.0438	14.29
1068	1	4.327	1.9045	20.97
1069	1	4.276	1.9904	20.63
1070	1	4.234	2.08	14.49
1071	1	4.269	2.1471	15.41
1072	1	4.235	1.9894	17.59
1073	1	4.219	1.9097	17.19
1074	1	4.173	2.1195	23.01
1075	1	4.187	2.0962	11.51
1076	1	4.184	1.9919	36.04
1077	1	4.172	1.9483	54.36
1078	1	4.14	2.0361	324.84
1079	1	4.138	2.2566	35.65
1080	1	4.09	2.3622	11.38
1081	1	4.103	2.2663	13.29
1082	1	4.075	2.1137	0.47
1083	1	4.018	1.9492	14.75
1502	2	3.593	0.8521	5.76
1503	2	3.585	1.0577	5.42
1504	2	3.635	1.1645	6.22
1505	2	3.666	1.2106	0.2

1506	2	3.566	1.3147	2.32
1507	2	3.726	0.9947	-0.13
1508	2	3.755	0.8368	-0.66
1510	2	4.359	0.7961	1.65
1511	2	4.358	0.9743	3.31
1512	2	4.355	0.89	-0.73
1513	2	4.284	0.9646	-2.31
1514	2	4.289	1.0262	-1.19
1515	2	4.251	1.1506	0
1516	2	4.262	1.493	2.31
1517	2	4.255	1.475	4.89
1518	2	4.18	1.3992	1.58
1519	2	4.235	1.6139	2.97
1520	2	4.219	1.6964	-1
1521	2	4.218	1.4952	-1.92
1522	2	4.123	1.1965	-1.72
1523	2	4.17	1.2897	-1.52
1524	2	4.187	1.4196	-0.4
1525	2	4.105	1.4205	4.89
1526	2	3.998	1.4944	6.61
1527	2	4.03	1.5615	6.75
1528	2	4.068	1.5196	1.78
1529	2	4.123	1.592	4.17
1530	2	4.091	1.6875	6.15
1531	2	3.992	1.549	7.01
1532	2	4.019	1.3411	7.27
1533	2	4.055	1.3137	12.63
1534	2	4.055	1.4466	2.98
1535	2	4.024	1.4849	6.28
1536	2	4.045	1.5714	7.08
1537	2	4.05	1.5892	7.28
1538	2	3.951	1.6094	7.21
1539	2	3.967	1.4386	2.18
1540	2	4.05	1.4543	0.6
1541	2	4.034	1.5978	2.18
1542	2	3.822	1.95	4.76
1543	2	4.028	1.886	3.57
1544	2	4.011	1.4575	1.72
1545	2	3.87	1.0949	3.77
1546	2	3.841	1.0267	3.9
1547	2	3.883	0.9535	-0.86
1548	2	3.761	1.0293	-0.86
1549	2	3.91	1.0493	-0.46
1550	2	3.351	1.2563	0
1572	3	3.849	1.6584	9.46

1573	3	3.806	1.7099	7.27
1574	3	3.795	1.5624	6.88
1575	3	3.77	1.4823	7.14
1576	3	3.841	1.3329	5.88
1577	3	3.82	1.2995	8.99
1578	3	3.933	1.0706	1.26
1581	3	3.917	0.8419	-1.19
1582	3	3.927	1.0328	-1.59
1583	3	4.046	1.2855	-0.92
1584	3	4.026	1.318	0.47
1585	3	4.043	1.2317	-1.39
1586	3	4.108	1.3002	-1.52
1587	3	4.214	1.0239	2.78
1588	3	4.131	0.9608	-0.2
1589	3	4.06	1.103	0.53
1590	3	4.051	0.991	-1.12
1591	3	4.076	0.8854	-0.59
1592	3	4.003	1.0446	-2.11
1593	3	4.078	1.051	4.36
1594	3	4.152	1.0538	4.17
1595	3	4.139	1.143	2.64
1596	3	4.146	1.3447	3.77
1597	3	4.133	1.4994	4.23
1598	3	4.13	1.4653	3.57
1599	3	4.14	1.6906	3.37
1600	3	4.141	1.8092	5.62
1601	3	4.109	1.834	5.23
1602	3	4.121	1.7494	6.61
1603	3	4.002	1.672	6.28
1604	3	4.097	1.5859	5.29
1605	3	4.093	1.5425	3.84
1606	3	4.111	1.5333	5.03
1607	3	4.033	1.5154	2.91
1608	3	4.039	1.5209	1.72
1609	3	4.039	1.7679	3.04
1610	3	4.066	1.8703	5.42
1611	3	3.957	1.9182	5.69
1612	3	4.017	1.8116	3.38
1613	3	4.05	1.6732	1.46
1614	3	4.077	1.5933	1.65
1615	3	4.077	1.7188	3.64
1616	3	4.091	1.5845	2.25
1622	4	4.348	1.3949	6.55
1623	4	4.38	1.4716	4.76
1624	4	4.374	1.3748	5.29

1625	4	4.367	1.4993	1.91
1626	4	4.332	1.6819	-1.12
1627	4	4.378	1.6857	-1.59
1628	4	4.368	1.3833	-1.45
1629	4	4.33	1.1803	1.58
1630	4	4.293	1.2842	-0.73
1631	4	4.398	1.2377	2.11
1632	4	4.343	1.1108	-1.06
1633	4	4.376	1.2249	-1.46
1634	4	4.34	1.1266	-0.27
1635	4	4.311	1.1183	7.67
1636	4	4.331	1.1028	5.56
1637	4	4.327	1.1538	3.31
1638	4	4.354	1.152	-0.33
1639	4	4.28	1.088	2.91
1640	4	4.295	1.1123	-0.13
1641	4	4.307	1.4052	-1.45
1642	4	4.319	1.361	-1.85
1643	4	4.257	1.2176	-1.98
1644	4	4.259	1.3332	-1.85
1645	4	4.221	1.4126	0.59
1646	4	4.277	1.309	1.45
1647	4	4.235	1.1334	5.95
1648	4	4.212	1.1863	-0.66
1649	4	4.231	1.3383	-1.59
1650	4	4.164	1.6061	-1.65
1651	4	4.206	1.547	6.81
1652	4	4.191	1.3116	6.94
1653	4	4.186	1.1632	8.13
1656	4	4.068	1.2304	0.26
1657	4	4.082	1.4552	-1.46
1658	4	4.096	1.5715	-1.19
1659	4	4.002	1.5231	0.73
1660	4	4.139	1.3333	-0.07
1661	4	4.171	1.1944	-1.52
1662	4	4.191	1.0913	-1.52
1663	4	4.209	1.003	-1.45
1664	4	4.188	1.023	-1.52
1665	4	4.233	1.1339	-1.19
1666	4	4.233	1.1232	-1.39
1667	4	4.264	1.0142	-1.25
1668	4	4.268	1.0814	-0.53
1669	4	4.191	1.3932	-0.53
1670	4	4.265	1.5921	1.06
1671	4	4.197	1.6022	0.66

1672	4	4.231	1.6127	-0.73
1673	4	4.27	1.3386	-0.99
1674	4	4.292	1.6084	4.96
1675	4	4.394	1.9164	8.99
1676	4	4.414	1.9185	7.67
1677	4	4.452	1.9291	6.68
1678	4	4.45	1.8129	5.29
1679	4	4.423	1.8211	7.08
1680	4	4.466	1.8555	4.83
1681	4	4.458	1.9641	5.69
1682	4	4.474	1.7216	5.22
1683	4	4.457	1.3148	2.91
1684	4	4.446	1.3435	7.87
1685	4	4.543	1.5797	6.02
1686	4	4.566	1.7525	5.75
1687	4	4.596	1.7433	3.17
1688	4	4.566	1.0698	0.13
1690	5	4.05	1.6947	12.57
1691	5	4.055	1.6959	13.82
1692	5	4.012	1.6044	14.22
1693	5	3.971	1.8352	15.14
1694	5	4.021	1.88	10.32
1695	5	3.983	1.8963	5.56
1696	5	4.006	1.9085	1.59
1697	5	3.97	1.9782	4.83
1698	5	3.975	1.8147	6.42
1699	5	3.958	1.7676	6.94
1700	5	4.015	1.5343	6.95
1701	5	3.977	1.2948	6.41
1702	5	3.998	1.5327	6.15
1703	5	3.992	1.2821	3.91
1704	5	3.809	1.336	8.14
1705	5	4.041	1.5032	8.87
1706	5	4.078	1.4552	7.94
1707	5	3.328	1.8687	8.47
1708	5	4.133	1.7582	4.37
1709	5	4.086	1.837	7.28
1710	5	4.096	1.8659	6.42
1711	5	3.994	1.8052	1.65
1712	5	4.11	1.6388	4.04
1713	5	4.096	1.5525	2.58
1714	5	3.602	1.8593	0.26
1715	5	3.853	1.9755	6.67
1716	5	4.056	1.9142	9.06
1717	5	4.09	1.7027	8.53

1718	5	3.939	1.3158	2.97
1719	5	4.178	1.6945	4.3
1720	5	4.195	2.0391	5.82
1721	5	4.178	1.8872	6.48
1722	5	4.229	1.8227	5.49
1723	5	4.182	1.7752	0.86
1724	5	4.236	1.7407	2.78
1725	5	4.161	1.7458	0.66
1726	5	4.195	1.7704	2.38
1727	5	4.063	1.728	1.46
1728	5	4.302	1.6981	2.38
1729	5	4.071	1.8219	1.66
1730	5	4.238	1.8318	9.65
1731	5	4.311	1.6605	3.64
1732	5	4.309	1.8243	3.77
1733	5	4.165	1.7622	4.7
1734	5	4.291	1.5421	3.17
1735	5	3.909	1.6836	2.84
1736	5	3.956	1.7055	2.84
1737	5	4.037	1.8536	2.04
1738	5	4.443	1.8166	3.04
1739	5	4.482	1.8166	4.43
1740	5	4.385	1.7057	4.29
1741	5	4.487	1.5998	3.24
1742	5	4.428	1.4923	2.71
1745	6	4.13	1.4748	10.45
1746	6	4.11	1.5362	8.46
1747	6	3.688	1.6747	6.48
1748	6	4.131	1.4598	6.94
1749	6	3.939	1.6915	7.47
1750	6	4.158	1.8256	11.3
1751	6	4.186	1.9595	12.23
1752	6	4.212	1.9761	9.46
1753	6	4.228	1.8542	9.52
1754	6	4.23	1.8943	2.51
1755	6	4.215	1.831	6.28
1756	6	4.242	1.5773	4.76
1757	6	4.278	1.5368	1.32
1758	6	4.008	1.4624	0.59
1759	6	3.375	1.5919	2.44
1760	6	4.351	1.2849	1.52
1761	6	3.861	1.5433	1.91
1762	6	4.327	1.4851	1.78
1763	6	4.384	1.769	2.91
1764	6	4.358	1.7197	5.56

1765	6	4.367	1.5643	5.82
1766	6	4.229	1.4449	4.43
1767	6	3.913	1.5719	2.45
1768	6	4.35	1.4052	2.97
1769	6	4.354	1.3649	1.39
1770	6	4.418	1.3463	0.2
1771	6	4.501	1.4944	3.04
1772	6	4.439	1.4649	3.3
1773	6	4.493	1.3896	3.37
1774	6	4.57	1.3564	3.77
1775	6	4.482	1.4164	3.57
1776	6	4.087	1.4329	3.9
1777	6	3.863	1.3946	0.79
1778	6	4.631	1.2215	0.46
1779	6	4.653	1.4953	-0.07
1780	6	4.786	1.5112	-0.4
1781	6	4.743	1.5102	0.79
1782	6	4.795	1.6968	3.5
1783	6	4.819	1.5663	2.25
1784	6	4.847	1.6663	2.45
1787	7	4.104	1.3411	3.18
1788	7	3.837	1.6005	5.1
1789	7	4.098	1.7824	2.98
1790	7	4.062	1.4864	3.64
1791	7	4.063	1.2099	1.66
1792	7	3.653	1.3865	0.34
1793	7	3.706	1.8767	0.33
1794	7	4.032	2.0305	1.52
1795	7	4.036	2.0589	1.52
1796	7	4.004	1.7303	1.25
1797	7	3.765	1.4897	3.24
1798	7	3.863	1.6463	-0.27
1799	7	3.756	1.73	-0.79
1800	7	3.191	1.5668	-0.93
1827	8	4.492	1.0874	2.97
1828	8	4.468	1.2465	4.69
1829	8	4.46	1.1002	5.43
1830	8	4.441	1.124	0.2
1831	8	4.481	1.2598	4.17
1832	8	4.008	1.4571	7.21
1833	8	4.246	1.528	7.74
1834	8	4.435	1.5532	7.8
1835	8	4.434	1.526	8.73
1836	8	4.448	1.4822	8.4
1837	8	4.443	1.3161	7.8

1841	8	3.449	0.8347	1.85
1842	8	4.136	0.8847	4.16
1843	8	4.147	0.9096	5.62
1844	8	3.852	0.9352	6.88
1845	8	4.174	1.048	6.29
1846	8	4.19	1.1797	6.55
1847	8	4.206	1.1626	8.33
1848	8	3.33	0.7615	6.68
1849	8	3.405	0.718	3.64
1850	8	3.698	0.9018	0.06
1851	8	4.218	0.9705	0
1853	8	3.849	1.0953	-0.86
1854	8	4.328	1.362	-1.06
1855	8	4.326	1.3156	-0.73
1856	8	3.965	1.1677	0.66
1857	8	4.033	1.4142	9.12
1858	8	4.278	1.7198	10.52
1859	8	4.248	1.8149	9.78
1860	8	4.221	1.914	7.67
1861	8	4.189	1.7111	5.75
1862	8	4.146	1.3585	-0.86
1863	8	3.874	1.7325	-1.39
1864	8	3.905	1.4397	-2.12
1865	8	3.907	0.8166	-2.12
1867	9	4.596	1.3955	10.98
1868	9	4.678	1.4112	4.43
1869	9	4.681	1.8865	6.48
1870	9	4.685	2.1041	6.08
1871	9	4.622	2.2025	6.61
1872	9	4.632	2.1599	5.69
1873	9	4.618	2.1436	5.43
1874	9	4.606	2.1412	4.89
1875	9	4.617	2.103	4.37
1876	9	4.617	2.0895	5.09
1877	9	4.605	1.8752	5.29
1878	9	4.6	1.866	5.82
1879	9	4.352	1.7034	1.72
1880	9	4.574	1.2009	1.33
1881	9	4.607	1.3154	-0.4
1882	9	4.571	1.4067	3.97
1883	9	4.584	1.3392	5.49
1884	9	4.415	1.3935	-1.25
1885	9	4.349	2.0963	-0.99
1886	9	4.529	2.1767	2.58
1887	9	4.512	2.1751	3.71

1888	9	4.535	2.1196	4.1
1889	9	4.516	1.8403	3.57
1890	9	4.496	1.9189	2.65
1891	9	4.456	1.8242	3.9
1892	9	4.499	1.6206	3.24
1893	9	4.52	1.3184	1.85
1894	9	4.255	1.3438	0.13
1895	9	4.26	1.5696	-1.32
1896	9	4.384	1.4896	-1.05
1897	9	4.451	1.8353	-0.46
1898	9	4.405	1.8794	2.12
1899	9	4.435	1.7777	4.63
1900	9	4.437	1.6641	1.85
1901	9	4.416	1.7355	3.37
1902	9	4.453	1.816	2.05
1903	9	4.466	1.9367	2.78
1904	9	4.474	2.0389	3.44
1905	9	4.454	2.0268	2.72
1906	9	4.429	1.962	2.12
1907	9	4.395	1.8637	2.58
1908	9	4.365	1.6467	2.64
1909	9	4.4	1.6827	2.25
1910	9	4.389	1.925	1.85
1911	9	4.37	2.0374	1.72
1912	9	4.377	2.0313	2.05
1913	9	4.363	2.0697	1.92
1914	9	4.378	2.0666	1.65
1915	9	4.357	2.0241	1.78
1916	9	4.357	2.0525	2.11
1917	9	4.26	1.9607	0.59
1918	9	3.986	1.8986	-0.26
1919	9	4.165	1.5485	0.14
1920	9	4.144	1.3769	-0.33
1921	9	4.139	1.2551	1.46
1922	9	4.078	1.041	0.53
1923	9	3.575	0.6648	-0.73
1926	10	3.625	0.9225	5.3
1927	10	3.639	1.0154	-2.25
1928	10	3.449	1.3464	-2.25
1929	10	3.351	2.1355	-1.65
1930	10	4.133	2.1062	3.5
1931	10	4.137	2.1201	1.65
1932	10	4.129	2.1058	0.72
1933	10	4.147	1.9104	-0.47
1934	10	4.153	1.6837	-1.59

1935	10	4.18	1.2717	-1.26
1936	10	3.318	1.5326	-2.25
1937	10	3.987	2.0257	1.59
1938	10	4.107	2.07	6.29
1939	10	4.104	2.1071	5.96
1940	10	4.116	2.1086	5.89
1941	10	4.164	2.107	6.16
1942	10	4.129	1.9734	6.02
1943	10	4.213	1.7443	7.41
1944	10	4.233	1.4874	6.88
1945	10	4.182	1.436	6.68
1946	10	4.239	1.6003	7.48
1947	10	4.245	1.6467	4.83
1948	10	4.284	1.5964	4.7
1949	10	3.953	1.6879	4.83
1950	10	4.319	1.5422	6.28
1951	10	4.352	1.4575	4.04
1952	10	3.759	1.4535	-1.12
1953	10	3.708	1.5863	-0.86
1954	10	4.15	1.6451	-1.46
1955	10	4.42	1.542	-0.53
1956	10	4.32	1.8766	2.71
1957	10	4.485	1.9938	5.56
1958	10	4.513	1.9821	6.22
1959	10	4.524	1.7818	6.02
1960	10	4.206	1.7377	6.48
1961	10	4.357	1.5479	2.91
1962	10	3.878	1.308	-0.53

Appendix 3b: BH-3 Geotek Scanner Density and Magnetic Susceptibility

Core Depth (cm)	**Section Number**	**Core Thickness (cm)**	**Density (g/cm^3)**	**Magnetic Susceptibility ($x10^{-5}$)**
80	1	3.528	1.0202	-0.06
81	1	4.137	1.1067	0
82	1	4.202	1.0595	0.34
83	1	4.199	1.0948	4.11
84	1	4.236	1.1028	0.86
85	1	4.294	1.056	0.99
86	1	4.117	1.0441	0.79
87	1	4.063	1.1055	0.73
88	1	4.108	1.0991	-0.59
89	1	4.1	1.1225	-1.25
90	1	4.14	1.1406	-1.12
91	1	4.209	1.0893	-1.32
92	1	4.206	1.1273	-0.93
93	1	4.226	1.1236	-1.06
94	1	4.26	1.1006	-0.73
95	1	4.246	1.1125	-1.32
96	1	4.253	1.1525	-1.25
97	1	4.294	1.1649	-1.32
98	1	4.326	1.1419	-0.86
99	1	4.287	1.1277	-1.45
100	1	4.236	1.1541	-1.85
101	1	4.226	1.1311	-0.13
102	1	4.319	1.1547	-1.52
103	1	4.297	1.1511	-1.19
104	1	4.359	1.1761	-0.99
105	1	4.288	1.2244	-0.19
106	1	4.332	1.1874	-0.13
107	1	4.307	1.1775	-1.78
108	1	4.329	1.1746	-0.06
109	1	4.256	1.2241	-0.59
110	1	4.199	1.2252	-0.46
111	1	4.32	1.1907	-0.33
112	1	4.295	1.2435	-0.06
113	1	4.352	1.2091	-0.72
114	1	4.406	1.2054	-1.52

115	1	4.401	1.2185	-1.52
116	1	4.417	1.1167	2.45
120	1	3.938	1.2809	-1.65
121	1	3.97	1.2322	-1.85
122	1	3.99	1.3016	-1.85
123	1	4.068	1.3046	-1.98
124	1	4.041	1.3103	-1.72
125	1	4.061	1.26	-2.18
126	1	4.072	1.3176	-2.18
127	1	4.117	1.2545	-2.38
128	1	4.104	1.2366	-0.6
129	1	4.141	1.232	-0.66
130	1	4.226	1.2815	-1.06
131	1	4.248	1.216	-0.99
132	1	4.27	1.2891	-1.06
133	1	4.304	1.2687	-1.06
134	1	4.35	1.2263	-1.06
135	1	4.343	1.2602	-1.32
136	1	4.448	1.1969	-1.06
137	1	4.498	1.2264	-1.19
138	1	4.522	1.1813	-0.6
139	1	4.537	1.1976	-0.86
140	1	4.524	1.2021	-0.99
141	1	4.62	1.2376	-0.33
142	1	4.608	1.2694	-0.07
143	1	4.669	1.2463	-0.2
144	1	4.702	1.2164	-0.27
145	1	4.715	1.2246	-0.53
146	1	4.687	1.1268	-0.66
150.87	2	4.088	1.1776	2.85
151.87	2	4.206	1.2622	3.37
152.87	2	4.204	1.2658	3.44
153.87	2	4.172	1.2123	3.51
154.87	2	4.141	1.2377	3.11
155.87	2	4.075	1.2553	3.5
156.87	2	4.11	1.2196	3.05
157.87	2	3.92	1.3291	2.84
158.87	2	4.06	1.2931	2.58
159.87	2	3.993	1.2977	2.58
160.87	2	3.988	1.1416	-0.73
164.87	2	4.479	1.2763	-2.31
165.87	2	4.536	1.2179	-2.11
166.87	2	4.516	0.9377	-2.05
170.87	2	3.989	0.9691	-0.72
173.87	2	4.232	1.241	-0.72

174.87	2	4.246	1.2395	-0.85
175.87	2	4.136	1.1458	-0.66
176.87	2	4.157	1.1631	-0.46
177.87	2	4.103	1.209	-0.26
178.87	2	4.17	1.2468	-0.33
179.87	2	4.1	1.2517	-0.19
182.82	3	4.291	1.1433	0.59
183.82	3	4.328	1.1822	0.66
184.82	3	4.313	1.2674	0.2
185.82	3	4.368	1.2788	0.13
186.82	3	4.399	1.2902	0.33
187.82	3	4.375	1.2669	-1.46
188.82	3	4.39	1.2269	-1.46
189.82	3	4.371	1.2526	-1.39
190.82	3	4.376	1.2703	-1.39
191.82	3	4.387	1.2735	-1.46
192.82	3	4.478	1.1765	-1.53
193.82	3	4.296	1.1688	-1.72
194.82	3	4.348	1.2295	-1.92
195.82	3	4.408	1.2373	-2.12
196.82	3	4.418	1.2485	-2.45
197.82	3	4.449	1.2695	-0.93
198.82	3	4.473	1.2873	-1.06
199.82	3	4.462	1.1771	1.98
203.82	3	4.051	1.3263	-1.59
204.82	3	4.054	1.2956	-1.39
205.82	3	4.127	1.2779	-1.33
206.82	3	4.124	1.3046	-1.52
207.82	3	4.138	1.272	-0.66
208.82	3	4.128	1.2831	-0.66
209.82	3	4.175	1.2903	-0.73
210.82	3	4.151	1.2523	-0.73
211.82	3	4.178	1.2608	-0.86
212.82	3	4.106	1.2723	-0.86
213.82	3	4.164	1.2582	-0.93
214.82	3	4.13	1.257	-0.93
215.82	3	4.164	1.2431	-0.93
216.82	3	4.16	1.2393	-1.13
217.82	3	4.226	1.2306	-1.39
218.82	3	4.215	1.2724	-1.53
219.82	3	4.236	1.2325	-1.66
220.82	3	4.298	1.2429	-1.79
221.82	3	4.253	1.2929	-1.79
222.82	3	4.32	1.2932	-1.92
223.82	3	4.345	1.2944	-2.18

224.82	3	4.354	1.2622	-2.39
225.82	3	4.318	1.3003	-2.31
226.82	3	4.401	1.2503	-2.32
227.82	3	4.371	1.2663	-0.53
228.82	3	4.45	1.1992	-0.66
229.82	3	4.38	1.1188	-0.86
231.78	4	4.429	1.2819	4.17
232.78	4	4.354	1.3362	2.45
233.78	4	4.496	1.2647	6.15
234.78	4	4.44	1.2774	4.96
235.78	4	4.503	1.2519	1.38
236.78	4	4.48	1.2866	1.05
237.78	4	4.469	1.2763	-0.66
238.78	4	4.372	1.3019	-0.73
239.78	4	4.378	1.2536	-1.39
240.78	4	4.449	1.278	-1.12
241.78	4	4.381	1.2774	-0.53
242.78	4	4.374	1.2837	1.71
243.78	4	4.513	1.2525	-0.4
244.78	4	4.522	1.2219	-1.72
245.78	4	4.439	1.2759	-0.53
246.78	4	4.48	1.2569	-0.93
247.78	4	4.519	1.2849	-0.66
248.78	4	4.556	1.2413	-0.6
249.78	4	4.563	1.2141	1.06
250.78	4	4.563	1.2762	-0.2
251.78	4	4.555	1.2461	0.46
252.78	4	4.567	1.233	0.07
253.78	4	4.583	1.2379	2.65
254.78	4	4.571	1.2635	0.93
255.78	4	4.546	1.2512	2.38
256.78	4	4.523	1.2758	0.47
257.78	4	4.536	1.2465	0
258.78	4	4.581	1.2149	-0.07
259.78	4	4.505	1.2449	-0.26
260.78	4	4.555	1.2707	-0.2
261.78	4	4.587	1.2244	0.07
262.78	4	4.592	1.155	-0.6
362.65	6	4.357	1.4268	55.55
363.65	6	3.94	1.6161	56.61
364.65	6	3.992	1.6374	25.06
365.65	6	4.13	1.4124	20.77
366.65	6	3.961	1.5154	28.96
367.65	6	4.199	1.7875	37.76
368.65	6	4.196	1.9018	26.39

369.65	6	4.186	1.9441	20.97
370.65	6	4.299	1.9024	36.31
371.65	6	4.031	1.7927	66.86
372.65	6	4.307	1.5596	31.62
373.65	6	3.86	1.7584	24.08
374.65	6	4.071	1.9403	79.96
375.65	6	4.07	2.0284	54.56
376.65	6	4.054	2.016	36.17
377.65	6	4.122	2.0113	30.88
378.65	6	4.169	1.9759	20.5
379.65	6	4.331	1.9199	13.95
380.65	6	4.229	2.0498	10.12
381.65	6	4.35	1.931	9.46
382.65	6	4.256	1.8287	36.84
383.65	6	4.318	1.756	16.14
384.65	6	4.393	1.6502	19.64
385.65	6	4.207	1.7929	30.36
386.65	6	4.298	1.7992	40.67
387.65	6	4.404	1.6896	58.26
388.65	6	4.268	1.7483	172.34
389.65	6	4.487	1.7444	26.32
390.65	6	4.294	1.8942	26.65
391.65	6	4.509	1.7926	56.15
392.65	6	4.33	1.7987	66.6
393.65	6	4.528	1.7274	43.32
394.65	6	4.422	1.6827	52.71
395.65	6	4.46	1.7032	27.51
396.65	6	4.49	1.792	46.49
397.65	6	4.502	1.8334	17.86
398.65	6	4.445	1.8434	22.61
399.65	6	4.432	1.7644	23.14
401.62	7	4.296	1.7903	52.11
402.62	7	4.33	1.7911	100.12
403.62	7	4.274	1.8543	79.49
404.62	7	4.118	1.9228	46.89
405.62	7	4.133	1.8971	66.13
406.62	7	4.315	1.937	309.23
407.62	7	4.207	1.8507	475.02
408.62	7	4.057	1.8991	75.85
409.62	7	4.181	1.9325	38.29
410.62	7	4.197	1.8544	42.92
411.62	7	4.156	1.6679	66.26
412.62	7	4.175	1.513	75.13
413.62	7	3.98	1.8312	46.49
414.62	7	4.06	1.9306	52.9

415.62	7	3.963	1.9396	60.51
416.62	7	4.102	1.9464	86.11
417.62	7	3.96	1.9127	80.29
418.62	7	3.949	1.9838	57.21
419.62	7	3.935	1.9176	57.73
420.62	7	3.825	1.9947	46.29
421.62	7	3.935	1.5741	27.18
422.62	7	3.888	1.2291	11.97
426.62	7	3.864	2.1951	47.35
427.62	7	4.038	1.7422	343.49
428.62	7	3.745	1.7543	18.85
429.62	7	3.843	1.7521	19.25
430.62	7	3.882	1.9228	32.14
431.62	7	4.016	2.0039	87.89
432.62	7	4.14	1.9587	43.78
433.62	7	4.099	1.7914	32.07
434.62	7	4.089	1.9333	38.75
435.62	7	4.18	2.0433	66.19
436.62	7	4.131	2.0511	38.82
437.62	7	4.091	1.999	59.58
438.62	7	4.198	1.9835	411.67
439.62	7	4.197	1.9129	193.63
440.62	7	4.149	1.9426	33.86
441.62	7	4.189	1.7492	67.19
442.62	7	4.018	1.8084	46.23
443.62	7	4.203	1.9085	19.97
444.62	7	4.233	1.9842	22.49
445.62	7	4.044	1.9686	26.06
446.62	7	4.205	1.8424	5.56
447.62	7	4.238	1.8037	6.22
448.62	7	4.228	1.952	19.51
449.62	7	4.272	2.0791	16.47
450.62	7	4.189	2.0251	14.15
451.62	7	4.309	1.9739	17.26
452.62	7	4.233	2.149	11.64
453.62	7	4.321	1.9583	10.12
454.62	7	4.167	2.1275	36.17
455.62	7	4.261	2.1245	26.19
456.62	7	4.347	1.9148	33.79
457.62	7	4.342	1.8368	41.93
458.62	7	4.337	1.7996	18.19
459.62	7	4.356	1.5508	20.17
1055.44	8	4.254	2.3141	9.85
1056.44	8	4.266	2.3574	9.99
1057.44	8	4.264	2.3442	10.12

1058.44	8	4.273	2.3312	9.59
1059.44	8	4.289	2.3742	9.46
1060.44	8	4.314	2.2964	6.48
1061.44	8	4.311	2.3014	6.41
1062.44	8	4.332	2.3523	5.89
1063.44	8	4.328	2.1592	7.01
1064.44	8	4.366	1.0767	5.09

Appendix 4a: BH-1 Loss-on-Ignition (LOI)

Depth	Batch-Index	Crucible #	Crucible (g)	Pre 550 Crucible + Sample Weight (g)	Post 550 Sample + Crucible Weight (g)	Pre 550 (g)	Post 550 (g) [Ash]	Lost (g)	LOI 550°C %	Post 550 Sample + Crusible Weight (g)	Pre 850 (g)	Post 850 (g) [Carbonates]	Lost (g)	LOI 850°C %
0.00	2-1	J	13.599	14.2222	13.7318	0.6232	0.1328	0.4904	78.6906	13.7182	0.1328	0.1192	0.0136	10.2410
0.20	1-5	T	16.6866	17.3861	16.7487	0.6995	0.0621	0.6374	91.1222	16.7451	0.0621	0.0585	0.0036	5.7971
0.40	2-9	VI	12.2980	13.5506	12.3969	1.2526	0.0989	1.1537	92.1044	12.3878	0.0989	0.0898	0.0091	9.2012
0.60	2-13	N	15.4206	15.8370	15.4454	0.4164	0.0248	0.3916	94.0442	15.4411	0.0248	0.0205	0.0043	17.3387
0.80	1-17	C	16.1637	16.4192	16.1814	0.2555	0.0177	0.2378	93.0724	16.1795	0.0177	0.0158	0.0019	10.7345
1.00	1-21	A	16.2046	16.5196	16.2299	0.3150	0.0253	0.2897	91.9683	16.2277	0.0253	0.0231	0.0022	8.6957
1.20	2-25	O	16.4915	16.965	16.5329	0.4735	0.0414	0.4321	91.2566	16.5273	0.0414	0.0358	0.0056	13.5266
1.40	2-29	B	15.7361	16.258	15.7801	0.5219	0.044	0.4779	91.5693	15.7747	0.0440	0.0386	0.0054	12.2727
1.60	1-33	G	14.5632	15.4147	14.6082	0.8515	0.0450	0.8065	94.7152	14.6044	0.0450	0.0412	0.0038	8.4444
1.80	2-37	E	13.8695	14.4634	13.9116	0.5939	0.0421	0.5518	92.9113	13.9068	0.0421	0.0373	0.0048	11.4014
2.10	1-43	S	15.1896	15.5818	15.2195	0.3922	0.0299	0.3623	92.3763	15.2165	0.0299	0.0269	0.0030	10.0334
2.20	2-45	I	14.7696	14.8012	14.7857	0.0316	0.0161	0.0155	49.0506	14.7815	0.0161	0.0119	0.0042	26.0870
2.60	2-53	V	12.7502	13.2920	12.8968	0.5418	0.1466	0.3952	72.9420	12.8841	0.1466	0.1339	0.0127	8.6630
2.80	1-57	R	15.4381	15.8946	15.5708	0.4565	0.1327	0.3238	70.9310	15.5621	0.1327	0.1240	0.0087	6.5561
3.00	2-61	K	16.3895	16.9487	16.5507	0.5592	0.1612	0.3980	71.1731	16.5352	0.1612	0.1457	0.0155	9.6154
3.20	2-65	III	11.4755	11.5425	11.4959	0.0670	0.0204	0.0466	69.5522	11.4926	0.0204	0.0171	0.0033	16.1765
3.60	2-73	IV	13.1444	13.3023	13.1849	0.1579	0.0405	0.1174	74.3509	13.1797	0.0405	0.0353	0.0052	12.8395
4.60	2-93	U	14.4377	14.5618	14.4604	0.1241	0.0227	0.1014	81.7083	14.4578	0.0227	0.0201	0.0026	11.4537

6.60	2-133	Q	15.7601	17.5895	17.5331	1.8294	1.7730	0.0564	3.0830	17.4019	1.7730	1.6418	0.1312	7.3999
6.80	1-137	J	13.5994	21.1057	20.8295	7.5063	7.2301	0.2762	3.6796	20.4938	7.2301	6.8944	0.3357	4.6431
7.20	1-145	F	14.1190	20.4581	20.1784	6.3391	6.0594	0.2797	4.4123	19.9646	6.0594	5.8456	0.2138	3.5284
7.40	1-149	O	16.4910	24.0192	23.7309	7.5282	7.2399	0.2883	3.8296	23.4277	7.2399	6.9367	0.3032	4.1879
7.45	1-150	D	15.0543	20.6655	20.3700	5.6112	5.3157	0.2955	5.2663	20.1683	5.3157	5.1140	0.2017	3.7944
7.60	1-153	E	13.8704	22.9256	22.5481	9.0552	8.6777	0.3775	4.1689	22.0686	8.6777	8.1982	0.4795	5.5257
7.85	1-158	M	16.0563	23.8576	23.4875	7.8013	7.4312	0.3701	4.7441	22.9702	7.4312	6.9139	0.5173	6.9612
8.00	2-161	R	15.4376	26.4294	26.0101	10.9918	10.5725	0.4193	3.8147	25.3703	10.5725	9.9327	0.6398	6.0515
8.20	1-165	Q	15.7601	23.7843	23.4784	8.0242	7.7183	0.3059	3.8122	23.0382	7.7183	7.2781	0.4402	5.7033
8.30	2-167	D	15.0541	23.8746	23.5307	8.8205	8.4766	0.3439	3.8989	23.0295	8.4766	7.9754	0.5012	5.9127
8.50	1-171	I	14.7393	21.8824	21.4459	7.1431	6.7066	0.4365	6.1108	21.2313	6.7066	6.4920	0.2146	3.1998
8.80	2-177	S	15.1091	23.0338	22.6862	7.9247	7.5771	0.3476	4.3863	22.2845	7.5771	7.1754	0.4017	5.3015
8.90	1-179	B	15.7363	21.8441	21.4522	6.1078	5.7159	0.3919	6.4164	21.2386	5.7159	5.5023	0.2136	3.7369
9.00	1-181	H	15.9677	23.0942	22.6557	7.1265	6.6880	0.4385	6.1531	22.4412	6.6880	6.4735	0.2145	3.2072
9.20	1-185	K	16.3888	25.1446	24.5877	8.7558	8.1989	0.5569	6.3604	24.3156	8.1989	7.9268	0.2721	3.3187
9.40	2-189	H	15.9675	25.5946	25.2233	9.6271	9.2558	0.3713	3.8568	24.7049	9.2558	8.7374	0.5184	5.6008
9.50	1-191	N	15.4200	22.7392	22.2837	7.3192	6.8637	0.4555	6.2234	22.0462	6.8637	6.6262	0.2375	3.4602
9.65	2-194	A	16.2049	23.1767	22.8831	6.9718	6.6782	0.2936	4.2113	22.4997	6.6782	6.2948	0.3834	5.7411
9.80	2-197	C	16.1641	24.3184	23.9523	8.1543	7.7882	0.3661	4.4897	23.4901	7.7882	7.3260	0.4622	5.9346
9.95	2-200	M	16.0562	23.4564	23.1197	7.4002	7.0635	0.3367	4.5499	22.7509	7.0635	6.6947	0.3688	5.2212
10.35	1-208	L	16.4860	17.8181	17.7335	1.3321	1.2475	0.0846	6.3509	17.6928	1.2475	1.2068	0.0407	3.2625
10.50	2-211	T	16.6866	24.9673	24.5309	8.2807	7.8443	0.4364	5.2701	24.0839	7.8443	7.3973	0.4470	5.6984
10.60	2-213	G	14.5628	21.2299	20.9462	6.6671	6.3834	0.2837	4.2552	20.5608	6.3834	5.9980	0.3854	6.0375
10.80	2-217	L	16.4861	22.9127	22.6337	6.4266	6.1476	0.2790	4.3413	22.302	6.1476	5.8159	0.3317	5.3956
10.95	2-220	F	14.1184	23.5247	23.1393	9.4063	9.0209	0.3854	4.0973	22.4599	9.0209	8.3415	0.6794	7.5314

Appendix 4b: BH-4 Loss-on-Ignition (LOI)

Depth	Batch-Index	Crucible #	Crucible (g)	Pre 550 Crucible + Sample Weight (g)	Post 550 Sample + Crucible Weight (g)	Pre 550 (g)	Post 550 (g) [Ash]	Lost (g)	LOI 550°C %	Post 550 Sample + Crusible Weight (g)	Pre 850 (g)	Post 850 (g) [Carbonates]	Lost (g)	LOI 850°C %
1.00	4-21	D	15.0537	16.0723	15.1741	1.0186	0.1204	0.8982	88.1799	15.1578	0.1204	0.1041	0.0163	13.5382
1.10	3-23	B	15.7361	16.6287	15.8455	0.8926	0.1094	0.7832	87.7437	15.8300	0.1094	0.0939	0.0155	14.1682
1.20	4-25	A	16.2040	17.4458	16.3758	1.2418	0.1718	1.0700	86.1652	16.3566	0.1718	0.1526	0.0192	11.1758
1.40	3-29	Q	15.7602	16.3270	15.8210	0.5668	0.0608	0.5060	89.2731	15.8123	0.0608	0.0521	0.0087	14.3092
1.50	4-31	N	15.4212	16.0187	15.4600	0.5975	0.0388	0.5587	93.5063	15.4545	0.0388	0.0333	0.0055	14.1753
1.60	4-33	H	15.9671	16.7467	16.0500	0.7796	0.0829	0.6967	89.3663	16.0346	0.0829	0.0675	0.0154	18.5766
1.70	4-35	I	14.7685	15.3907	14.8271	0.6222	0.0586	0.5636	90.5818	14.8183	0.0586	0.0498	0.0088	15.0171
1.80	3-37	N	15.4206	16.5281	15.5494	1.1075	0.1288	0.9787	88.3702	15.5294	0.1288	0.1088	0.0200	15.5280
1.90	3-39	L	16.4873	17.4829	16.5879	0.9956	0.1006	0.8950	89.8955	16.5707	0.1006	0.0834	0.0172	17.0974
2.00	3-41	S	15.1902	16.3956	15.3410	1.2054	0.1508	1.0546	87.4896	15.3232	0.1508	0.1330	0.0178	11.8037
2.20	3-45	K	16.2895	17.2658	16.4917	0.9763	0.2022	0.7741	79.2892	16.4822	0.2022	0.1927	0.0095	4.6983
2.40	4-49	B	15.7356	16.7086	15.8528	0.9730	0.1172	0.8558	87.9548	15.8382	0.1172	0.1026	0.0146	12.4573
2.60	3-53	U	14.4382	15.3466	14.6004	0.9084	0.1622	0.7462	82.1444	14.5847	0.1622	0.1465	0.0157	9.6794
2.80	3-57	G	14.5627	15.3286	14.6476	0.7659	0.0849	0.6810	88.9150	14.6414	0.0849	0.0787	0.0062	7.3027
3.00	3-61	F	14.1187	16.4023	15.5192	2.2836	1.4005	0.8831	38.6714	15.4959	1.4005	1.3772	0.0233	1.6637
3.20	4-65	R	15.4373	16.5130	15.9195	1.0757	0.4822	0.5935	55.1734	15.9099	0.4822	0.4726	0.0096	1.9909
3.40	3-69	3	11.4755	11.9485	11.8397	0.4730	0.3642	0.1088	23.0021	11.8294	0.3642	0.3539	0.0103	2.8281
3.60	3-73	6	12.2982	13.9659	13.7052	1.6677	1.4070	0.2607	15.6323	13.6751	1.4070	1.3769	0.0301	2.1393
3.80	4-77	G	14.5627	21.4654	20.7364	6.9027	6.1737	0.7290	10.5611	20.6894	6.1737	6.1267	0.0470	0.7613
4.10	4-83	K	16.3896	20.3463	19.7244	3.9567	3.3348	0.6219	15.7176	19.6912	3.3348	3.3016	0.0332	0.9956

4.30	3-87	5	12.7506	15.0752	14.7720	2.3246	2.0214	0.3032	13.0431	14.7369	2.0214	1.9863	0.0351	1.7364
4.60	4-93	L	16.4859	21.7179	21.3844	5.2320	4.8985	0.3335	6.3742	20.5260	4.8985	4.0401	0.8584	17.5237
4.65	3-94	4	13.1436	16.9845	16.7456	3.8409	3.6020	0.2389	6.2199	16.6598	3.6020	3.5162	0.0858	2.3820
4.80	4-97	E	13.8697	18.0560	17.6142	4.1863	3.7445	0.4418	10.5535	17.5433	3.7445	3.6736	0.0709	1.8934
5.05	4-102	F	14.1195	21.6537	21.3791	7.5342	7.2596	0.2746	3.6447	21.1736	7.2596	7.0541	0.2055	2.8307
5.40	3-109	R	15.4384	21.3619	21.1826	5.9235	5.7442	0.1793	3.0269	20.9734	5.7442	5.5350	0.2092	3.6419
5.50	4-111	O	16.4907	22.9576	22.7758	6.4669	6.2851	0.1818	2.8112	22.5294	6.2851	6.0387	0.2464	3.9204
5.70	4-115	J	13.5992	22.3100	22.0787	8.7108	8.4795	0.2313	2.6553	21.7868	8.4795	8.1876	0.2919	3.4424
5.95	3-120	A	16.2047	21.9771	21.8061	5.7724	5.6014	0.1710	2.9624	21.6267	5.6014	5.4220	0.1794	3.2028
6.00	4-121	U	14.4382	20.9311	20.7099	6.4929	6.2717	0.2212	3.4068	20.2978	6.2717	5.8596	0.4121	6.5708
6.05	3-122	T	16.6869	19.8945	19.7848	3.2076	3.0979	0.1097	3.4200	19.6885	3.0979	3.0016	0.0963	3.1086
6.26	3-126	J	13.5994	18.1800	18.0355	4.5806	4.4361	0.1445	3.1546	17.8834	4.4361	4.2840	0.1521	3.4287
6.40	1-129	H	15.9677	22.6347	22.4256	6.6670	6.4579	0.2091	3.1363	22.0528	6.4579	6.0851	0.3728	5.7728
6.60	3-133	I	14.7690	19.3403	19.1842	4.5713	4.4152	0.1561	3.4148	18.9757	4.4152	4.2067	0.2085	4.7223
6.75	4-136	M	16.0558	21.8296	21.6469	5.7738	5.5911	0.1827	3.1643	21.3144	5.5911	5.2586	0.3325	5.9470
6.90	3-139	C	16.1637	21.8681	21.6509	5.7044	5.4872	0.2172	3.8076	21.2149	5.4872	5.0512	0.4360	7.9458
7.00	3-141	E	13.8706	19.8128	19.6088	5.9422	5.7382	0.2040	3.4331	19.3497	5.7382	5.4791	0.2591	4.5154
7.15	3-144	D	15.0538	20.3687	20.2066	5.3149	5.1528	0.1621	3.0499	19.5076	5.1528	4.4538	0.6990	13.5654
7.20	4-145	C	16.1627	23.0865	22.8666	6.9238	6.7039	0.2199	3.1760	22.4476	6.7039	6.2849	0.4190	6.2501
7.40	3-149	O	19.4817	19.8683	19.7556	0.3866	0.2739	0.1127	29.1516	19.4069	0.2739	-0.0748	0.3487	127.3092

Appendix 4c: BH-8 Loss-on-Ignition (LOI)

Depth	Batch-Index	Crucible #	Crucible (g)	Pre 550 Crucible + Sample Weight (g)	Post 550 Sample + Crucible Weight (g)	Pre 550 (g)	Post 550 (g) [Ash]	Lost (g)	LOI 550°C %	Post 550 Sample + Crusible Weight (g)	Pre 850 (g)	Post 850 (g) [Carbonates]	Lost (g)	LOI 850°C %
0.20	8-4	I	14.7684	15.8950	14.9157	1.1266	0.1473	0.9793	86.9253	14.9062	0.1473	0.1378	0.0095	6.4494
0.40	6-8	Q	15.7609	16.4146	15.8636	0.6537	0.1027	0.5510	84.2894	15.8583	0.1027	0.0974	0.0053	5.1607
0.60	8-12	R	15.4373	16.1156	15.5277	0.6783	0.0904	0.5879	86.6726	15.5239	0.0904	0.0866	0.0038	4.2035
0.83	5-17	T	16.6858	16.7289	16.6890	0.0431	0.0032	0.0399	92.5754	16.6889	0.0032	0.0031	0.0001	3.1250
1.00	8-20	M	16.0553	17.5692	16.4520	1.5139	0.3967	1.1172	73.7962	16.4439	0.3967	0.3886	0.0081	2.0418
1.23	5-24	J	13.5989	14.4121	13.9014	0.8132	0.3025	0.5107	62.8013	13.8953	0.3025	0.2964	0.0061	2.0165
1.40	8-27	A	16.2038	16.6685	16.4208	0.4647	0.2170	0.2477	53.3032	16.4184	0.2170	0.2146	0.0024	1.1060
1.60	8-31	S	15.1883	17.8027	17.0077	2.6144	1.8194	0.7950	30.4085	16.7940	1.6219	1.6057	0.0162	0.9988
1.78	8-34	D	15.0534	17.8047	16.9632	2.7513	1.9098	0.8415	30.5855	16.9437	1.9098	1.8903	0.0195	1.0210
1.98	5-38	L	16.4852	18.5379	17.9166	2.0527	1.4314	0.6213	30.2675	17.9027	1.4314	1.4175	0.0139	0.9711
2.03	8-39	J	13.5984	15.7571	14.9569	2.1587	1.3585	0.8002	37.0686	14.9434	1.3585	1.3450	0.0135	0.9937
2.40	7-45	T	16.6855	18.8858	18.2878	2.2003	1.6023	0.5980	27.1781	18.2686	1.6023	1.5831	0.0192	1.1983
2.55	6-47B	G	14.5627	15.8710	14.9286	1.3083	0.3659	0.9424	72.0324	14.9183	0.3659	0.3556	0.0103	2.8150
2.78	6-51	L	16.4852	17.9425	16.9339	1.4573	0.4487	1.0086	69.2102	16.9224	0.4487	0.4372	0.0115	2.5630
2.98	6-54	1	12.3083	14.1797	13.5853	1.8714	1.2770	0.5944	31.7623	13.5631	1.2770	1.2548	0.0222	1.7384
3.21	7-58	G	15.5622	16.8356	16.0959	1.2734	0.5337	0.7397	58.0886	16.0682	0.5337	0.5060	0.0277	5.1902
3.40	6-62	F	14.1184	15.2225	14.8846	1.1041	0.7662	0.3379	30.6041	14.8662	0.7662	0.7478	0.0184	2.4015
3.60	6-66	6	12.2984	13.7676	13.3613	1.4692	1.0629	0.4063	27.6545	13.3443	1.0629	1.0459	0.0170	1.5994
3.92	5-72	1	12.3081	15.0732	14.6020	2.7651	2.2939	0.4712	17.0410	14.5682	2.2939	2.2601	0.0338	1.4735
4.15	5-76	K	16.3880	17.7873	17.2244	1.3993	0.8364	0.5629	40.2273	17.2085	0.8364	0.8205	0.0159	1.9010

4.41	5-81	5	12.7502	15.4354	15.0551	2.6852	2.3049	0.3803	14.1628	15.0003	2.3049	2.2501	0.0548	2.3775
4.60	5-85	E	13.8694	18.3138	17.7909	4.4444	3.9215	0.5229	11.7654	17.7869	3.9215	3.9175	0.0040	0.1020
4.79	5-89	3	11.4752	14.5676	14.2243	3.0924	2.7491	0.3433	11.1014	14.1610	2.7491	2.6858	0.0633	2.3026
5.00	5-93	U	14.4373	18.9720	18.4481	4.5347	4.0108	0.5239	11.5531	18.3655	4.0108	3.9282	0.0826	2.0594
5.20	5-97	Q	15.7598	20.0621	19.5620	4.3023	3.8022	0.5001	11.6240	19.1617	3.8022	3.4019	0.4003	10.5281
5.56	7-103	B	15.7353	22.3976	22.0883	6.6623	6.3530	0.3093	4.6425	21.9188	6.3530	6.1835	0.1695	2.6680
5.78	7-107	H	15.9332	23.1461	22.8507	7.2129	6.9175	0.2954	4.0954	22.7158	6.9175	6.7826	0.1349	1.9501
6.00	5-112	H	15.9660	23.0398	22.7516	7.0738	6.7856	0.2882	4.0742	22.6244	6.7856	6.6584	0.1272	1.8746
6.20	8-116	E	13.8697	19.9634	19.6341	6.0937	5.7644	0.3293	5.4039	19.5334	5.7644	5.6637	0.1007	1.7469
6.40	5-120	F	14.1181	21.5332	21.1626	7.4151	7.0445	0.3706	4.9979	21.0627	7.0445	6.9446	0.0999	1.4181
6.60	7-123	K	16.3876	22.4060	22.1439	6.0184	5.7563	0.2621	4.3550	22.0283	5.7563	5.6407	0.1156	2.0082
6.78	5-127	4	13.1441	17.2184	17.0519	4.0743	3.9078	0.1665	4.0866	16.9553	3.9078	3.8112	0.0966	2.4720
7.00	7-131	U	14.4371	19.3294	19.1071	4.8923	4.6700	0.2223	4.5439	19.0155	4.6700	4.5784	0.0916	1.9615
7.17	6-134	T	16.6862	20.1569	19.9800	3.4707	3.2938	0.1769	5.0970	19.9201	3.2938	3.2339	0.0599	1.8186
7.17	7-134	1	12.3076	13.8476	13.7738	1.5400	1.4662	0.0738	4.7922	13.7470	1.4662	1.4394	0.0268	1.8279
7.43	7-139	F	14.1179	19.5632	19.2035	5.4453	5.0856	0.3597	6.6057	19.1867	5.0856	5.0688	0.0168	0.3303
7.54	7-141	L	16.4850	21.4943	21.2733	5.0093	4.7883	0.2210	4.4118	21.1816	4.7883	4.6966	0.0917	1.9151
7.80	7-146	Q	15.7595	19.4107	19.2299	3.6512	3.4704	0.1808	4.9518	19.1600	3.4704	3.4005	0.0699	2.0142
8.00	6-150	K	16.3880	21.9265	21.6766	5.5385	5.2886	0.2499	4.5121	21.5776	5.2886	5.1896	0.0990	1.8720
8.29	6-155	H	15.9655	21.7679	21.5057	5.8024	5.5402	0.2622	4.5188	21.4058	5.5402	5.4403	0.0999	1.8032
8.60	6-156B	C	16.1636	21.3868	21.1414	5.2232	4.9778	0.2454	4.6983	21.0538	4.9778	4.8902	0.0876	1.7598
8.79	5-160	G	14.5623	19.9091	19.6673	5.3468	5.1050	0.2418	4.5223	19.5780	5.1050	5.0157	0.0893	1.7493
9.00	5-164	O	16.4904	22.1700	21.9010	5.6796	5.4106	0.2690	4.7362	21.8231	5.4106	5.3327	0.0779	1.4398
9.20	5-168	D	15.0539	21.1305	20.8780	6.0766	5.8241	0.2525	4.1553	20.7305	5.8241	5.6766	0.1475	2.5326
9.40	5-180	B	15.7359	21.7655	21.4647	6.0296	5.7288	0.3008	4.9887	21.3631	5.7288	5.6272	0.1016	1.7735
9.40	5-172	R	15.4376	22.0784	21.8077	6.6408	6.3701	0.2707	4.0763	21.6537	6.3701	6.2161	0.1540	2.4175

9.60	5-176	A	16.2041	23.4092	23.1113	7.2051	6.9072	0.2979	4.1346	22.9523	6.9072	6.7482	0.1590	2.3019
10.00	5-183	C	16.1634	22.0638	21.7478	5.9004	5.5844	0.3160	5.3556	21.6653	5.5844	5.5019	0.0825	1.4773
10.20	5-186	S	18.1892	22.2806	21.9916	4.0914	3.8024	0.2890	7.0636	21.8166	3.8024	3.6274	0.1750	4.6024
10.37	5-189	I	14.7686	21.1953	20.9201	6.4267	6.1515	0.2752	4.2821	20.7596	6.1515	5.9910	0.1605	2.6091
10.61	5-194	M	16.0553	21.7917	21.5535	5.7364	5.4982	0.2382	4.1524	21.4118	5.4982	5.3565	0.1417	2.5772
10.78	8-197	O	16.4903	21.4564	21.2038	4.9661	4.7135	0.2526	5.0865	21.1164	4.7135	4.6261	0.0874	1.8542
10.95	6-200	U	14.4375	19.8722	19.5874	5.4347	5.1499	0.2848	5.2404	19.4900	5.1499	5.0525	0.0974	1.8913
11.19	6-205	B	15.7365	22.0214	21.6750	6.2849	5.9385	0.3464	5.5116	21.5332	5.9385	5.7967	0.1418	2.3878
11.34	7-208	N	15.4192	23.3407	22.8758	7.9215	7.4566	0.4649	5.8688	22.6328	7.4566	7.2136	0.2430	3.2589